To the Graduate Council:

I am submitting herewith a thesis written by Gary R. Mattasits entitled "An Investigation of Wind Tunnel Carriage Position Airloads Using Flight Test Data as Criterion." I recommend that it be accepted in partial fulfillment of the requirements for the degree of Master of Science, with a major in Aerospace Engineering.

Trevor H. Moulden, Major Professor

We have read this thesis
and recommend its acceptance:

William B. Baker Jr

C. F. L.

Accepted for the Council:

L Evans Roth

Vice Chancellor
Graduate Studies and Research

Thesis
78
.M392
cop 2

AN INVESTIGATION OF WIND TUNNEL CARRIAGE POSITION AIRLOADS USING FLIGHT TEST DATA AS CRITERION

A Thesis

Presented for the

Master of Science

Degree

The University of Tennessee, Knoxville

Gary R. Mattasits

December 1978

139411

ACKNOWLEDGEMENTS

The author wishes to express his appreciation to Mr. R. E. Dix, Research Engineer, Arnold Research Organization, for his comments regarding this work.

Special thanks are due to Mrs. Wanda Bush for the preparation of figures.

The work was conducted by the Arnold Engineering Development Center (AEDC), Air Force Systems Command (AFSC), at the request of the Air Force Armament Laboratory (AFATL), under Program Element 62602F. The results were obtained by ARO, Inc., AEDC Division (a Sverdrup Corporation Company), operating contractor for the AEDC, AFSC, Arnold Air Force Station, Tennessee. The test was conducted under ARO Project Numbers P34A-C4A and P34A-K6A.

ABSTRACT

Many analytical programs used to determine weapon trajectories rely on experimental aerodynamic loads data obtained in wind tunnels. A recent study of two techniques used to obtain carriage position airloads data in wind tunnels has indicated disagreement between the test techniques. At present the lack of any data base has made it impossible to decide which wind tunnel technique is best. As a result, a flight test was conducted in order to obtain a data base for the evaluation of wind tunnel carriage position airloads. Flight test hardware and one-twentieth-scale wind tunnel models of the F-4 aircraft, inboard pylon, triple ejector rack, and MK-83 bomb were tested at Mach numbers from 0.6 to 0.9 at aircraft angles of attack from minus three to plus thirteen degrees. The effects of rack design, data acquisition techniques, store afterbody modifications, Reynolds number, wall porosity, and sting interference were investigated during the wind tunnel test. Experimental and analytical techniques were used to evaluate the effect of carriage position airloads on the separation trajectories of a MK-83 bomb from the number one triple ejector rack station on the F-4 inboard pylon. Flight test results were good with the exception of data obtained during high "g" maneuvers. Wind tunnel data obtained using the internal bracket support test technique compared well with flight test results.

Comparisons between flight test and wind tunnel test data were not significantly changed by modeling triple ejector rack details for this aircraft-store configuration. Analytical trajectories based on wind tunnel internal bracket support data compared well with trajectories computed using flight test results.

TABLE OF CONTENTS

CHAPTER		PAGE
I.	INTRODUCTION	1
II.	APPARATUS	4
	Flight Test	4
	Wind Tunnel Test	18
III.	DATA ACQUISITION	31
	Flight Test	31
	Wind Tunnel Test	38
IV.	RESULTS AND DISCUSSION	54
V.	CONCLUSIONS	116
LIST OF REFERENCES		119
APPENDIXES		122
A.	ESTIMATION OF INERT SHELL ELEMENT EFFECTS	123
B.	AN OUTLINE OF THE DATA REDUCTION PROGRAM	134
C.	DERIVATION OF FLIGHT TEST UNCERTAINTY EQUATIONS.	138
VITA		144

LIST OF FIGURES

FIGURE		PAGE
1.	A Photograph of the Flight Test Configuration . . .	5
2.	A Sketch of the Inert-Shell Elements and Isolation Gaps	8
3.	A Photograph of the Pastushin Balance	9
4.	A Photograph Showing the Exterior Routing and Attachment of the MK-83 Bomb Instrumentation Cable	11
5.	Details and Dimensions of Both the Standard and Extended Sway Brace	13
6.	Details and Dimensions of the Standard and Modified MK-83 Afterbodies	14
7.	An Isometric Drawing of a Typical CTS Test Installation	20
8.	An Isometric Drawing of a Typical IBS Test Installation	23
9.	Details and Dimensions of the F-4C Aircraft Model	24
10.	Details and Dimensions of the Inboard Pylon Model	26
11.	Details and Dimensions of the Detailed TER Model	27
12.	Details and Dimensions of the MK-83 Bomb Models . .	28
13.	Photographs of a Typical IBS and CTS Test Installation	29

FIGURE PAGE

14. Digitized Data Showing Two Values of Aircraft Angle of Attack 35

15. A Spike in the Digitized Coefficient Data Curve Indicating an Error in the Recording and/or Digitizing Process 36

16. Estimated Uncertainties for the Flight Test Mach Number 40

17. Estimated Uncertainties for the Flight Test Dynamic Pressure 41

18. Estimated Uncertainties in the Flight Test Aerodynamic Coefficient Data 42

19. Ejector Force as a Function of Time 50

20. A Preliminary Comparison of the Aerodynamic Coefficients Obtained During the Flight Test and an Early Wind Tunnel Test, IBS Data 55

21. A Preliminary Comparison of the Aerodynamic Coefficients Obtained During the Flight Test and an Early Wind Tunnel Test, CTS Data 59

22. The Effect of TER Geometric Details on the Aerodynamic Coefficients of the MK-83 Model, Standard Afterbody 66

23. The Effect of TER Geometric Details on the Aerodynamic Coefficients of the MK-83 Model, Modified Afterbody 68

FIGURE PAGE

24. The Effect of Venting Slots and Sway Brace Arms on the Aerodynamic Coefficients of the MK-83 Model 70

25. Comparisons of IBS Data Obtained in the Flow Field of the Detailed TER Model and Flight Test Data, Standard Afterbody 75

26. Comparisons of IBS Data Obtained in the Flow Field of the Detailed TER Model and Flight Test Data, Modified Afterbody 79

27. An Example of Aircraft Load Factors at Various Mach Numbers and Store Angles of Attack 84

28. A Comparison of CTS Data Obtained in the Flow Field of the Detailed TER Model and the Flight Test Data 85

29. The Effects of the CTS Sting on the Aerodynamic Coefficients of the MK-83 Model 91

30. The Effects of Afterbody Modification on the Aerodynamic Coefficients of the MK-83 Model . . . 93

31. The Effect of Reynolds Number on the Aerodynamic Coefficients of the MK-83 Model 95

32. The Effects of Wind Tunnel Wall Porosity on the Aerodynamic Coefficients of the MK-83 Model . . . 98

33. The Effects of TER Geometry on Wind Tunnel Trajectory Simulations 101

34. One Example of a Family of Interference Coefficient Data Curves 106

FIGURE PAGE

35. The Effects of Experimental Carriage Position Airloads on the Predicted Pitch Orientation of the MK-83 Bomb, M_∞ = 0.6 108

36. The Effects of Experimental Carriage Position Airloads on the Predicted Pitch Orientation of the MK-83 Bomb, M_∞ = 0.8 110

37. The Effect of Experimental Carriage Position Airloads on the Predicted Ground Dispersion of the MK-83 Bomb at Various Angles of Attack . . 113

A-1. Details and Dimensions of the Pressure Model . . . 124

A-2. Details and Dimensions of the Nielsen Model 125

A-3. Circumferential Pressure Coefficient Distributions 126

A-4. Circumferential Pressure Coefficient Distributions Associated with Various Inert Elements 128

A-5. Examples of Local Normal-Force and Pitching-Moment Coefficient Distributions With and Without Simulated Inert-Shell Elements 131

NOMENCLATURE

AB1,AB2	Store afterbody designation; standard and modified, respectively
A_x, A_y, A_z	Acceleration of the store center of gravity; positive in the negative X_E, positive Y_E, and positive Z_E directions, respectively, g's
b, $\bar{c}$	Store lateral and longitudinal reference dimension, respectively, feet full scale
BL	Aircraft buttock line from plane of symmetric, inches model scale
$B_1 \rightarrow B_9$	Bridge power supplied to the store balance and accelerometer gages, volts
C_A, C_N, C_Y	Store aerodynamic axial-force, normal-force, and side-force coefficients; positive in the negative X_B, negative Z_B, and positive Y_B direction, respectively
C_ℓ, C_m, C_n	Store aerodynamic rolling-moment, pitching-moment, and yawing-moment coefficients; the positive vectors are coincident with the positive X_B, Y_B, and Z_B axes, respectively
$C_{\ell_p}, C_{m_q}, C_{n_r}$	Store roll-damping, pitch-damping, and yaw-damping derivatives, respectively, per radian
$C_{N_w}, C_{N_{wo}}$	Store normal-force coefficient with and without simulated inert-shell elements, respectively; positive in the negative Z_B direction
$C_{m_w}, C_{m_{wo}}$	Store pitching-moment coefficient with and without simulated inert-shell elements, respectively; the positive vector is coincident with the positive Y_B axes
C_p	Local pressure coefficient, $(P_\ell - P)/q_\infty$
$C_0 \rightarrow C_5$	Initial polynomial curve fit coefficients for the ejector force as a function of time
$C_{11} \rightarrow C_{66}$	Diagonal terms of the balance coefficient matrix

D_B, D_S	Store model body diameter and store model sting support diameter, respectively
$DR_1 \rightarrow DR_6$	Differential balance reading, flight minus wind-off reading, microvolts
$d_0 \rightarrow d_5$	Final polynomial curve fit coefficients for the ejector force as a function of time
FS	Aircraft fuselage station, inches model scale
F_A, F_N, F_Y	Store aerodynamic axial, normal, and side force; positive in the negative X_B, negative Z_B, and positive Y_B direction, respectively, pounds
$F_{A_g}, F_{N_g}, F_{Y_g}$	Store gross axial, normal, and side force; positive in the negative X_B, negative Z_B, and positive Y_B direction, respectively, pounds
$F_{A_{st}}, F_{N_{st}}, F_{Y_{st}}$	Store inertial axial, normal, and side force; positive in the negative X_B, negative Z_B, and positive Y_B direction, respectively, pounds
H	Altitude, feet
I_{xx}, I_{yy}, I_{zz}	Full-scale moments of inertia about the store X_B, Y_B, and Z_B axes, respectively, slug-feet^2
I_{xz}	Full-scale product of inertia in the store X_B-Z_B plane, slug-feet^2
$[K_{ij}]$	Balance coefficient matrix
$K_{BP1} \rightarrow K_{BP9}$	Balance and accelerometer bridge power shunt ratio
K_{SX}, K_{SY}, K_{SZ}	Accelerometer shunt ratio
$K_{S1} \rightarrow K_{S6}$	Balance shunt ratio
$L_1 \rightarrow L_6$	Balance gage total load, pounds
ℓ	Store length, feet full scale or inches model scale
LIB	Left inboard pylon designation

$\bar{m}$	Full-scale store mass, slugs
M_ℓ, M_m, M_n	Store aerodynamic rolling, pitching, and yawing moment; the positive vectors are coincident with the positive X_B, Y_B, and Z_B axes, respectively, foot-pounds
$M_{\ell_g}, M_{m_g}, M_{n_g}$	Store gross rolling, pitching, and yawing moment; the positive vectors are coincident with the positive X_B, Y_B, and Z_B axes, respectively, foot-pounds
$M_{\ell_{st}}, M_{m_{st}}, M_{n_{st}}$	Store inertial rolling, pitching, and yawing moment; the positive vectors are coincident with the positive X_B, Y_B, and Z_B axes, respectively, foot-pounds
M_∞	Free-stream Mach number
N_z	Aircraft load factor, g's
P	Free-stream static pressure, pounds per foot^2
P_ℓ	Local static pressure measured at the model orifices, pounds per foot^2
P_o	Sea level static pressure, 2116.22 pounds per foot^2
P_t	Free-stream total pressure, pounds per foot^2
q_∞	Free-stream dynamic pressure, pounds per foot^2
R	Universal gas constant, 1716 ft^2 per second^2 degrees Rankin
Re	Free-stream Reynolds number
Re/ℓ	Free-stream unit Reynolds number, per foot
R_{AX}, R_{AY}, R_{AZ}	Accelerometer gage readings, millivolts
R_{AX_o}, R_{AY_o}, AZ_o	Accelerometer reference zero gage readings, millivolts
R_H	Altitude instrument reading, millivolts

$R_P, R_{T_T}, R_{V_{CAL}}$	Free-stream static pressure, total temperature and calibrated airspeed instrument reading, respectively, millivolts
$R_1 \rightarrow R_6$	Balance gage reading, millivolts
$R_{1_o} \rightarrow R_{6_o}$	Balance reference zero gage reading, millivolts
$R_\alpha, R_\beta, R_\theta$	Aircraft angle of attack, sideslip angle, and dive angle instrument reading, millivolts
S	Store reference area, feet^2 full scale
$S_{0,1} \rightarrow S_{0,9}$	Intercept coefficient for the calculation of balance and accelerometer shunt ratios
$S_{1,1} \rightarrow S_{1,9}$	Slope coefficient for the calculation of balance and accelerometer shunt ratios
T, T_T	Free-stream static and total temperature, respectively, degrees Rankin
t	Cumulative time for the trajectory, seconds of full-scale flight time following the release of the store
TAU	Wind tunnel wall porosity, percent open
V_∞	Free-stream velocity, feet per second
V_{a_o}	Sea level speed of sound, 1116.45 feet per second
V_{CAL}	Free-stream calibrated airspeed, feet per second
WL	Aircraft waterline, inches model scale
W_A, W_N, W_Y	Store static tare weight as measured by the balance axial-force, normal-force, and side-force gages, respectively, pounds
X	Distance along the store longitudinal axis or wing chord, inches model scale
XDIS,YDIS	Store longitudinal and lateral ground dispersion, respectively, feet full scale
X_{cg}	Axial distance from the store nose to the center of gravity location, feet full scale

X_L	Distance between the center of gravity and the ejector piston location; positive when the center of gravity location is aft of the ejector piston location, feet full scale
$\overline{X}_m, \overline{X}_n$	Axial distance between the store center of gravity location and the effective pitching moment and yawing moment center of the balance, respectively; positive when the center of gravity is forward of the effective center of the balance, feet full scale
X_{m_T}, X_{n_T}	Axial distance between the store moment reference point and the effective pitching-moment and yawing-moment center of the balance, respectively; positive when the moment reference point is forward of the effective center of the balance, feet full scale
X_1, X_7	Axial distance between the forward and aft pitching-moment and yawing-moment gages, respectively, feet full scale
Y	Distance perpendicular to the wing-chord plane, inches model scale
$\overline{Y}$, $\overline{Z}$	Distance between the store center of gravity location and the X_B axis, measured perpendicular to the X_B axis in the X_B-Y_B and X_B-Z_B plane, respectively; positive when the center of gravity is to the right and below of the X_B axis, respectively, feet full scale
α, α_s	Aircraft and store angle of attack relative to the free-stream velocity vector, degrees
β	Aircraft sideslip angle relative to the free-stream velocity vector, degrees
γ	Ratio of specific heats of air, 1.4
θ	Aircraft dive angle, positive for decreasing altitude, degrees
μ	Viscosity of air, pound-second per foot^2
ρ	Density of air, pound-second^2 per foot^4

Prescript Notations:

Δ	Uncertainty
∂	Partial derivative

STORE BODY-AXIS SYSTEM DEFINITIONS

Coordinate Directions

X_B	Parallel to the store longitudinal axis, positive direction is upstream at store release
Y_B	Perpendicular to X_B and Z_B directions, positive to the right looking upstream when the store is at zero yaw and roll angles
Z_B	Perpendicular to the X_B direction and parallel to the X_I-Z_I plane when the store is at zero yaw and roll angles, positive downward as seen by the pilot when the store is at zero pitch and roll angles

Origin

The store body-axis system origin is coincident with the store cg at all time. The X_B, Y_B, and Z_B coordinate axes rotate with the store in pitch, yaw, and roll so that mass moments of inertia about the three axes are not time-varying quantities.

EARTH-AXIS SYSTEM DEFINITIONS

Coordinate Directions

X_E	Parallel to a projection of the X_I axis on the earth surface, positive direction is forward as seen by the pilot
Y_E	Perpendicular to the X_E and Z_E directions, positive to the right as seen by the pilot
Z_E	Perpendicular to the earth surface, positive direction is down

Origin

The earth-axis system origin is fixed at the point in space coincident to the store cg at release.

FLIGHT-AXIS SYSTEM DEFINITIONS

Coordinate Directions

X_F	Parallel to the current aircraft flight path direction, positive forward as seen by the pilot
Y_F	Perpendicular to the X_F and Z_F directions, positive to the right as seen by the pilot
Z_F	Parallel to the aircraft plane of symmetry and perpendicular to the current aircraft flight path direction, positive downward as seen by the pilot

Origin

The flight-axis system origin is coincident with the store cg at release. The origin is fixed with respect to the aircraft and thus translates along the current aircraft flight path at the free-stream velocity. The coordinate axes rotate to maintain alignment of the X_F axis with the current aircraft-flight path direction.

INERTIAL-AXIS SYSTEM DEFINITIONS

Coordinate Directions

X_I	Parallel to the aircraft flight path direction at store release, positive forward as seen by the pilot
Y_I	Perpendicular to the X_I and Z_I direction, positive to the right as seen by the pilot
Z_I	Parallel to the aircraft plane of symmetry and perpendicular to the aircraft flight path direction at store release, positive downward as seen by the pilot

Origin

The inertial axis system origin is coincident with the store cg at release and translates along the initial aircraft flight path direction at the free-stream velocity. The coordinate axes do not rotate with respect to the initial aircraft flight path direction.

PYLON-AXIS SYSTEM DEFINITIONS

Coordinate Directions

X_P	Parallel to the store longitudinal axis at release and at constant angular orientation with respect to the current aircraft flight path direction, positive forward as seen by the pilot
Y_P	Perpendicular to the X_P direction and parallel to the X_F-Y_F plane, positive to the right as seen by the pilot
Z_P	Perpendicular to the X_P and Y_P directions, positive downward as seen by the pilot

Origin

The pylon-axis system origin is coincident with the flight-axis system origin and the store cg at release. It is fixed with respect to the aircraft and thus translates along the current aircraft flight path at the free-stream velocity. The coordinate axes rotate to maintain constant angular orientation with respect to the current aircraft flight path direction.

Positions

X_P	Separation distance of the store cg with respect to the flight-axis system origin in the X_P direction, feet, full scale
Y_P	Separation distance of the store cg with respect to the flight-axis system origin in the Y_P direction, feet, full scale
Z_P	Separation distance of the store cg with respect to the flight-axis system origin in the Z_P direction, feet, full scale

Attitudes (Yaw, Pitch, Roll Sequence)

DPSI	Angle between the projection of the store longitudinal axis in the X_P-Y_P plane and the X_P-axis, positive for store nose to the right as seen by the pilot, degrees
DTHA	Angle between the store longitudinal axis and its projection in the X_P-Y_P plane, positive when the store nose is raised as seen by the pilot, degrees

DPHI	Angle between the store lateral (Y_B) axis and the intersection of the Y_B-Z_B and X_P-Y_P planes, positive for clockwise rotation when looking upstream, degrees

CHAPTER I

INTRODUCTION

The separation of a weapon from an aircraft is influenced by many aerodynamic as well as inertial phenomena. A successful separation is one which not only clears the aircraft but also follows a predictable path from release to impact. Both experimental and analytical techniques are used in practice to determine weapon trajectories. Analytical calculations which employ such techniques as small perturbation theory or vortex-lattice methods, are being routinely used and continually refined. These techniques are summarized in Reference 1. Such methods yield trajectories which are in reasonably good agreement with experimental results when the necessary geometric features of the aircraft and weapon are correctly modeled and the flight speed is below the critical speed. In the transonic flight region, where local sonic flow and local shock wave interactions with boundary layers exist, the analytical methods are not as yet fully developed. In this region, analytical methods rely heavily on experimental aerodynamic loads data obtained in the wind tunnel. The purpose of this investigation is to examine carriage position aerodynamic loads data obtained in the wind tunnel using flight test data as the criterion and to evaluate the effect of any discrepancies on the separation characteristics of a weapon.

Test data were obtained for a MK-83 bomb at the bottom (number one) station of a triple ejector rack (TER) mounted on the inboard pylon of an F-4 aircraft. Weapons separating from TER station one are generally characterized by large nose down pitch rates that increase with increasing Mach number and decreasing aircraft angle of attack. The nose down pitch rate is a direct result of aerodynamically induced downwash at the nose and upwash at the tail of the weapon at the carriage location. Therefore, the success or failure of separation depends largely on carriage position aerodynamics. A more detailed experimental investigation into the physical behavior of the flow at TER station one can be found in Reference 2.

A recent study of the two major methods used to obtain wind tunnel carriage position airloads is described in Reference 3. The study indicates some disagreement between the two methods; disagreement which may influence separation trajectories. The methods of obtaining carriage position airloads are the dual sting support and the internal bracket support techniques. At present the lack of any data base, for a meaningful comparison between wind tunnel and flight test data has made it impossible to decide which, if any, wind tunnel method truely simulates weapon aerodynamics at the carriage position. A need for in-flight measurements of carriage position airloads was therefore established.

The acquisition of flight test data has, thus far, met with limited success. Early attempts were thwarted by

improper balance design and large dynamic forces which made it difficult to interpret oscillograph traces of the balance and accelerometer output data. Later attempts were made with advanced balance designs capable of obtaining useful captive loads data. Although anticipated loads were within the design load range and electrical filters were used to reduce dynamic signal interference, the validity of the reduced data was questionable for two major reasons. First, measured forces and moments were not corrected for store weight tares; and secondly, no provisions were made to determine an accurate flight attitude. The acquisition, reduction, and analysis of the flight test data presented herein is an attempt to improve upon past experience.

This thesis describes the most recent attempt to acquire valid in-flight carriage loads data and the use of those data as a criterion for carriage loads data obtained in the four-foot Transonic Wind Tunnel (4T) at the Arnold Engineering Development Center (AEDC). It is hoped that these comparisons will verify a wind tunnel method of obtaining carriage loads data in 4T that simulate actual weapon aerodynamics. Both experimental and computer simulated trajectories will be used to evaluate the effect of carriage position airloads on the separation characteristics of the MK-83 bomb from TER station one.

CHAPTER II

APPARATUS

I. FLIGHT TEST

The flight test was conducted at the Naval Air Test Center (NATC) at Patuxent River, Maryland from June 18 through June 22, 1976. Atmospheric conditions on the ground were approximately those of a standard day with the exception of temperature which was about twenty to twenty-five degrees Fahrenheit above the standard, winds were mild. The flights were conducted using an F-4J aircraft assigned to the United States Navy. A United States Air Force pylon was fitted to the left inboard pylon station of the aircraft. A TER-9A was mounted to the pylon and was fitted with inert MK-83 bombs at stations two and three (left and right shoulder stations, respectively). TER station one (bottom center) was occupied by an instrumented MK-83 bomb. A photograph of the flight test configuration is shown in Figure 1. A TER and TER adaptor of United Kingdom (UK) design were mounted to a United States Navy pylon at the right wing inboard pylon station of the aircraft. Weapons of the UK were mounted on TER stations two and three. The UK test articles were tested simultaneously with, but completely independent of, the American test and hence will not be discussed.

The F-4J aircraft was equipped with special

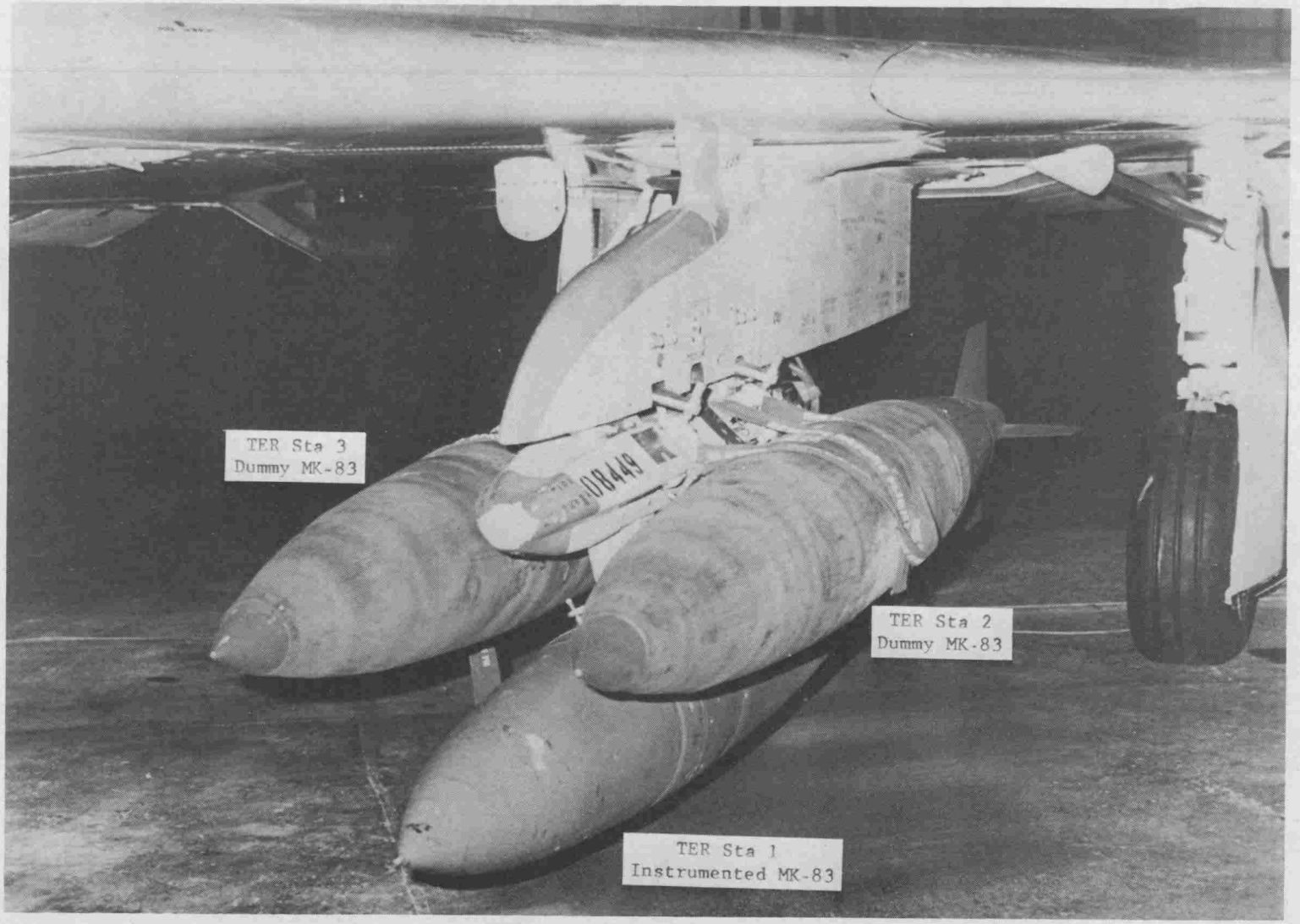

Figure 1. A photograph of the flight test configuration.

instrumentation subsystems for the flight test. A signal conditioning subsystem served as an interface for all signal wiring and provided the means for conditioning balance and accelerometer output signals for the MK-83 bomb. The balance output signals required bridge balance circuits, low level amplifiers, low pass Butterworth filters, high pass filters, voltage substitution calibration circuits, and differential input amplifiers with gain and offset for the bridge voltage monitor circuits. The accelerometer output signals required differential amplifiers and low pass Butterworth filters. The boom subsystem consisted of a probe extending from the aircraft nose tip. The probe sensed an averaged static pressure, total temperature, airspeed, altitude, angle of attack, and sideslip angle. Output signals from the boom subsystem required no conditioning. All data were synchronized by the time correlation subsystem which consisted of a time code generator, a cockpit time display, a pilot event mark, an aircraft bomb button firing pulse, and a UHF radio. The pulse code modulation subsystem consisted of a Vector (PAS507) pulse code modulation unit. A data rate of eighty-eight thousand bits per second was selected to ensure data reconstruction up to twenty cycles per second. All channels were filtered to remain within the twenty-cycle per second limit. Output signals from the pulse code modulation subsystem were recorded by the magnetic tape recorder subsystem. The magnetic tape recorder subsystem was a fourteen track, MARS 2000, intermediate band magnetic tape recorder with a

maximum frequency response of two hundred and fifty cycles per second at sixty inches of tape per second. A record speed of thirty inches per second was selected to handle the data bandwidth requirement for this test. All aircraft instrumentation subsystems were calibrated by the Technical Support Division of the NATC.

The instrumented MK-83 bomb was furnished by the Naval Weapons Center in China Lake, California. The bomb shell was of standard munition production. The centerbody, which housed the Pastushin balance, was modified to provide inert-shell elements to which the TER suspension hooks and sway brace pads could be attached. These inert elements were isolated from the remainder of the bomb shell by isolation gaps to avoid physical interactions. A sketch of the inert-shell elements and isolation gaps is presented in Figure 2.

The Pastushin balance consisted of an upper and lower platform which were interconnected by six strain-gaged elements. The lower platform bolted directly to the bomb shell. The inert-shell elements were fastened to the upper platform. A photograph of the Pastushin balance is shown in Figure 3. With the exception of the inert-shell elements, aerodynamic loads acting on or inertial loads attributable to the bomb shell were sensed by the balance. An estimation of the effects caused by the inert-shell elements is given in Appendix A.

The strain-gaged elements which connected the

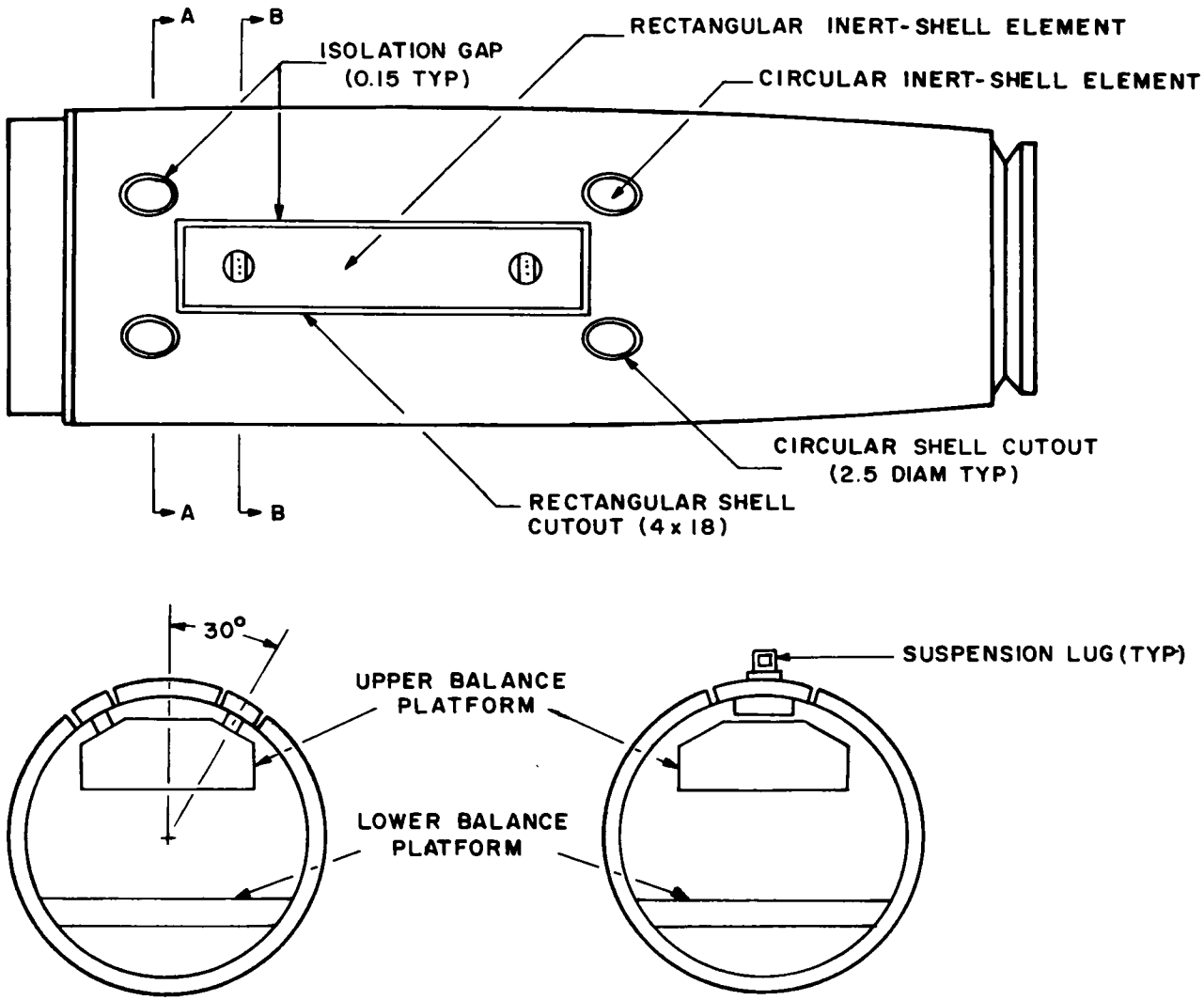

Figure 2. A sketch of the inert-shell elements and isolation gaps.

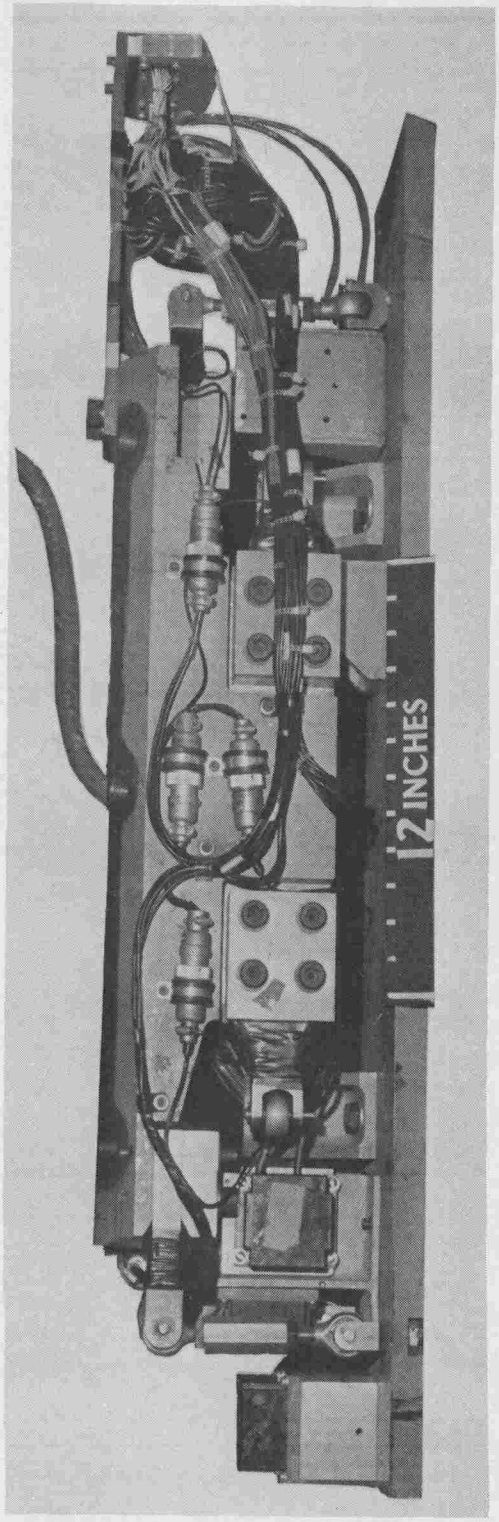

Figure 3. A photograph of the Pastushin balance.

upper and lower balance platforms were designed to transmit loads along one axis; thereby resolving any applied load into its components in a three-dimensional orthogonal coordinate system. The coordinate system was aligned with, and therefore identical to, the MK-83 bomb body-axis system. The body-axis system coordinate directions are defined in the Nomenclature. Three Statham accelerometers were mounted to the lower balance platform in each of the primary directions of the body-axis system. To eliminate the possibility of interference between strain-gage and accelerometer wiring and the metric bomb shell, all wiring internal to the bomb shell was fastened to the sides of the upper (non-metric) balance platform. The internal wiring was then formed into one cable which was routed through the upper platform, attached to the TER, and connected to the aircraft instrumentation receptacles. A photograph showing the exterior routing and attachment of the MK-83 bomb instrumentation cable is shown in Figure 4.

Also shown in Figure 4 are the TER sway brace arms. The span of the sway brace arms associated with the instrumented bomb, TER station one, are larger than the standard sway brace arms, TER stations two and three. The arms were extended so that the sway brace pads could be positioned on the inert-shell elements of the MK-83 bomb without effecting the nominal carriage position. The design and fabrication of the extended sway braces was done at the Arnold Engineering Development Center (AEDC). Details and dimensions of

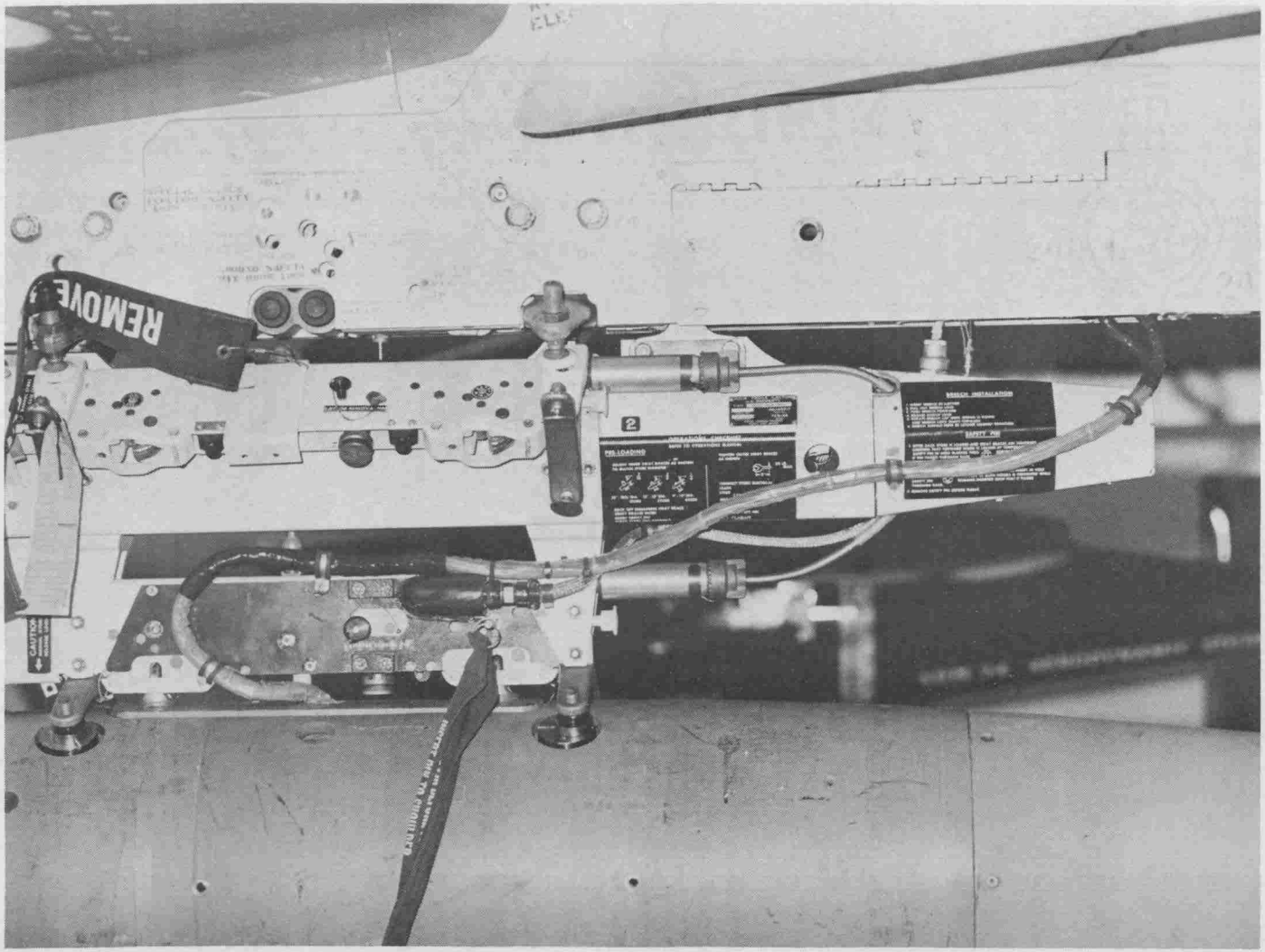

Figure 4. A photograph showing the exterior routing and attachment of the MK-83 bomb instrumentation cable.

both the standard and extended sway brace are given in Figure 5.

Flight test data were obtained for the MK-83 bomb with both a standard and a modified afterbody. The modified afterbody was a full-scale version of a one-twentieth-scale model afterbody used to allow sting mounting during captive trajectory support (CTS) testing in the 4T wind tunnel. The design and fabrication of the modified afterbody was also accomplished at AEDC. Details and dimensions of the standard and modified MK-83 afterbodies are given in Figure 6.

Numerous preflight and post-flight test procedures were developed at AEDC. The procedures helped substantiate the operational reliability of the MK-83 instrumentation package. Among these procedures was a shunt calibration which provided the means of correlating balance and accelerometer outputs obtained during the flight test to those obtained during the laboratory calibrations. The shunt calibration was performed before and after each day's flights so that each of the gage amplifier outputs could be checked and adjusted if necessary. A shunt box, designed and built at AEDC, was attached to the shunt box receptacles located on the end of an extension bar which was fastened to the upper balance platform. Access to the receptacles was obtained by removing the tail section of the bomb. The shunt box consisted of calibration resistors and switches which enabled the resistors to be placed across each leg of each strain gage and accelerometer.

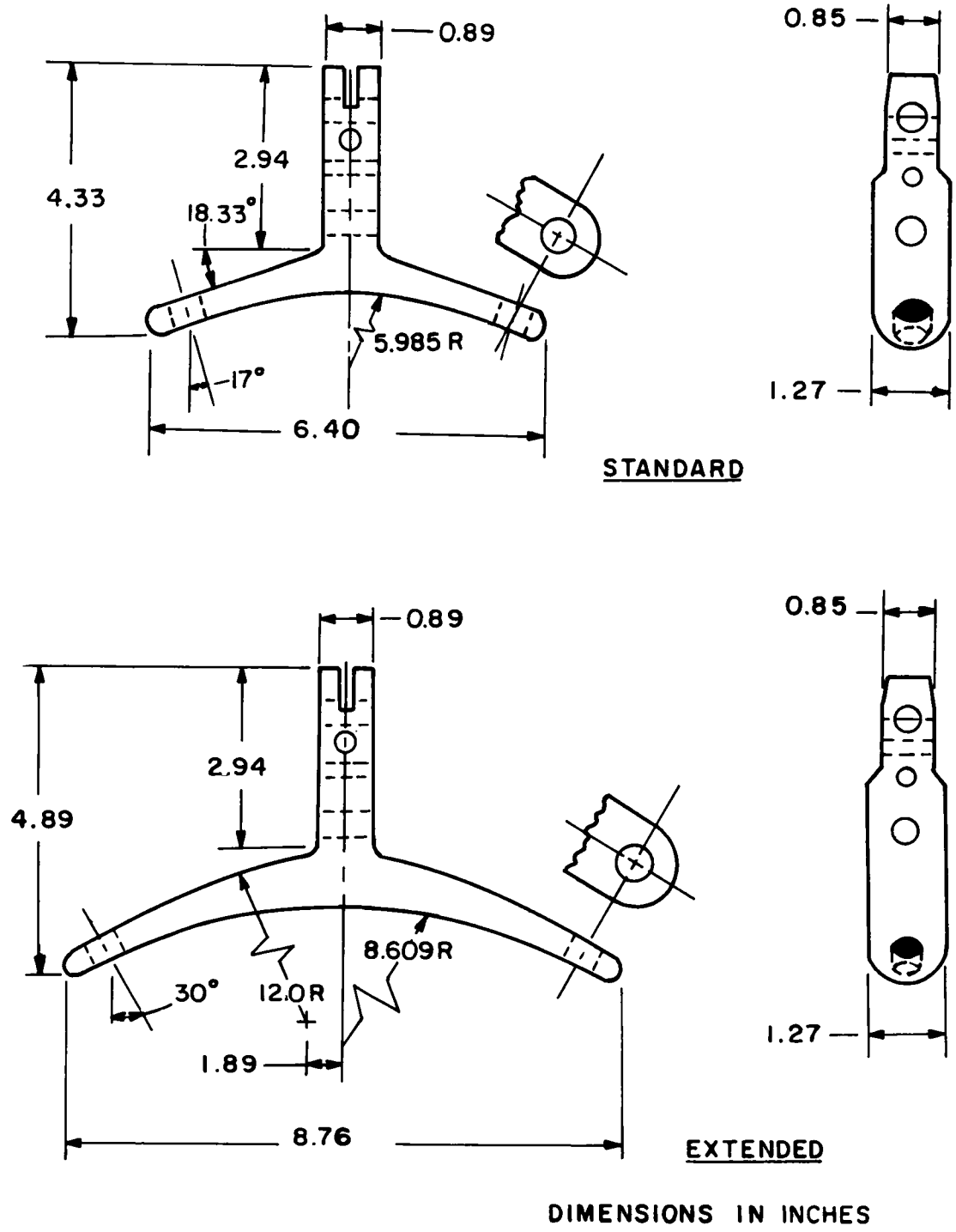

Figure 5. Details and dimensions of both the standard and extended sway brace.

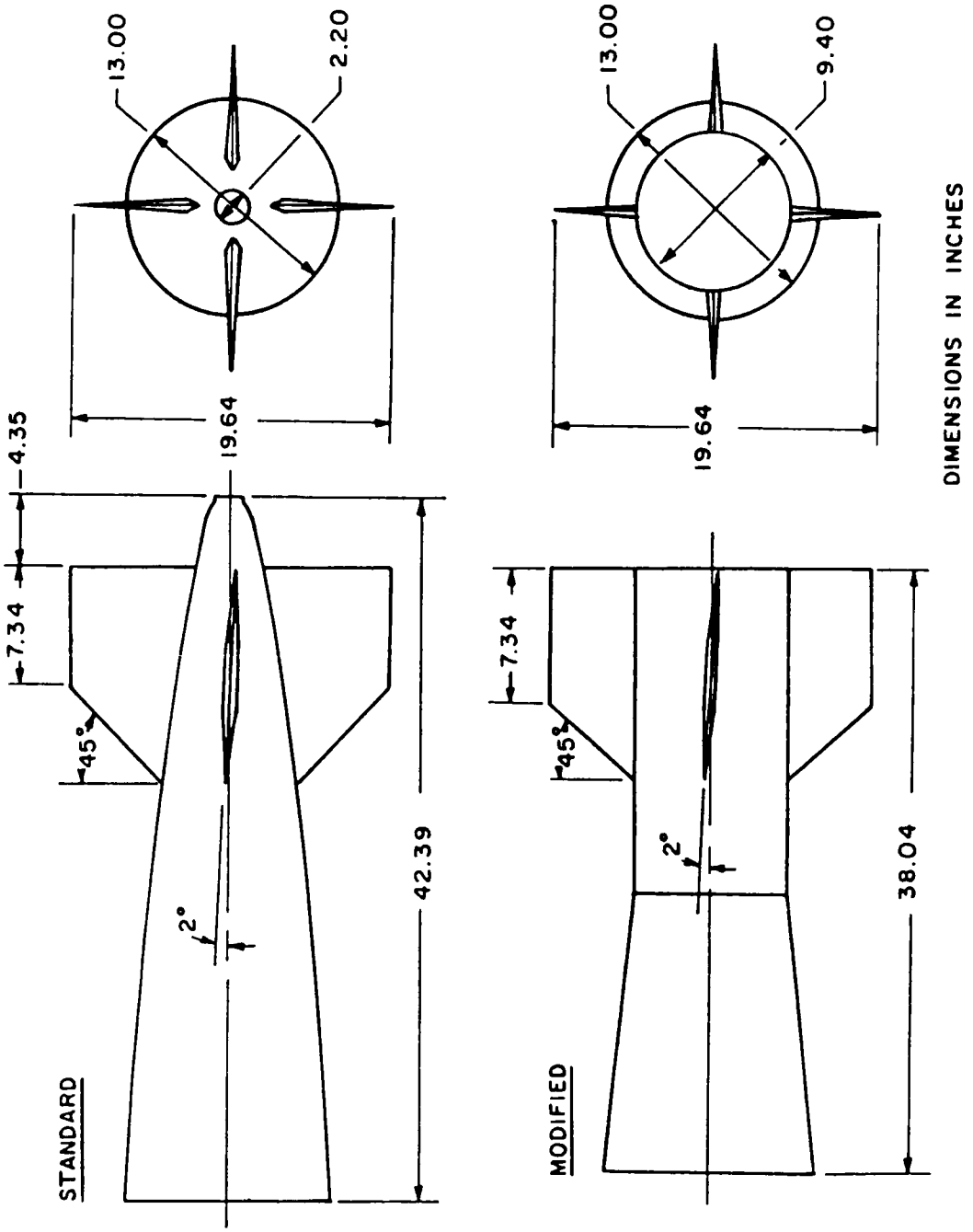

Figure 6. Details and dimensions of the standard and modified MK-83 afterbodies.

Holes, drilled and tapped into the MK-83 bomb shell, served as load points during both the laboratory calibration and the preflight and post-flight check loading procedures. Cap screws were used to plug these holes during flight.

The balance was calibrated at AEDC by the Instrumentation Branch of the Propulsion Wind Tunnel Facility. A preliminary inspection of the balance, showed that three load measuring strain gages could not be electrically suppressed (the electrical resistance between the elements of the strain gage would not balance to a common reference zero). Resistors were added to those elements. Four strain gages were modified by reversing the gage polarities such that the output of the Pastushin balance was identical to the standard moment-type balance calibrated at AEDC. The overall condition of the gaging, moisture proofing compound, flexures, et cetera, was satisfactory.

A large calibration rig was used to support the balance during the laboratory balance calibration. The upper balance platform was attached to the rig by conventional bomb lugs and sway brace pads. The balance was installed inside the bomb midsection during the calibration procedure. The midsection served as the calibration body to which known loads at known positions were applied. The balance calibration consisted of three load cycles. During each load cycle both positive and negative incremental

loads were applied in each of the three primary balance-axis system directions. Balance outputs were recorded for each incremental load only after the balance was leveled in pitch and roll to ensure that the load was properly applied. All calibration data were recorded using the force and moment readout system (FAMROS). The FAMROS is a multi-channel, parallel readout system for digitizing the output of strain-gage balances.

The electrical output of a good balance, as a function of applied load, is linear in nature; however, the linearity in one direction may differ slightly from the linearity in the opposite direction. Therefore, the bi-linear or two-slope method was used to reduce the balance calibration data. The slopes were determined by the method of least squares which was applied to all digitized calibration data in determining the final balance calibration constants. The final constants were calculated using a Raytheon 520 computer. The constants were defined by two six-by-six balance coefficient matrixes; one matrix for positive strain-gage outputs and the other for negative strain-gage outputs. The diagonal term of each matrix was large in relation to the off-diagonal terms. The off-diagonal terms are commonly referred to as interaction terms. These terms, for example, define the output of the side-force gages due to an applied load in the normal-force direction.

A balance calibration is used to relate the

electrical output of strain gages to applied loads. Although the laboratory FAMROS and the aircraft recording system were electrically equivalent, differences in the length or gage diameter of circuit wiring can effect the magnitude of electrical outputs. A shunt ratio is therefore used to relate in-flight strain-gage outputs to laboratory strain-gage outputs. The basic assumption is that the ratio of flight-to-laboratory strain-gage outputs is equivalent to the ratio of flight-to-laboratory shunts (shunt ratio). During the laboratory calibration, the balance power supply was adjusted to eleven volts direct current. The balance gages were allowed time to reach thermal equilibrium before shunt values from the four elements of each strain gage were recorded; six shunt values were thus obtained. The same procedure was used before each flight. A shunt ratio for each strain gage was then calculated for each flight.

The four Statham accelerometers were calibrated at AEDC. Each accelerometer was statically calibrated by rolling the instrument through plus and minus ninety degrees. A dynamic calibration was made at fifty cycles per second as a check on the operational reliability of each accelerometer. The sensitivity for both static and dynamic calibrations was approximately equal.

The accelerometers were used in conjunction with the MK-83 bomb mass properties to determine inertial loadings. The mass properties of the instrumented bomb were determined by means of a static tare calibration. The bomb was

completely assembly and suspended from the calibration rig where balance output data were obtained at bomb roll orientations of zero, plus and minus ninety, and one hundred and eighty degrees at a pitch orientation of zero degrees. Data were also obtained at pitch attitudes of minus four and positive three degrees with roll equal to zero degrees. These data were reduced using the balance coefficient matrixes obtained from the balance calibration procedure. The results were three values of the bomb weight as measured by the balance gages in the three primary balance-axis directions. The location of the bomb's center of gravity was also determined by this procedure. Static tare calibrations were done for both the standard and modified bomb afterbodies. The static tare calibration results are given below:

Store	Afterbody	W_N	W_Y	W_A	$\bar{X}_m$	$\bar{X}_n$	$\bar{Y}$	$\bar{Z}$
MK-83	Standard	669	667	657	0.247	0.288	0.004	0.072
MK-83	Modified	689	688	671	0.145	0.158	0.023	0.070

The axial static tare results (W_A), obtained by pitching the bomb, vary slightly from the normal and side static tare results (W_N and W_Y). The variation is most likely due to the limited range through which the bomb was pitched.

II. Wind Tunnel Test

A test was conducted in the Aerodynamic Wind Tunnel (4T) of the Arnold Engineering Development Center (AEDC), Propulsion Wind Tunnel Facility (PWT), from February

11 through February 18, 1977. The wind tunnel is a closed-loop, continuous flow, variable-density tunnel in which the Mach number can be varied from 0.1 to 1.3 and can be set at discrete Mach numbers of 1.6 and 2.0 by placing nozzle inserts over the permanent sonic nozzle. At all Mach numbers, the stagnation pressure can be varied from three hundred to thirty-seven hundred pounds per square foot (absolute). The test section is four-feet square and twelve and one-half feet long. The walls are perforated with sixty-degree slant holes and can be set automatically at wall porosities from one-half to 10-percent open. The test section is completely enclosed in a plenum chamber from which air can be evacuated, allowing part of the airflow to be removed through the perforated walls of the test section. A more complete description of the test facility can be found in Reference 4.

Two data acquisition techniques were used to obtain carriage position airloads in 4T. The first to be discussed is the dual support or captive trajectory support (CTS) technique. Two separate and independent support systems are used to support the test articles. The aircraft model is inverted in the test section and supported by an offset sting attached to the main pitch sector. The MK-83 store model is supported by the CTS which extends down from the tunnel top wall and provides store movement (six degrees of freedom) independent of the aircraft model. An isometric drawing of a typical CTS test installation is shown in Figure 7.

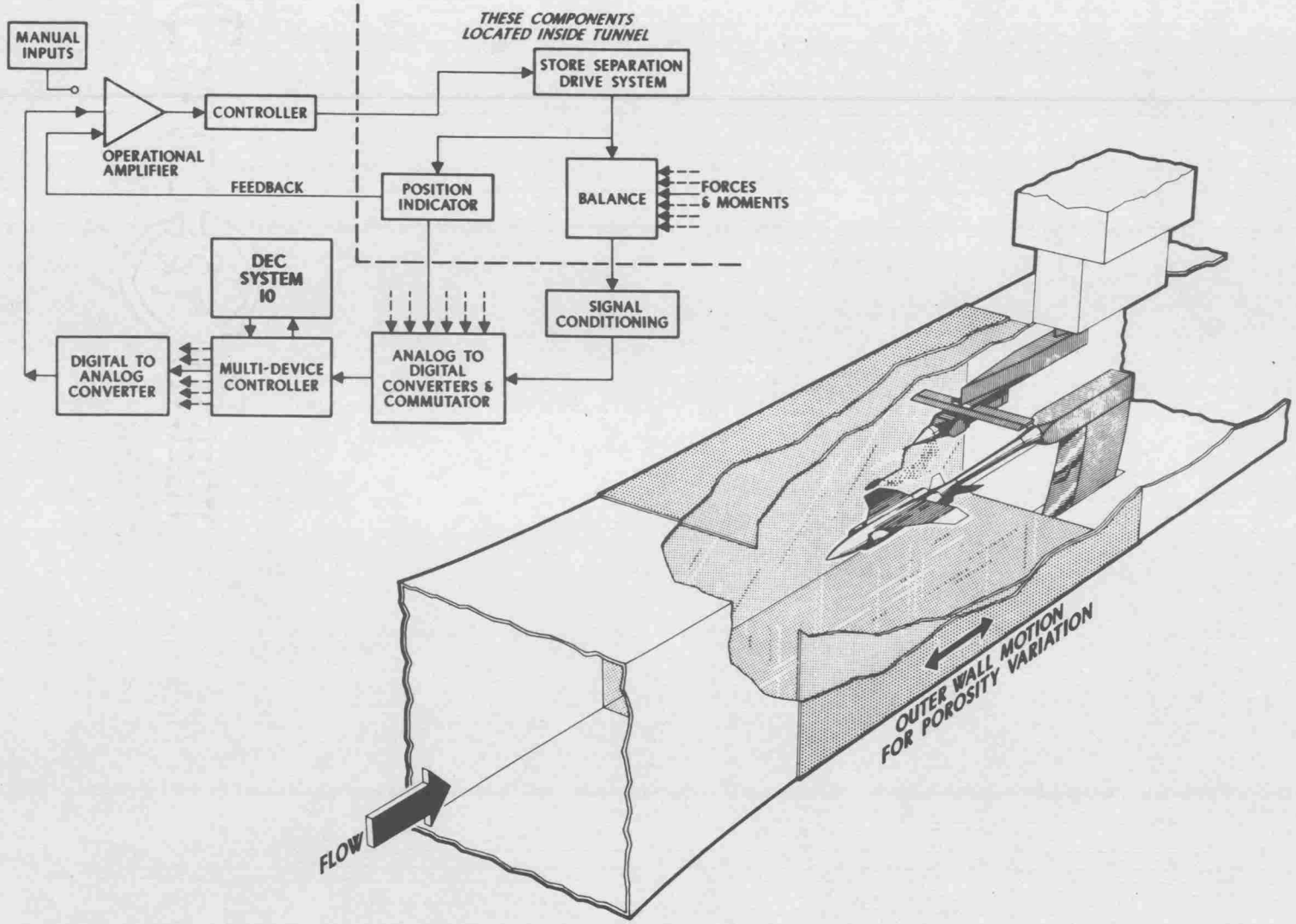

Figure 7. An isometric drawing of a typical CTS test installation.

A block diagram of the computer control loop used during CTS testing is also shown in Figure 7. The analog system and the digital computer work as an integral unit, utilizing required input information, to position the store model. Positioning is accomplished by use of six individual, direct current, electrical motors.

Since the aircraft and store model are moved independently of each other, the CTS technique is extremely versatile. Store model aerodynamic loads data can be obtained at almost any position in the aircraft's flow field and, with appropriate computer programs, separation trajectories can be simulated. However, modifications to the store afterbody, in most cases, must be made in order to accommodate the rear-entry sting support structure. Modifications such as increasing the store base area or shortening the store length, can produce sizeable differences in store aerodynamic characteristics; coefficient increments as large as 0.6 are shown in Reference 5. Afterbody modifications are also discussed in Reference 6.

The second method of obtaining carriage loads data is the internal bracket support (IBS) technique. The aircraft model is inverted in the test section and supported by an offset sting attached to the main pitch sector. The MK-83 store model and its internal balance are mounted directly to the TER at the carriage position. The IBS technique has an advantage in that the exact store geometry can be modeled since the balance is fitted completely within the

store model. A rigid structural member provides the necessary physical link between the store balance and the aircraft pylon or TER. However, to establish the physical link, surface area of the store must be removed. Although this area is small, its aerodynamic significance can be important (see Appendix A). An isometric drawing of a typical IBS test installation is shown in Figure 8.

A block diagram of the computer control loop used to set the aircraft model angle of attack is also shown in Figure 8. The automatic model attitude positioning system (AMAPS) utilizes a digital-to-analog converter to position the aircraft model.

A six-component internal strain-gage balance was used to measure wind tunnel store aerodynamic force and moment data. The procedures followed during the calibration of the store model balance were identical to the procedures followed during the calibration of the Pastushin balance. The aircraft model angle of attack was measured by an absolute angle-of-attack indicator (dangleometer). The procedure used during the calibration of the dangleometer was similar to the procedure used to calibrate the MK-83 bomb accelerometers.

One-twentieth-scale models of the F-4C aircraft, inboard pylon, TER, and MK-83 bomb were used during the wind tunnel test. The aircraft model was geometrically similar to the full-scale F-4J aircraft. Details and dimensions of the F-4C aircraft model are given in Figure 9. Details and

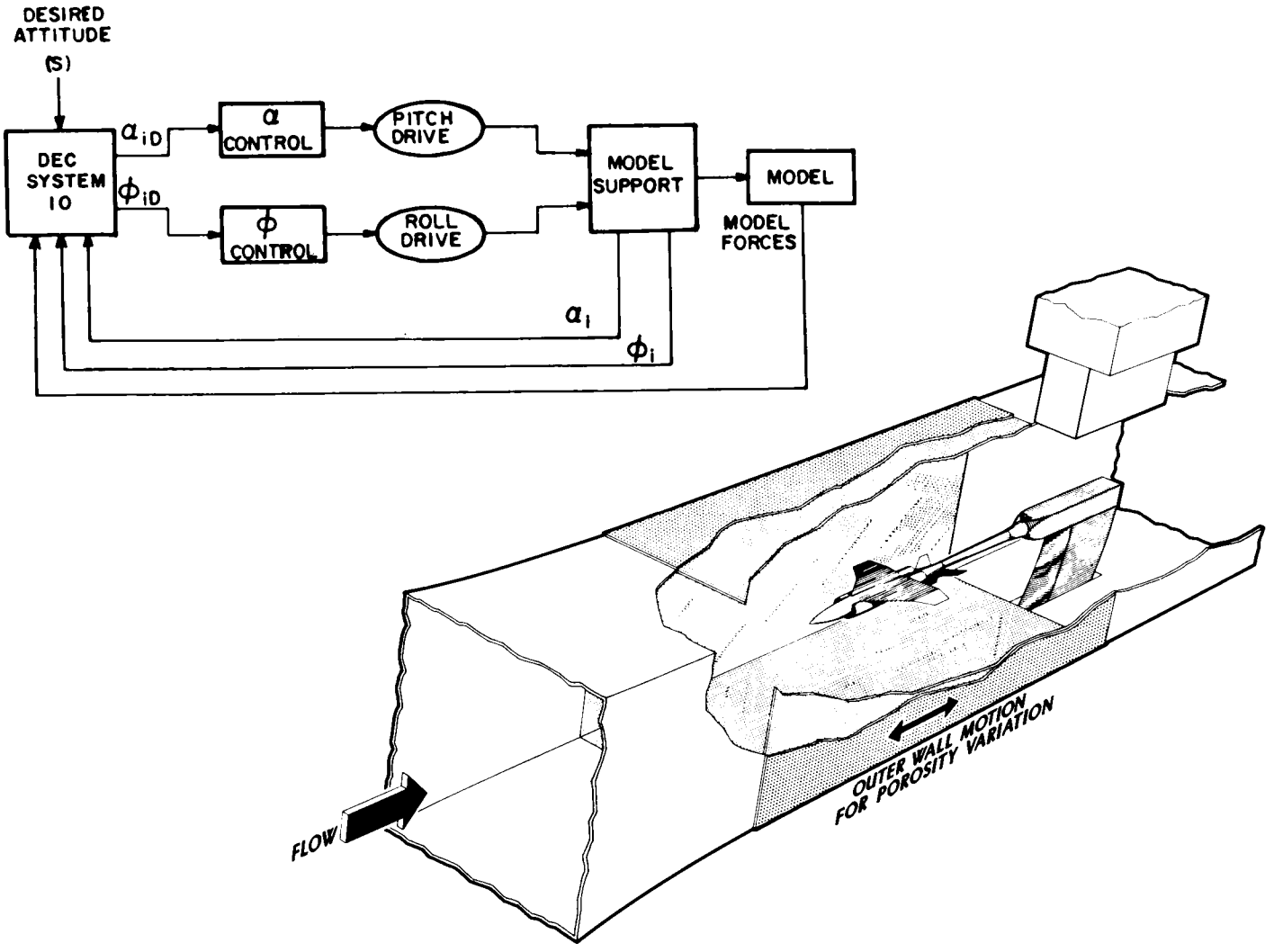

Figure 8. An isometric drawing of a typical IBS test installation.

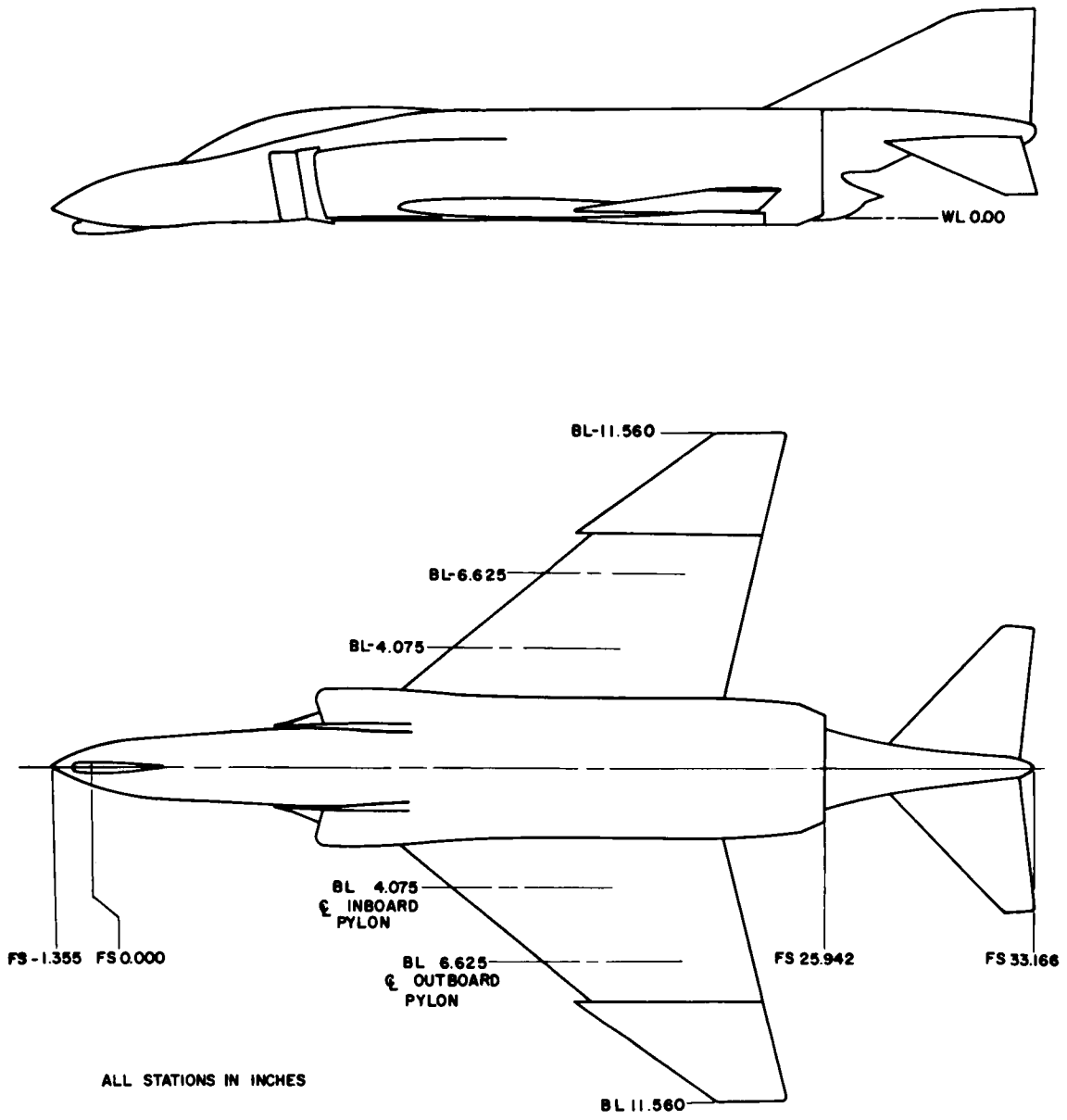

Figure 9. Details and dimensions of the F-4C aircraft model.

dimensions of the inboard pylon model are shown in Figure 10. In previous investigations of MK-83 carriage position airloads, no attempt was made to simulate spacings between the main TER body and its ejector units, sway brace arms, or sway brace pads. These intricate details are difficult and expensive to machine at one-twentieth scale. However, a detailed TER model was designed and fabricated at AEDC. The details and dimensions of the detailed TER model are given in Figure 11. Note the extended sway brace arms at TER station one which were used during wind tunnel testing to simulate the full-scale flight test hardware.

The TER model contained a touch wire system which aided in the positioning of the MK-83 model at the carriage positioning during CTS testing.

The MK-83 model was tested with both a standard and modified afterbody during IBS testing. Details and dimensions of the MK-83 bomb models are shown in Figure 12. Photographs of a typical IBS and CTS test installation are shown in Figure 13.

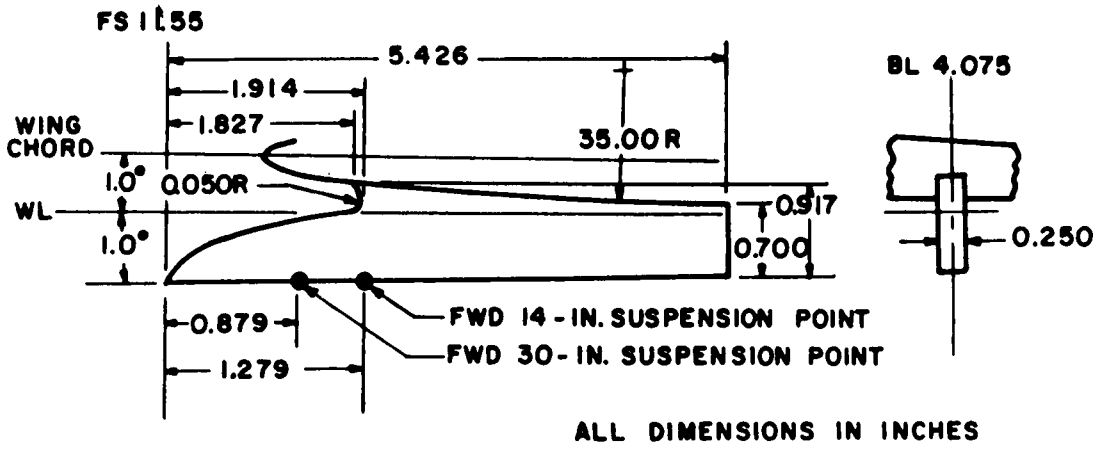

Figure 10. Details and dimensions of the inboard pylon model.

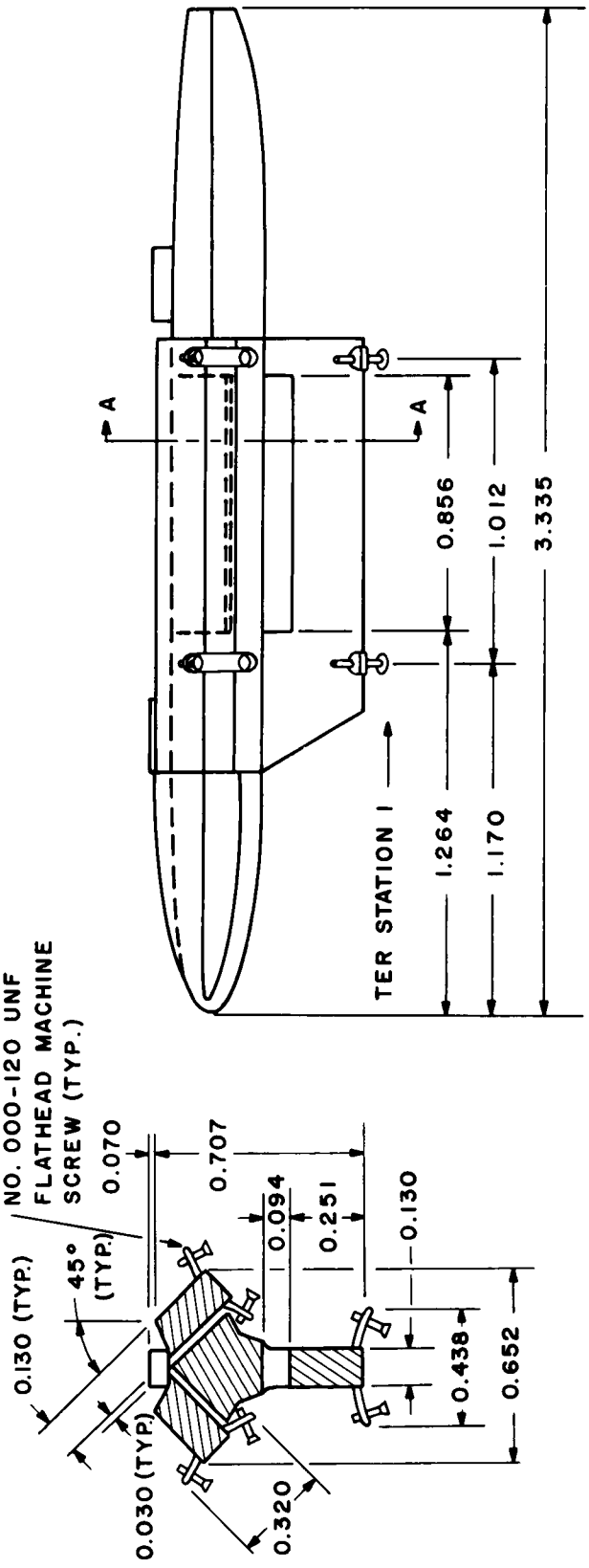

Figure 11. Details and dimensions of the detailed TER model.

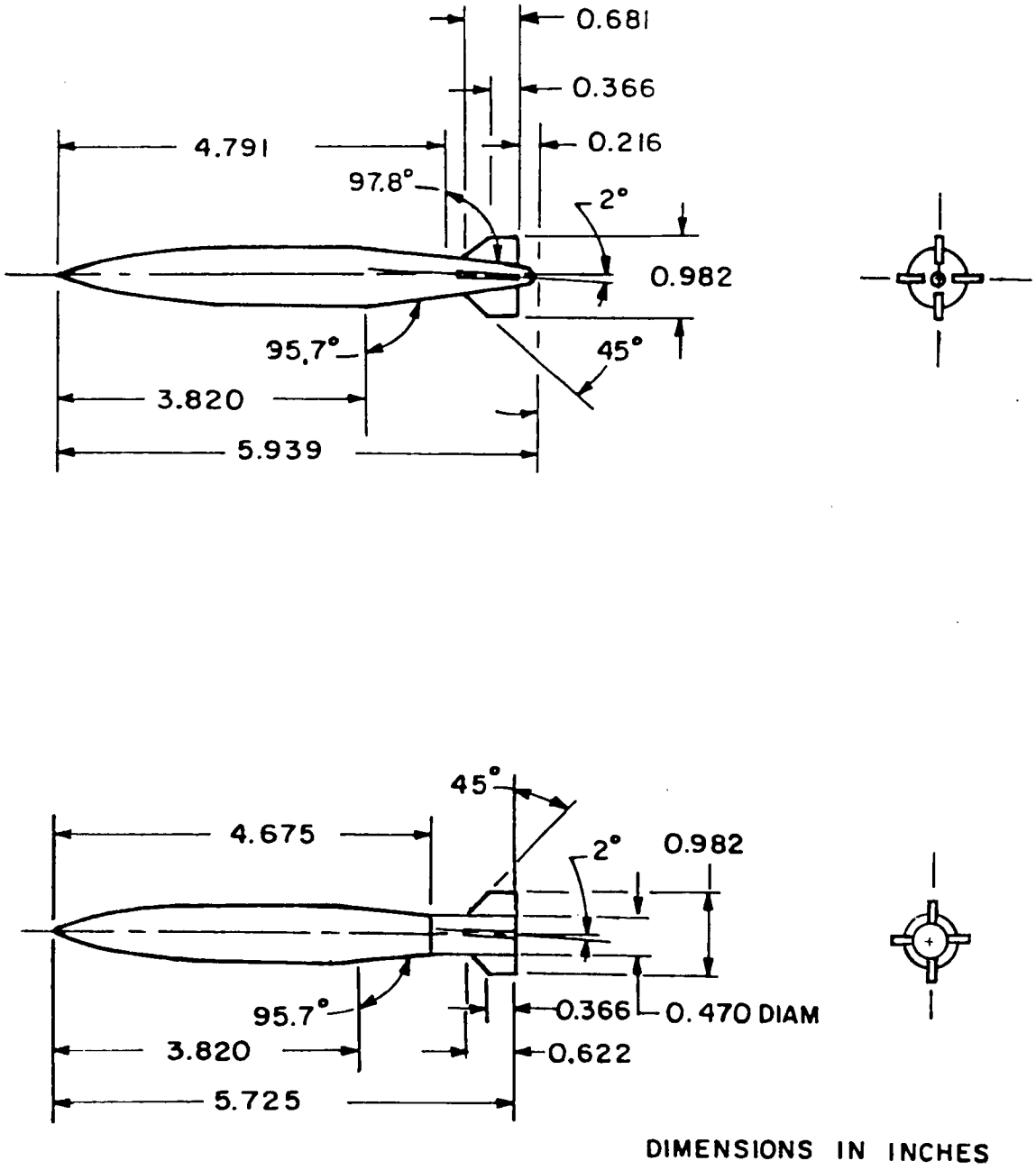

Figure 12. Details and dimensions of the MK-83 bomb models.

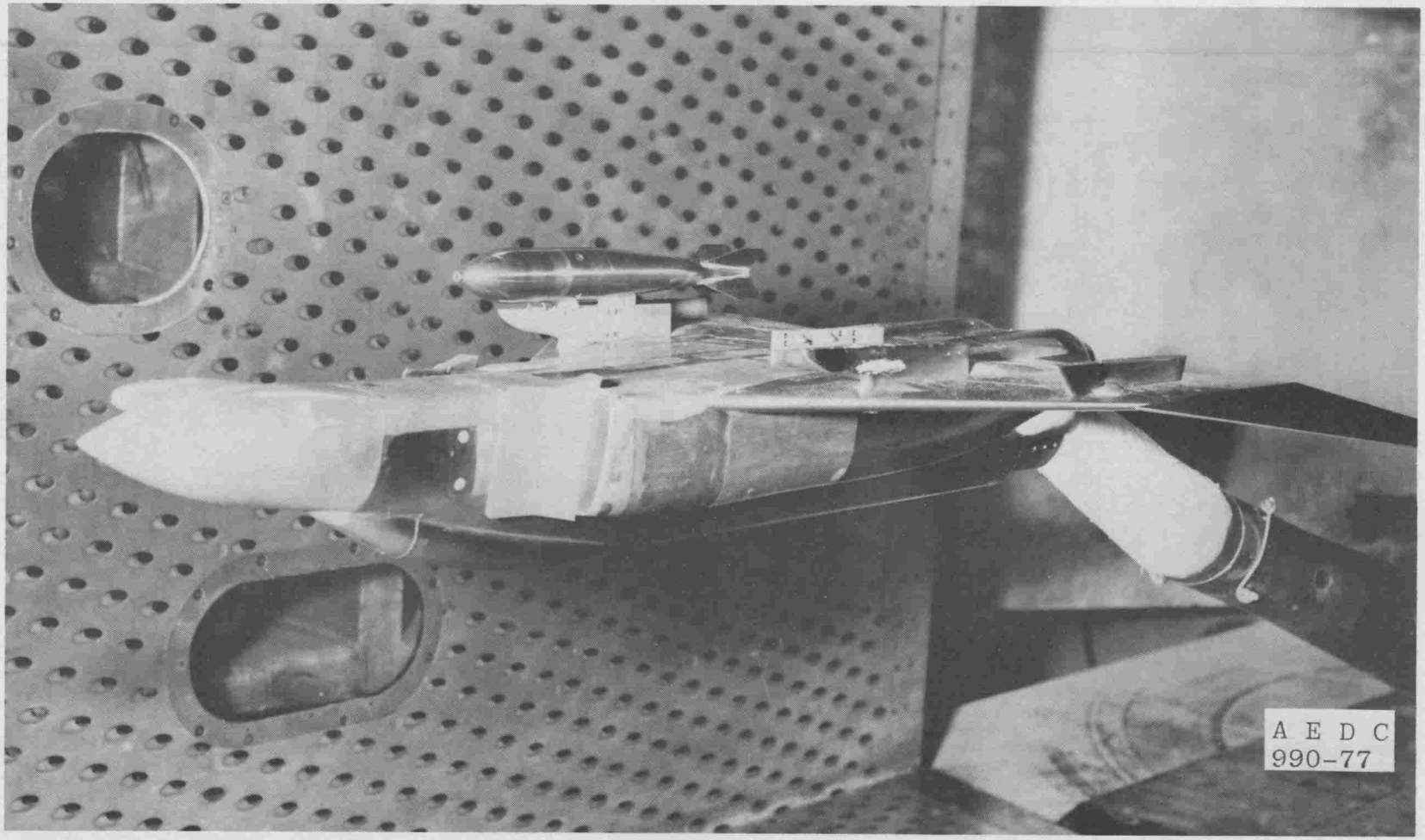

a. IBS test installation

Figure 13. Photographs of a typical IBS and CTS test installation.

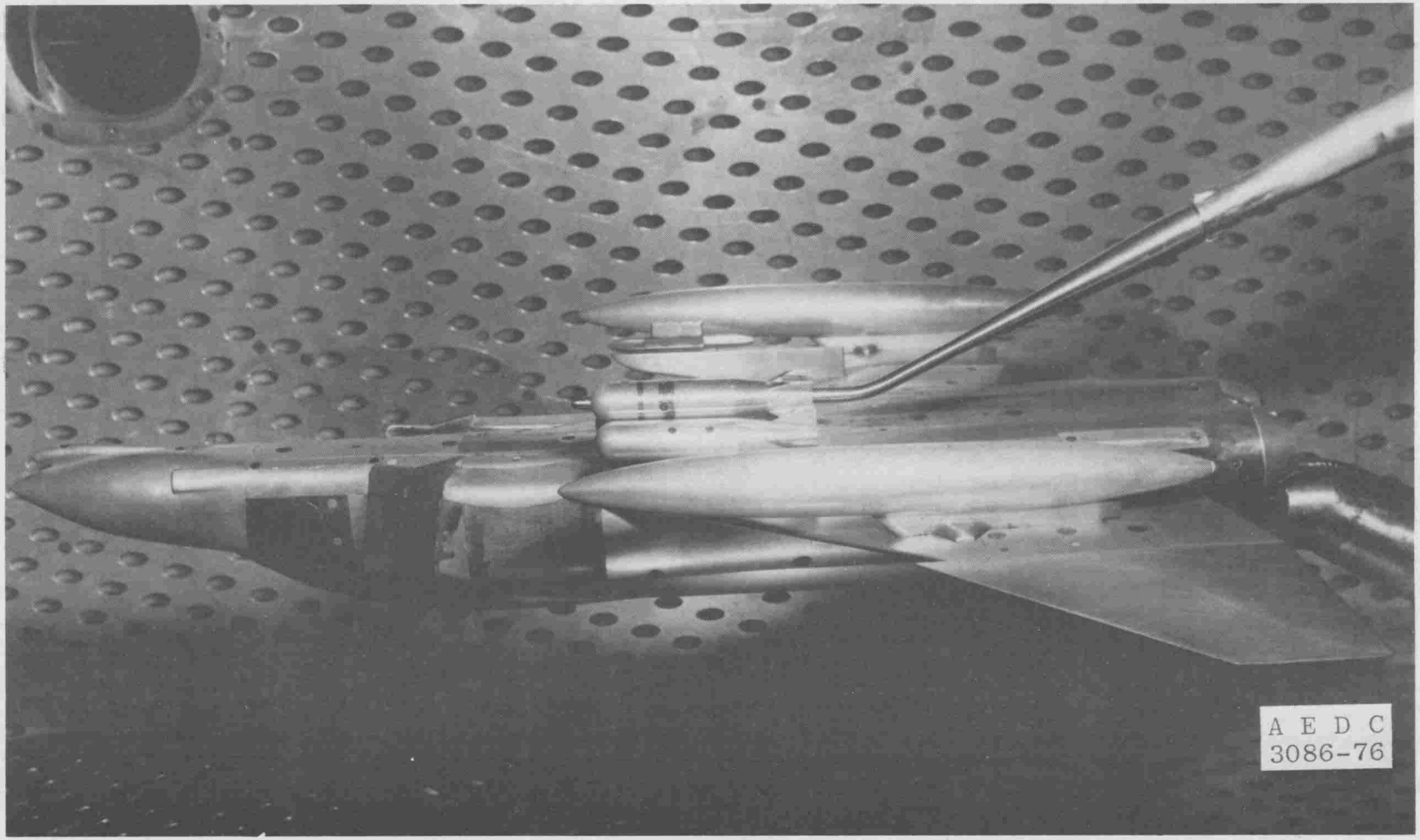

b. CTS test installation

Figure 13. (Continued)

CHAPTER III

DATA ACQUISITION

I. FLIGHT TEST

Preflight test procedures were used to obtain reference zero readings for all instrumentation systems. Differences between the in-flight measurements and the reference zero readings were used to determine flight test conditions and aerodynamic coefficients. The effect of atmospheric turbulence on flight measurements was not considered.

The first of six flights was flown with the instrumented store on TER station one only, leaving TER stations two and three empty. The flight was made in order to familiarize the pilot with the handling qualities of the instrumented aircraft as well as to correlate cockpit instrumentation with flight test instrumentation for the required Mach number and aircraft angle-of-attack ranges. During the remaining flights, the pilot acquired data at Mach numbers from 0.6 to 0.9 at aircraft angles of attack from minus two to positive seven degrees. Since the aircraft angle of attack was primarily a function of weight, altitude, and velocity, the pilot maneuvered the aircraft into push-overs, dives, pull-outs, and climbs, as well as trim conditions to obtain data at the required conditions. The data recording process was initiated by the pilot depressing the bomb release button. Output from all instrumented systems were recorded at a rate

of ten samples per second until the bomb button was released. The data were digitized by the Technical Support Division of NATC. The digitized data were reduced to engineering units by ARO, Inc. An outline of the data reduction program is given in Appendix B. In general, output from the balance and accelerometers was used to calculate gross and inertial loads about the balance electrical centers. The gross and inertial loads were used to calculate aerodynamic forces and moments; moments being transferred to the moment reference point (the nominal full-scale center-of-gravity location). The flight dynamic pressure, calculated from aircraft boom probe measurements of static pressure and indicated airspeed, was used along with the store reference dimensions to reduce the aerodynamic forces and moments to coefficient form.

The final selection of flight test data was based primarily on Mach number. Wind tunnel data were obtained at Mach numbers of 0.6, 0.7, 0.8, and 0.9; hence only those flight data acquired at similar values were reduced to their final form. The flight Mach number was calculated as function of pressure by the following equation:

$$M_\infty = \left[\left(P/P_t \right)^{\frac{1-\gamma}{\gamma}} - 1\right) \frac{2}{\gamma-1}\right]^{1/2} \quad \text{(isentropic flow)} \qquad (1)$$

The static pressure (P) was obtained from direct boom measurements. The total pressure (P_t) was derived from the following boom airspeed calibration equation:

$$V_{CAL}^2 = 2Va_o^2/\gamma-1 \left[\left(P_t-P/P_o + 1 \right)^{\frac{\gamma-1}{\gamma}} - 1 \right] \quad (2)$$

Solving Equation (2) for P_t yields:

$$P_t = \left[\left(V_{CAL}^2 \ (\gamma-1)/2Va_o^2 + 1 \right)^{\frac{\gamma}{\gamma-1}} - 1 \right] P_o + P \quad (3)$$

The dynamic pressure, used to reduce aerodynamic load measurements to coefficient form, was calculated as a function of the measured static pressure and the calculated Mach number by the following equation:

$$q_\infty = \frac{1}{2} \gamma \ P \ M_\infty^2 \quad \text{(thermally perfect fluid)} \quad (4)$$

The Reynolds number per unit length is defined by the following equation:

$$Re/\ell = \rho \ V_\infty/\mu \quad (5)$$

The velocity (V_∞) may be expressed by the following equation derived from the definitions of Mach number and speed of sound:

$$V_\infty = M_\infty \sqrt{\gamma RT} \quad \text{(thermally perfect fluid)} \quad (6)$$

The density (ρ) may be expressed by the following equation:

$$\rho = P/RT \quad \text{(thermally perfect fluid)} \quad (7)$$

The viscosity of air (μ) is expressed by the following:

$$\mu = 2.27 \ \frac{T^{3/2}}{T + 198.6} \times 10^{-8} \quad (8)$$

Substituting Equations (6), (7), and (8) into Equation (5) yields the following equation used to calculate the unit

Reynolds number as a function of the calculated Mach number and the boom static temperature (T) measurement:

$$Re/\ell \times 10^{-6} = 1.798\, q_\infty\, (T + 198.8)/M_\infty T^2 \qquad (9)$$

The correlation of digitized flight test parameters was made on the basis of recorded NATC time signals. Data from all flights were analyzed using the IBM 370 computer and associated interactive graphics system. A graph of Mach number versus time was displayed to identify time intervals during which data were obtained at the required Mach numbers. The Mach number was allowed to deviate within ±0.005 of the quoted Mach number; a deviation corresponding to wind tunnel Mach number uncertainties. During each time interval, the aircraft angle of attack was reviewed. A time interval was divided into sub-intervals if more than one angle of attack was indicated. Presented in panel a of Figure 14 are digitized data showing two values of aircraft angle of attack. This time interval was divided into the two sub-intervals shown in panels b and c. Occasionally, errors in the recording and/or digitizing process were encountered. A spike in the digitized coefficient data curve indicating an error in the recording and/or digitizing process is shown in Figure 15. All such errors were eliminated.

The graphics system analysis indicated that the coefficient data in each time interval could be satisfactorily described by a least-squares first-order curve fit. The slopes of the curve fits indicated little, if any, time rate

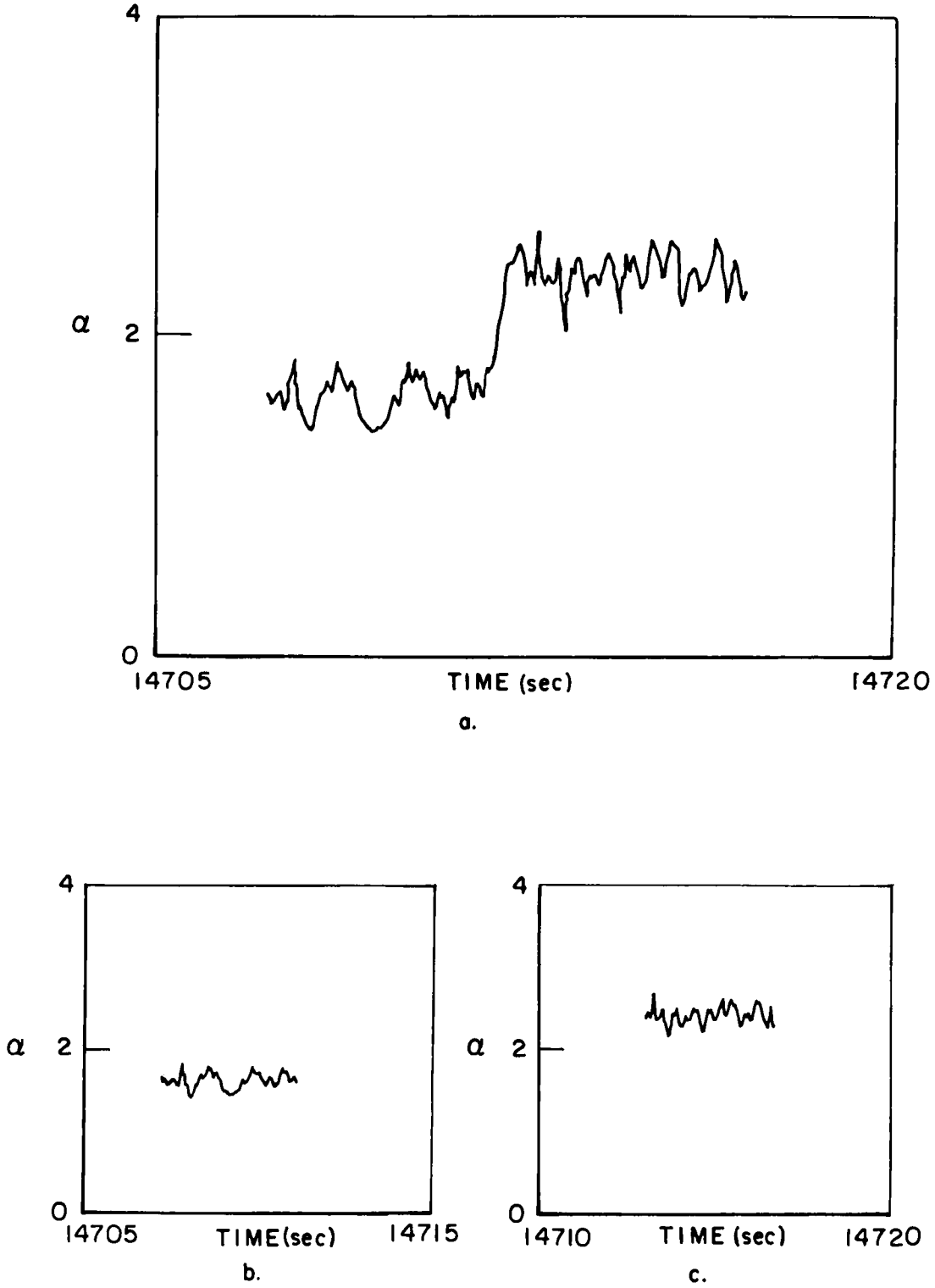

Figure 14. Digitized data showing two values of aircraft angle of attack.

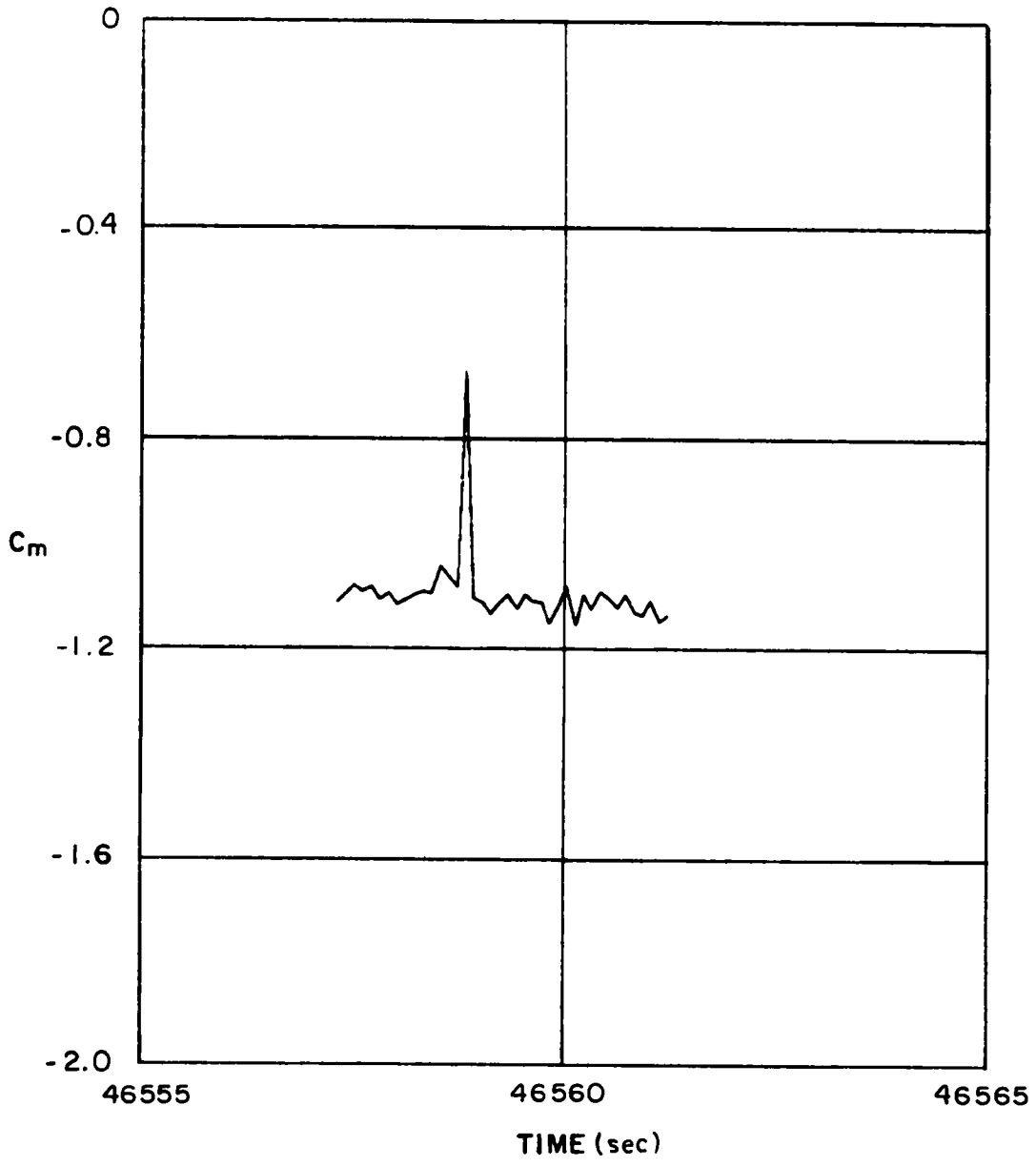

Figure 15. A spike in the digitized coefficient data curve indicating an error in the recording and/or digitizing process.

of change. Hence, a simple arithmetic average was used to evaluate each coefficient curve within a given time interval. Standard deviations for each curve fit were calculated: the results were on the order of one-tenth the uncertainty in measured coefficients.

The number of data samples within a given time interval was a direct result of the flight maneuver. During straight and level flight, Mach number remained within the ±0.005 tolerance for several seconds, generally five to ten seconds and as long as twenty-five seconds. During the more transient flight maneuvers, Mach number was held for as little as 0.4 seconds. Data average over time intervals of less than one second (less than ten data samples) were considered statistically small and were re-examined after the data from all flights were tabulated. Although increasing the Mach number deviation by a factor of ten would have increased the number of data samples within a time interval, the arithmetic average of the coefficient data was virtually unchanged. A comparison of data obtained at equivalent Mach numbers and aircraft angles of attack was made for steady and transient flight maneuvers. The comparisons showed that the magnitudes of the calculated coefficient data obtained at aircraft pitch rates equal to or less than 0.6 degrees per second were consistently the same. Therefore, on the basis of repeatability, data obtained at aircraft pitch rates greater than 0.6 degrees per second were omitted.

The basic aircraft instrumentation uncertainties

were determined by a root-mean-square analysis of the calibration data and are presented in Table 1. Since Mach number and dynamic pressure were derived as a function of basic aircraft measurements, uncertainties were calculated using the Taylor series method of error propagation. The derivation of the Mach number and dynamic pressure uncertainty equations is given in Appendix C. The estimated uncertainties in the flight test Mach number and dynamic pressure are presented in Figures 16 and 17 for various altitudes as a function of Mach number.

The aerodynamic coefficient data were also derived as a function of basic measurements and again uncertainties were calculated using the Taylor series method of error propagation. The derivation of the aerodynamic coefficient uncertainty equations is also given in Appendix C. The major contributing elements to the aerodynamic coefficient uncertainties were the weight of the instrumented test weapon and the uncertainty of the accelerometer measurements. Both elements combined to yield large inertial load uncertainties and therefore large aerodynamic coefficient uncertainties. The estimated uncertainties in the flight test aerodynamic coefficient data are shown in Figure 18.

II. WIND TUNNEL TEST

Aerodynamic carriage loads data for the MK-83 model were obtained at TER station one on the right inboard pylon of an F-4C aircraft model. Data were obtained using the

Table 1

Basic Aircraft Instrumentation Uncertainties

Parameter	Symbol	Uncertainty
Balance Strain Gages	$R_1 \rightarrow R_6$	±200 μV
Accelerometers	A_x, A_y, A_z	±3.2 ft/sec^2
Boom Static Pressure	P	±28.8 psfa
Boom Airspeed	V_{CAL}	±0.7 ft/sec
Boom Angle of Attack	α	±0.3 deg
Boom Sideslip Angle	β	±0.3 deg
Boom Total Temperature	T_T	±2.2°R
Altitude	H	±200 ft

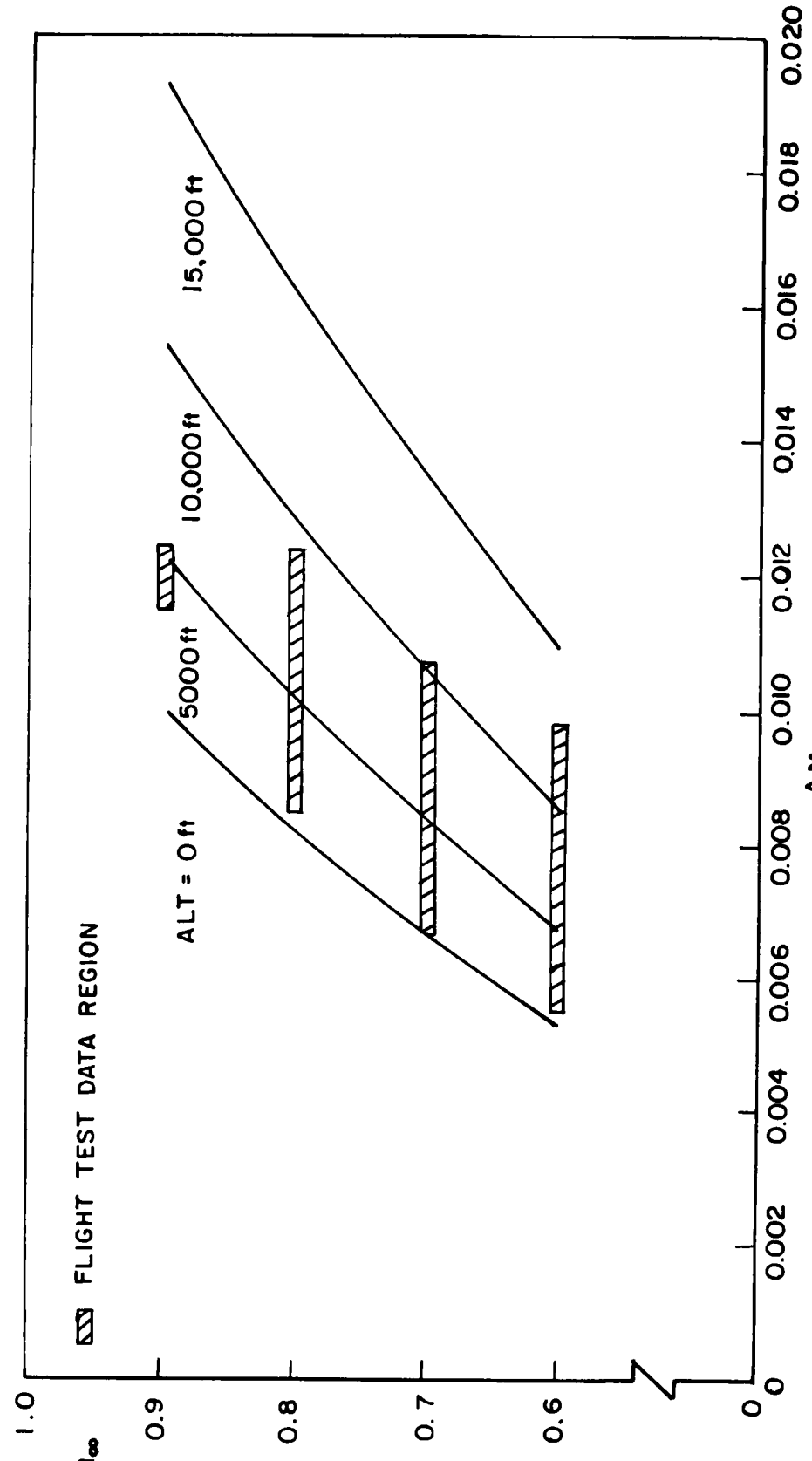

Figure 16. Estimated uncertainties for the flight test Mach number.

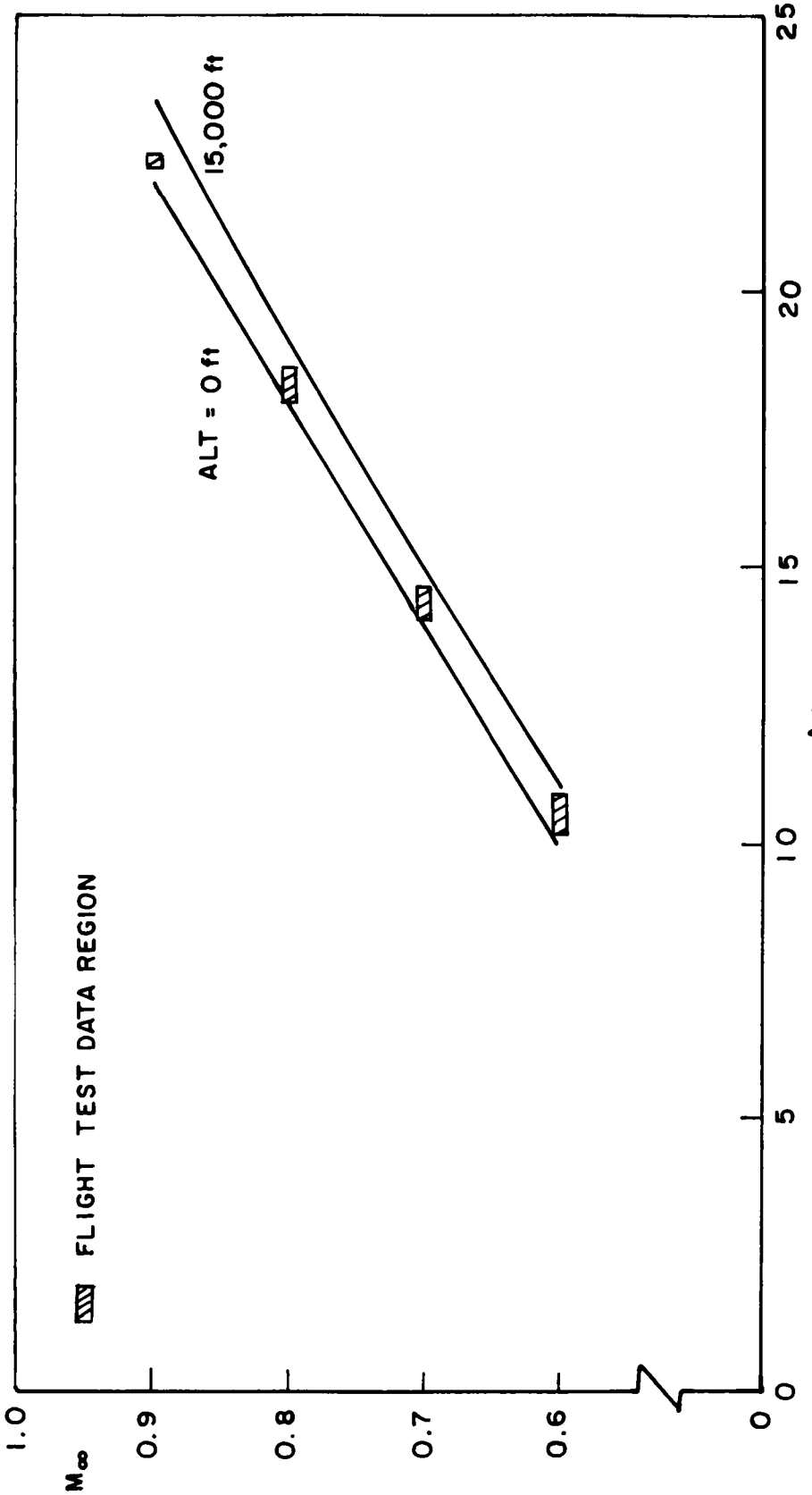

Figure 17. Estimated uncertainties for the flight test dynamic pressure.

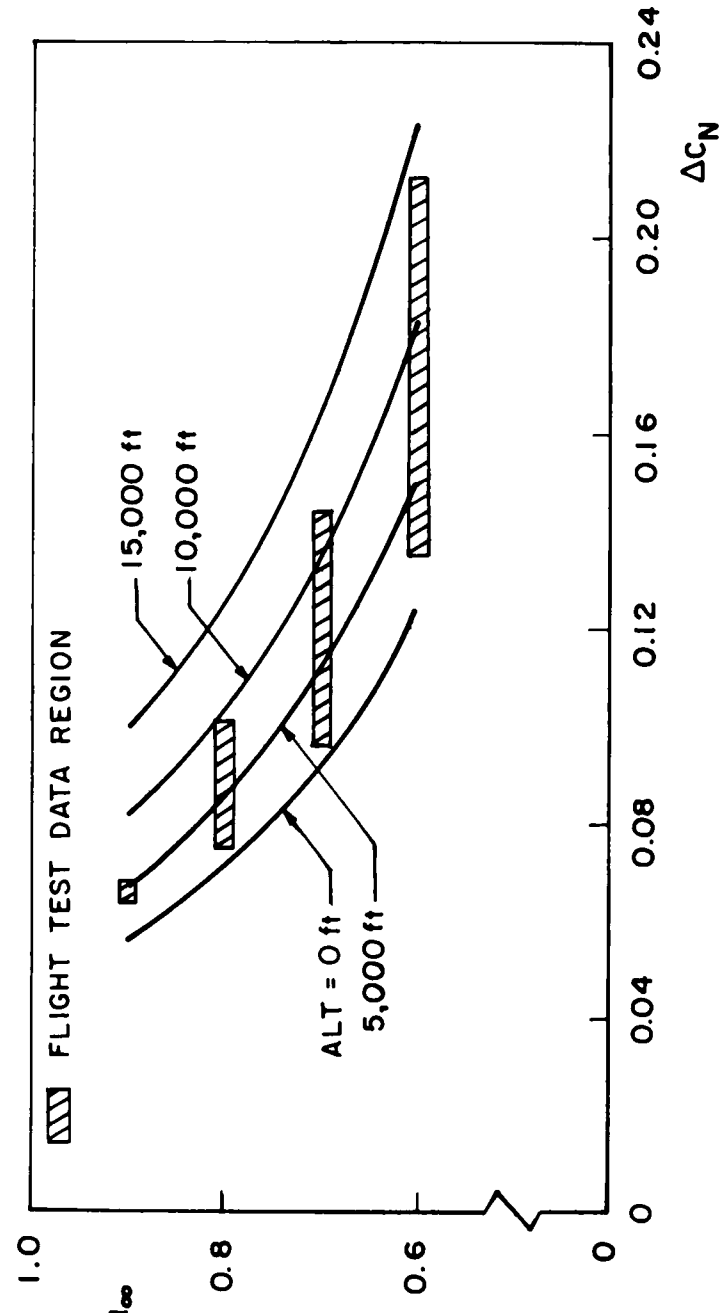

a. Normal-force coefficient

Figure 18. Estimated uncertainties in the flight test aerodynamic coefficient data.

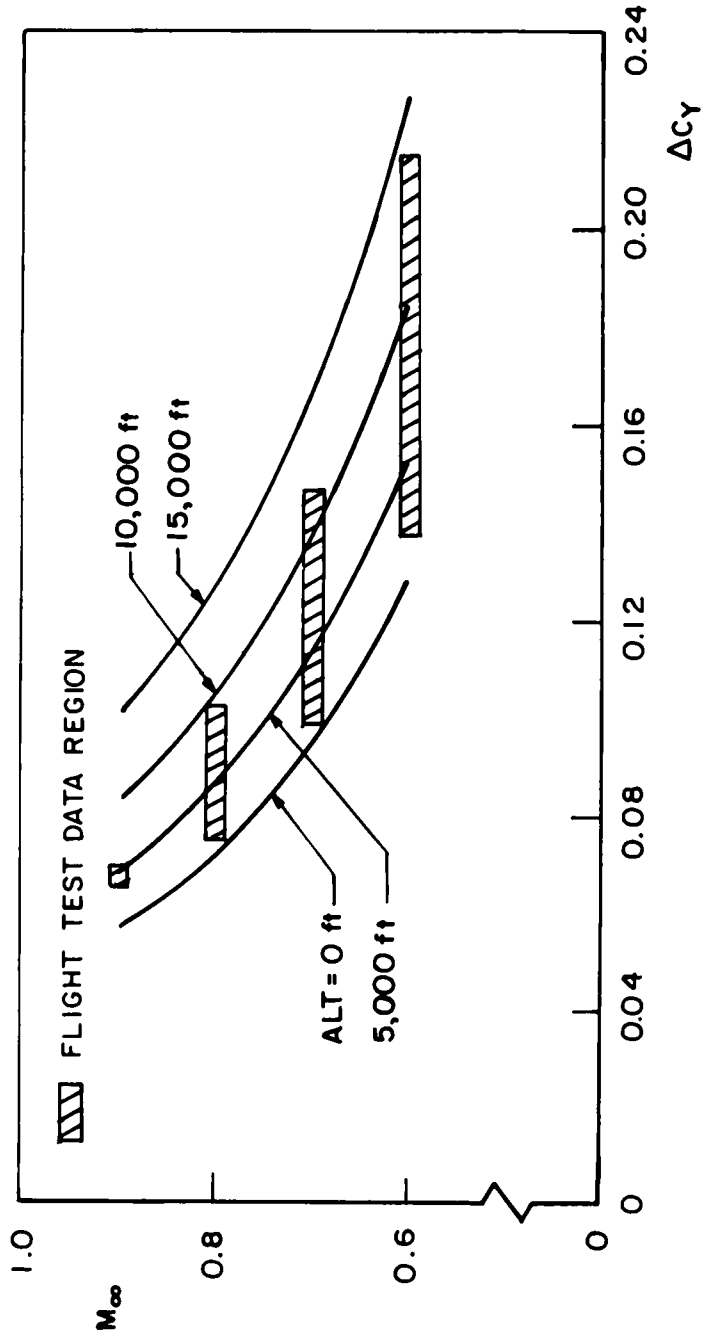

b. Side-force coefficient

Figure 18. (Continued)

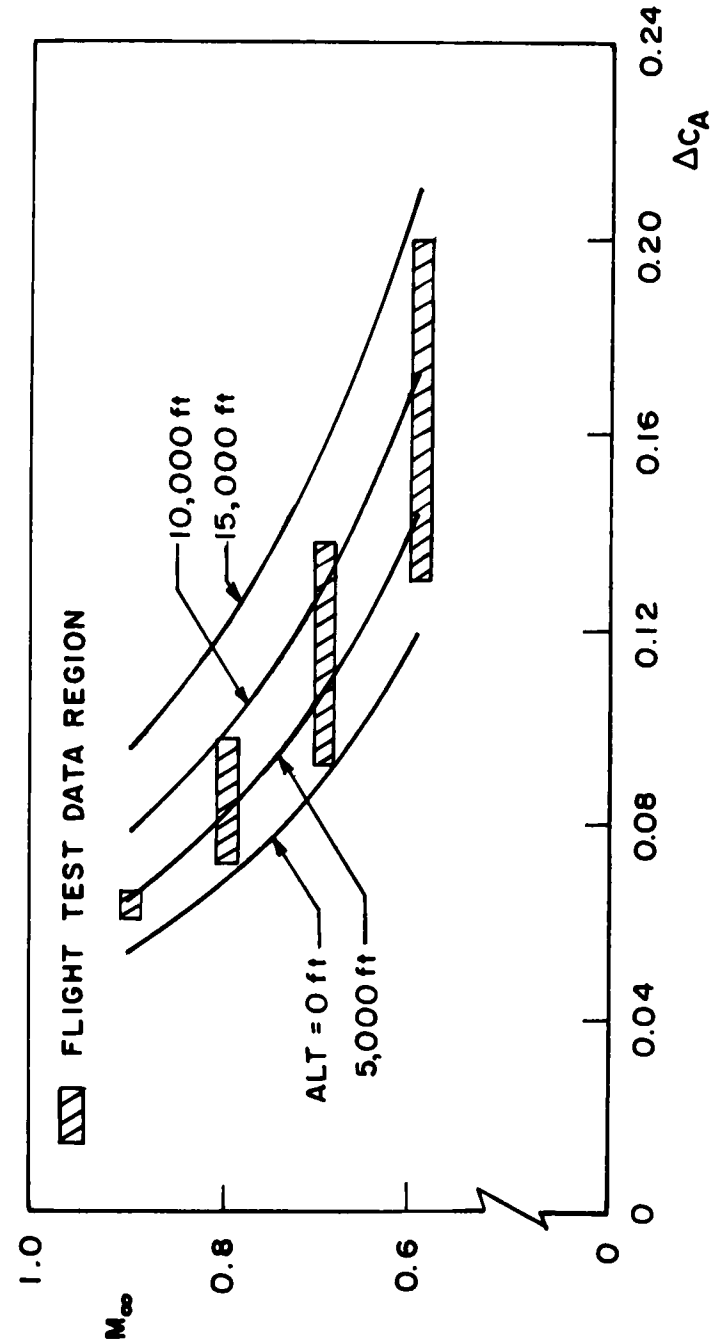

c. Axial-force coefficient

Figure 18. (Continued)

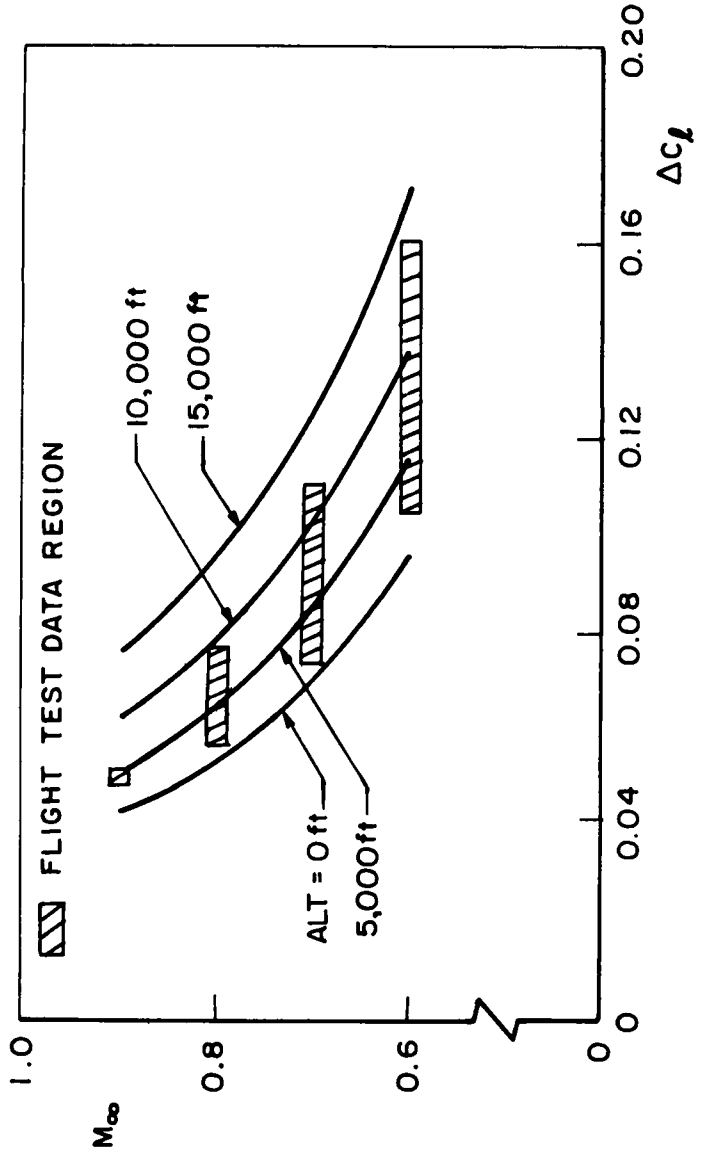

d. Rolling-moment coefficient

Figure 18. (Continued)

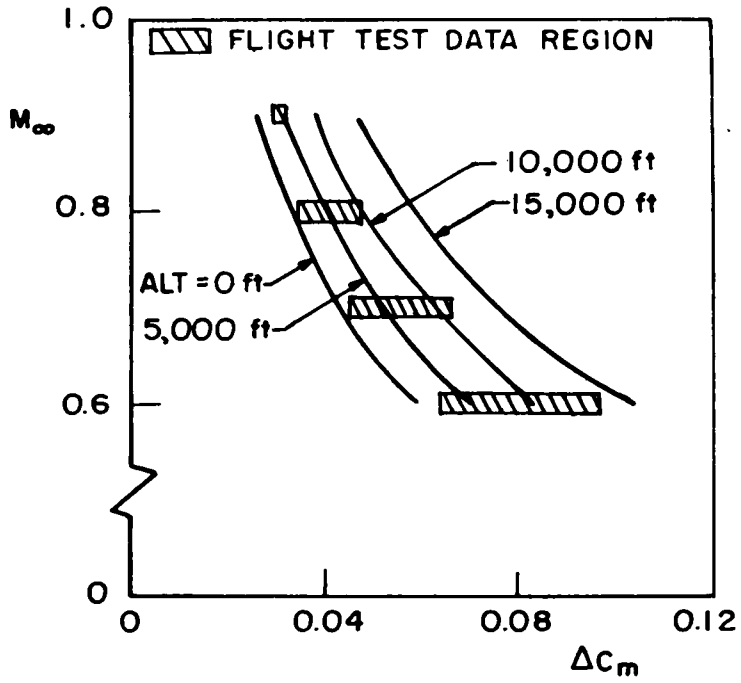

e. Pitching-moment coefficient

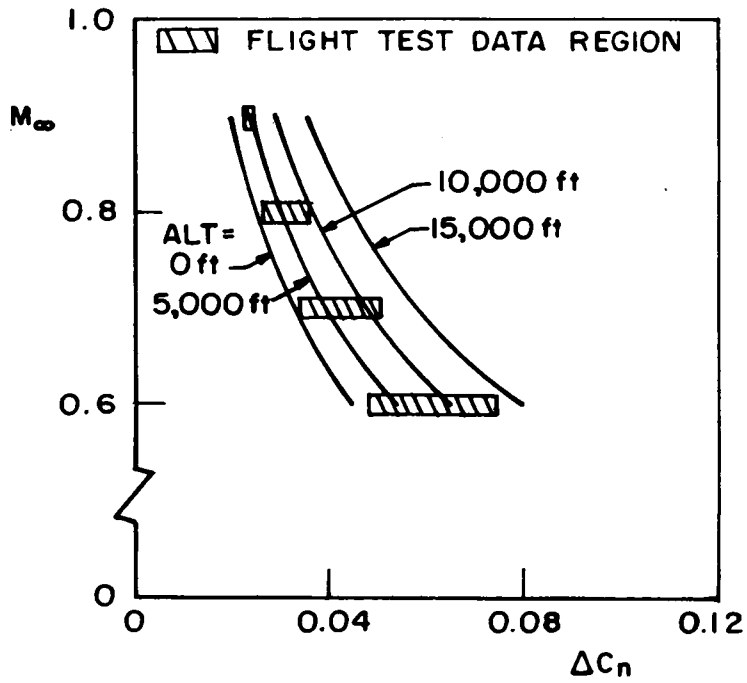

f. Yawing-moment coefficient

Figure 18. (Continued)

internal bracket support (IBS) and the captive trajectory support (CTS) techniques.

During IBS testing, the MK-83 model was attached directly to the TER model at station one. To obtain data, test conditions were established in the wind tunnel before the operational control of the AMAPS was switched to the digital computer. The digital computer controlled the angular positions of the aircraft at which data were obtained (see Figure 8, page 23, block diagram).

During CTS testing, both the aircraft model and the MK-83 model were independently supported in the wind tunnel. To obtain data, test conditions were established in the wind tunnel and the aircraft model angle of attack was set before the operational control of the CTS was switched to the digital computer. The computer was used to set the MK-83 model to the carriage position at TER station one through commands to the CTS (see Figure 7, page 20, block diagram). TER station one was equipped with the spring-loaded plunger (touch wire), extending approximately 0.05 inches below the rack surface, which provided an indication of when the MK-83 model was at the carriage position. The touch wire system was electrically wired to give a visual indication on the control console when contact was made between the model and touch wire. The system was also electrically connected to automatically stop the CTS movement should the MK-83 model or its sting support contact the aircraft model or its sting support.

During both IBS and CTS testing, data obtained at the carriage position, consisting of measured forces and moments and wind tunnel operating conditions, were input into the digital computer which was programmed to calculate aerodynamic loads and reduce them to coefficient form.

In addition to carriage position airloads, trajectory data were obtained for the MK-83 bomb during CTS testing. To obtain a trajectory, test conditions were established in the tunnel and the aircraft model was set at the desired angle of attack. Operational control of the CTS was then switched to the digital computer which automatically sets the MK-83 model at the carriage position. Store movement during a trajectory was controlled by the computer through commands to the CTS analog system. The computer was programmed to solve a set of six-degree-of-freedom equations which predicted store angular and linear displacements relative to the aircraft model. In general, the trajectory program utilizes the last two successive calculated values of each aerodynamic coefficient to predict new coefficients over the next time interval. The predicted coefficients are used to calculate a new position for the store model at the end of that time interval. The CTS is then commanded to move the store model to the new position where aerodynamic coefficients are calculated. If these coefficients agree with predicted values, the process is continued over another time interval. If all the aerodynamic coefficients do not agree to within ±0.1, the prediction calculation is repeated over a time interval

of one-half the previous value. The entire process is repeated until a complete trajectory has been obtained.

To use wind tunnel data to predict full-scale weapon trajectories, measured forces and moments are reduced to aerodynamic coefficients. The wind tunnel coefficients, along with the full-scale store properties and the flight dynamic pressure, are used to determine full-scale forces and moments. No attempt is made to correct coefficient data for the characteristic mismatch between wind tunnel and full-scale Reynolds number. The dynamic pressure is calculated using a flight velocity equal to the wind tunnel free-stream velocity component plus the components of store velocity relative to the aircraft, and a density corresponding to a simulated altitude.

The initial portion of each simulated trajectory incorporated a simulated ejector force in addition to simulated inertial and calculated aerodynamic loads. The ejector force as a function of time is presented in Figure 19. Two fifth-order polynomials were used to analytically model the ejection force as a function of time. The polynomial coefficients are given in Figure 19. Other full-scale MK-83 parameters used during wind tunnel testing are listed in Table 2.

Wind tunnel data were obtained at Mach numbers from 0.6 to 0.9 at aircraft angles of attack from minus three to positive thirteen degrees. The aircraft angle of attack was set with an absolute angle-of-attack indicator which accounted for aircraft model support deflections caused by

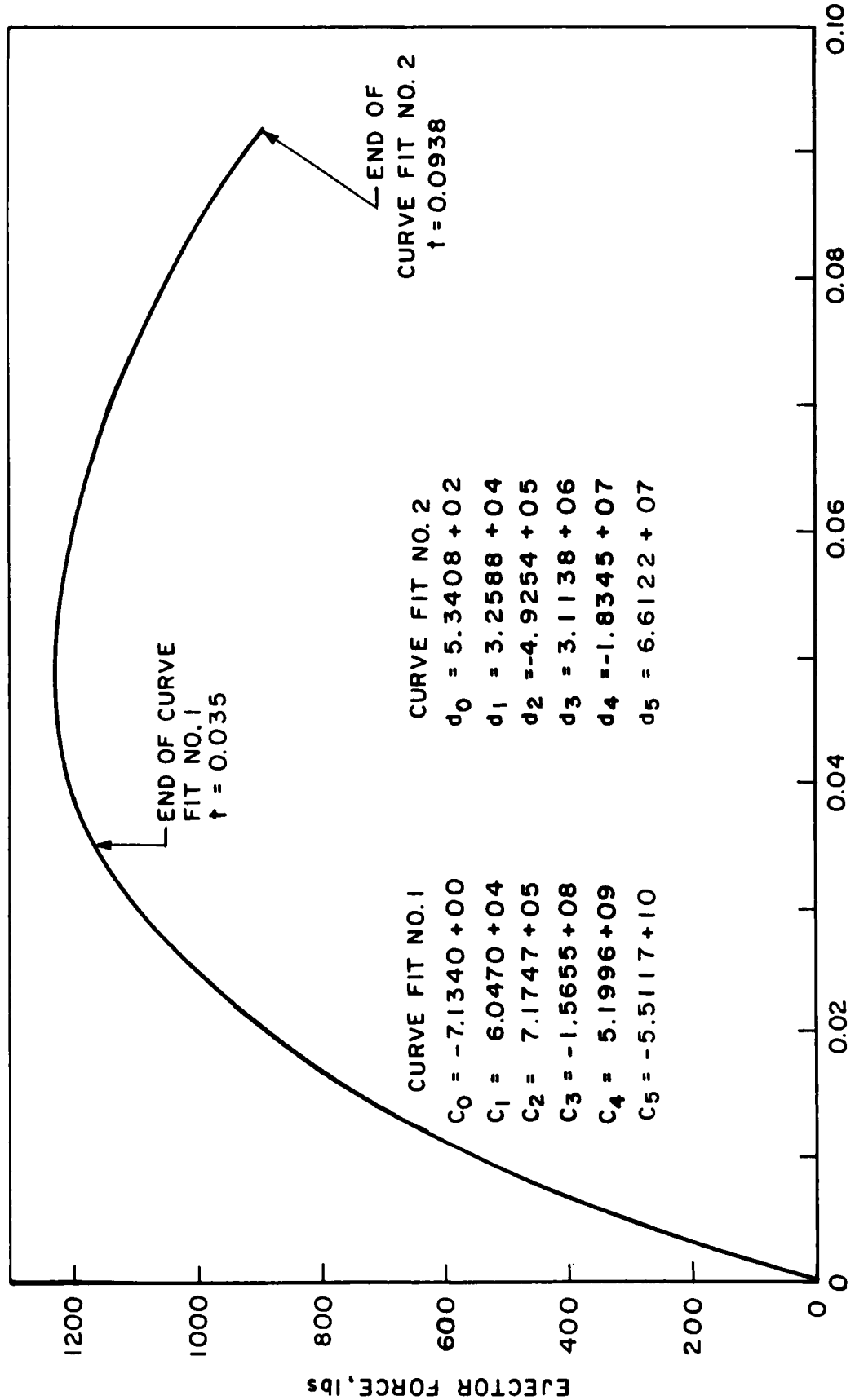

Figure 19. Ejector force as a function of time.

Table 2

Full-Scale MK-83 Parameters

Parameter	Value
S	1.069 ft
b, $\bar{c}$	1.167 ft
$\bar{m}$	30.615 slug
I_{xx}	5.4 slug-ft^2
I_{yy}, I_{zz}	114.0 slug-ft^2
I_{xz}	3.73 slug-ft^2
X_{cg}	4.208 ft
C_{ℓ_p}	-0.75 per radian
C_{m_q}, C_{m_r}	-75.0 per radian
X_L	- 0.172 ft

aerodynamic loads acting on the aircraft model. Trajectory data were obtained at a simulated pressure altitude of five thousand feet and a simulated aircraft load factor equal to the acceleration of gravity.

Corrections were made for store model weight tare components in order to calculate aerodynamic forces and moments on the MK-83 model. During CTS testing, balance sting and support deflections caused by aerodynamic loads on the model were accounted for in the data reduction program.

The uncertainty in determining the aircraft model angle of attack was estimated to be ±0.10 degrees. The Mach number was held within ±0.005 of the desired Mach number with an estimated uncertainty of ±0.003. Data obtained using the CTS are subject to positioning errors resulting from the ability of the CTS to set to a specified position. The maximum error in CTS positioning was estimated to be ±0.05 inches (0.083 feet full scale) for translational settings, ±0.15 degrees for pitch and yaw settings, and ±1.0 degree for roll settings. Uncertainties in the coefficient data were calculated taking into consideration the probable inaccuracies in balance measurements and tunnel conditions. The wind tunnel coefficient uncertainties are based on a ninety-five-percent confidence level, ignoring bias errors, and are given in Table 3. Estimates of the uncertainties in the trajectory data attributable to balance precision limitations were made for the store model at given times in a trajectory and are presented in Table 4.

Table 3

Wind Tunnel Coefficient Uncertainties

M_∞	C_N	C_y	C_A	C_ℓ	C_m	C_n
0.6	±0.04	±0.05	±0.04	±0.05	±0.08	±0.08
0.7	±0.04	±0.04	±0.03	±0.05	±0.07	±0.08
0.8	±0.03	±0.04	±0.03	±0.04	±0.07	±0.07
0.9	±0.03	±0.04	±0.03	±0.04	±0.06	±0.06

Table 4

Uncertainties in the Trajectory Data

M_∞	t	XP	YP	ZP	DTHA	DPSI	DPHI
0.6	0.2	±0.005	±0.008	±0.008	±0.2	±0.2	±1.4
	0.4	±0.02	±0.03	±0.03	±0.8	±0.9	±5.6
	0.6	±0.04	±0.07	±0.07	±1.9	±2.7	±12.6
0.8	0.2	±0.006	±0.008	±0.008	±0.3	±0.3	±2.0
	0.4	±0.02	±0.04	±0.05	±1.2	±1.2	±8.1
	0.6	±0.06	±0.08	±0.08	±2.7	±2.5	±18.6

CHAPTER IV

RESULTS AND DISCUSSION

The primary emphasis of this investigation was to identify a means of obtaining accurate carriage position airloads data in the four-foot transonic (4T) Aerodynamic Wind Tunnel at the Arnold Engineering Development Center (AEDC) and to evaluate the effects of carriage position airloads on the separation characteristics of the stable MK-83 bomb. Trajectories were evaluated experimentally in the wind tunnel and analytically with a six-degree-of-freedom trajectory-prediction program. The analytical program used interference flow field and free-stream coefficient data obtained in the wind tunnel. Full-scale flight test data were used to evaluate wind tunnel test results. The full-scale data were obtained during a flight test conducted at the Naval Air Test Center (NATC) during which carriage position airloads data were obtained for an MK-83 bomb at the number one TER station on the left wing inboard pylon of an F-4J aircraft. Data were obtained at Mach numbers from 0.6 to 0.9 at aircraft angles of attack from minus two to plus seven degrees. Two bomb afterbody configurations were tested. Inert MK-83 bombs occupied TER stations two and three.

A preliminary comparison of the aerodynamic coefficients obtained during the flight test and an early wind tunnel test (Reference 7) is presented in Figures 20 and 21

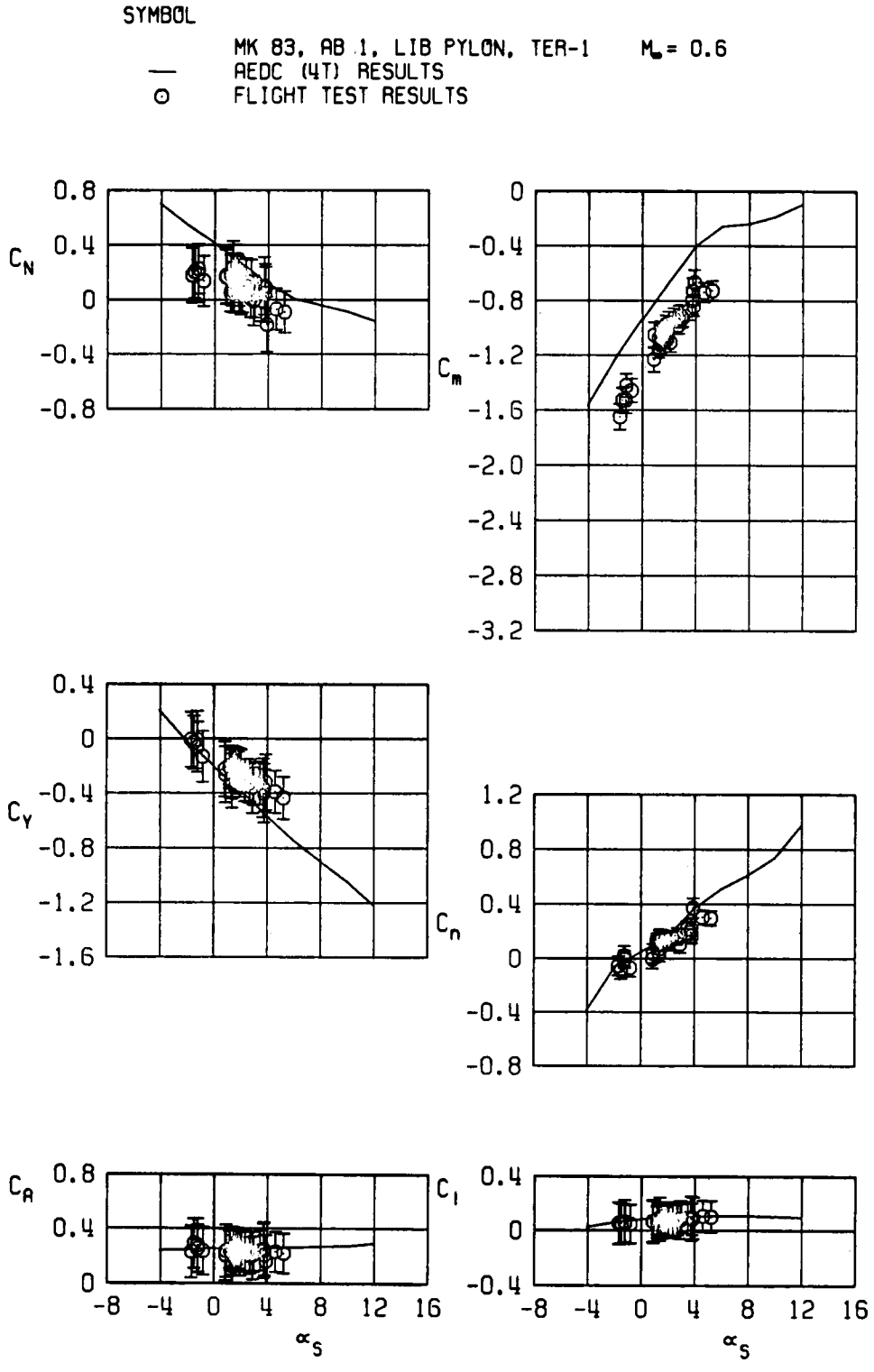

a. $M_\infty = 0.6$

Figure 20. A preliminary comparison of the aerodynamic coefficients obtained during the flight test and an early wind tunnel test, IBS data.

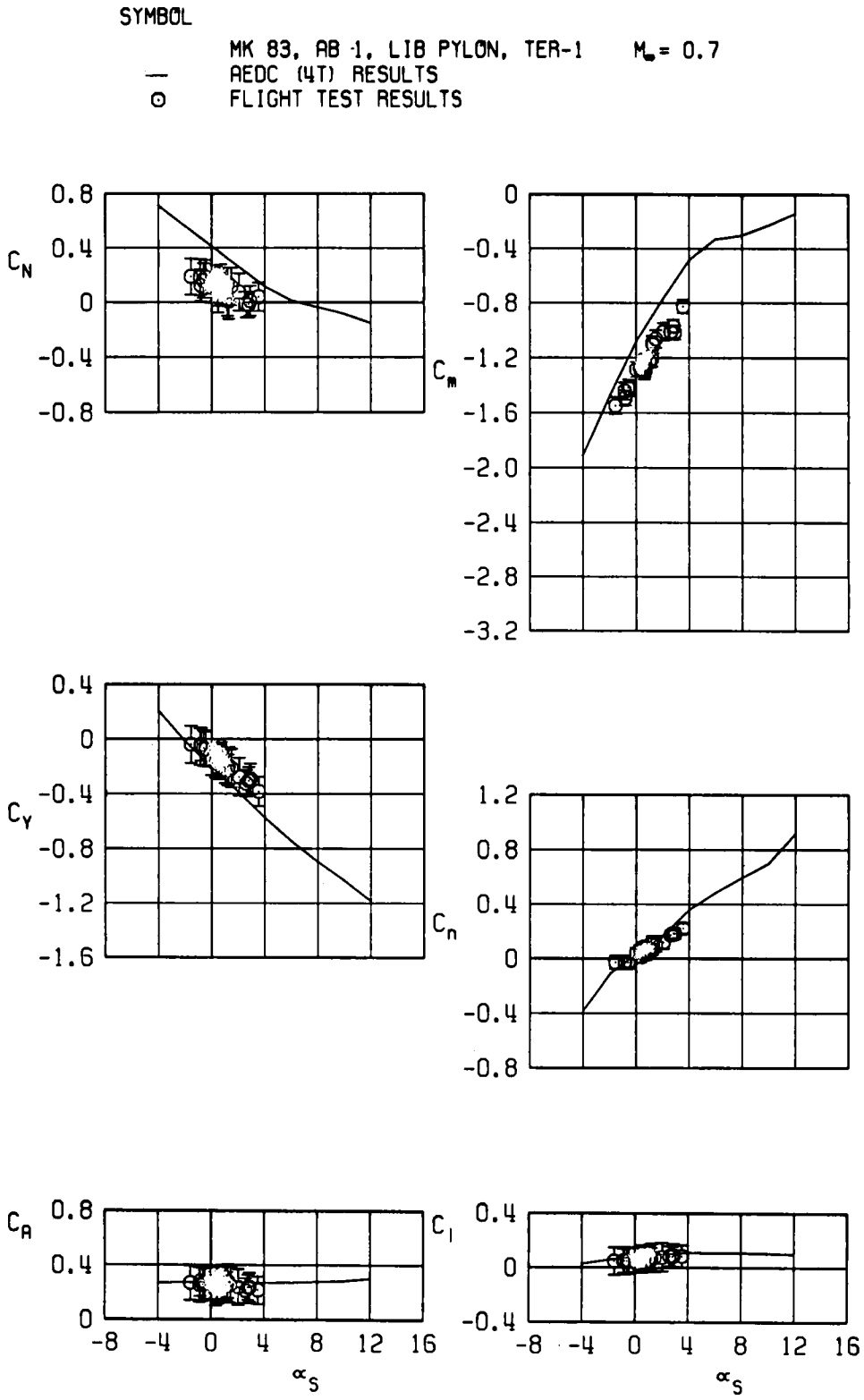

b. $M_\infty = 0.7$

Figure 20. (Continued)

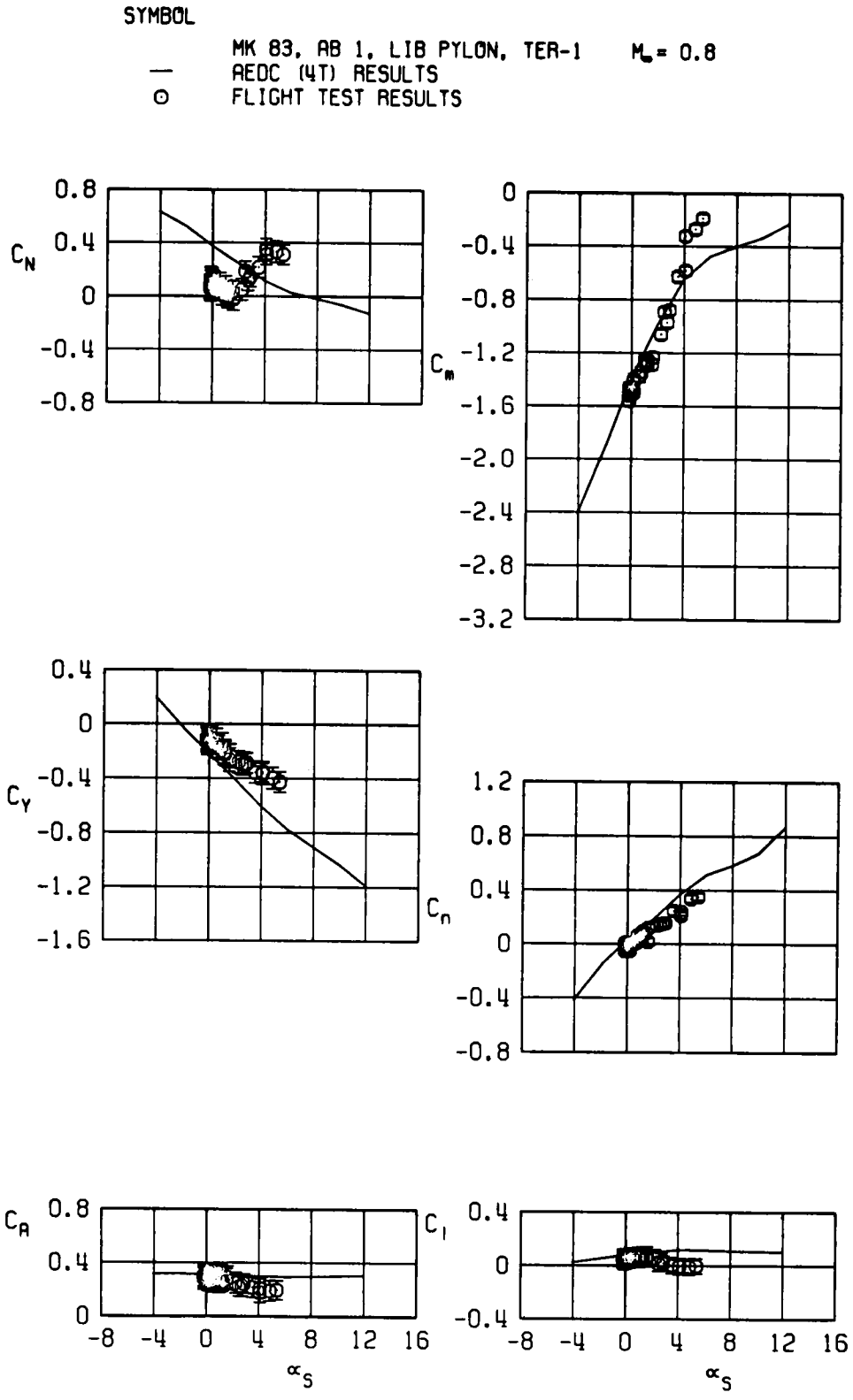

c. $M_\infty = 0.8$

Figure 20. (Continued)

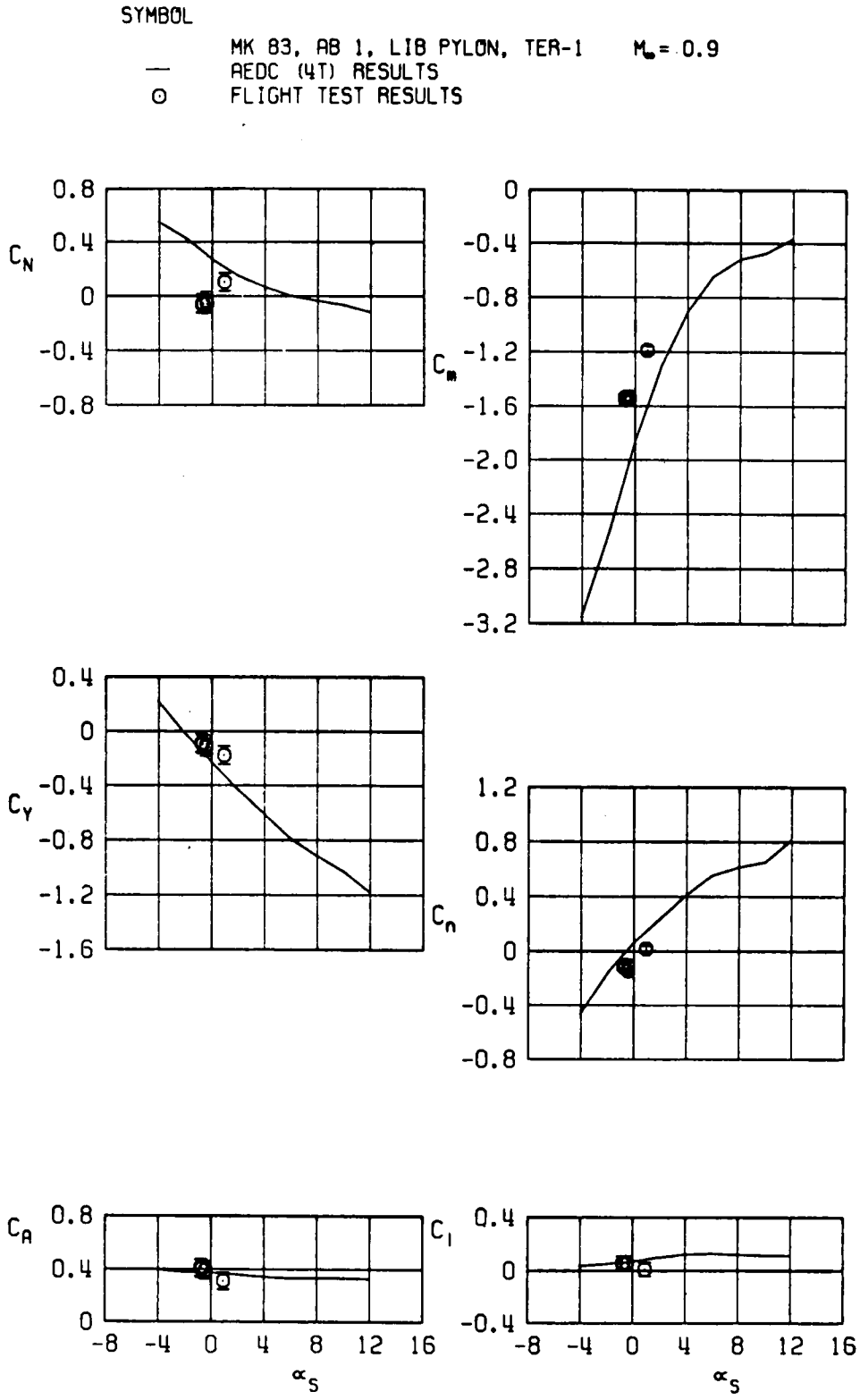

d. $M_\infty = 0.9$

Figure 20. (Continued)

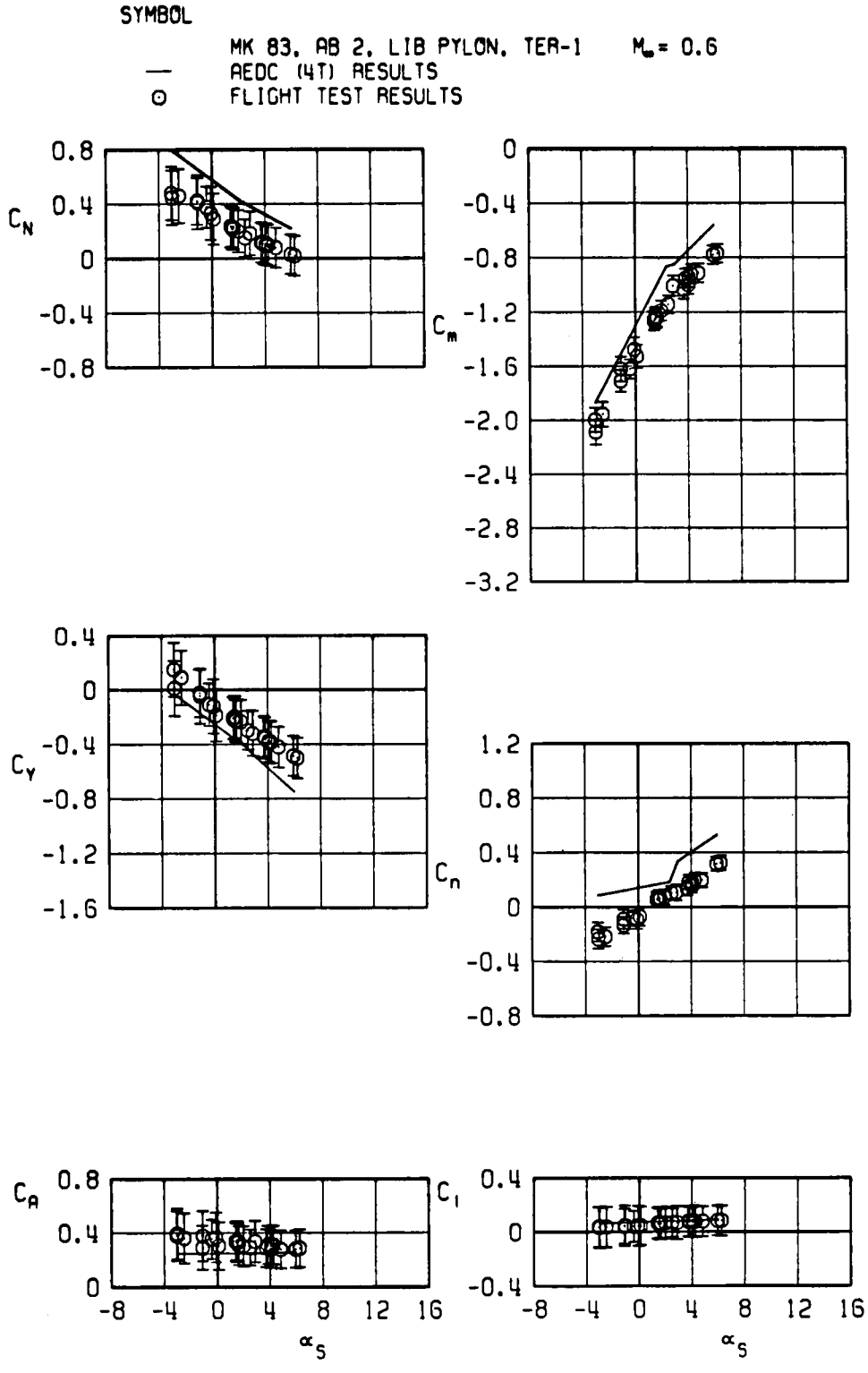

a. $M_\infty = 0.6$

Figure 21. A preliminary comparison of the aerodynamic coefficients obtained during the flight test and an early wind tunnel test, CTS data.

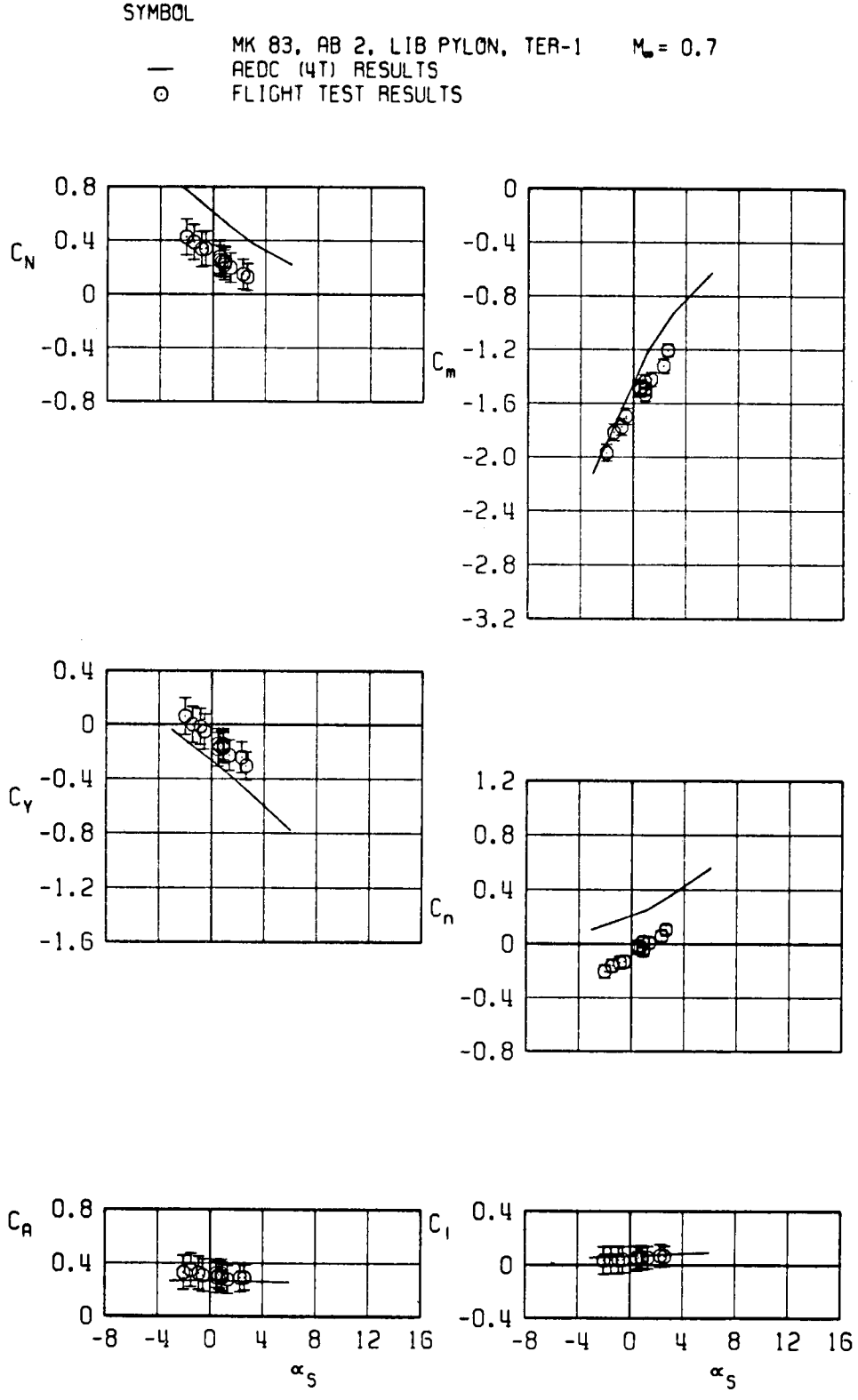

b. $M_\infty = 0.7$

Figure 21. (Continued)

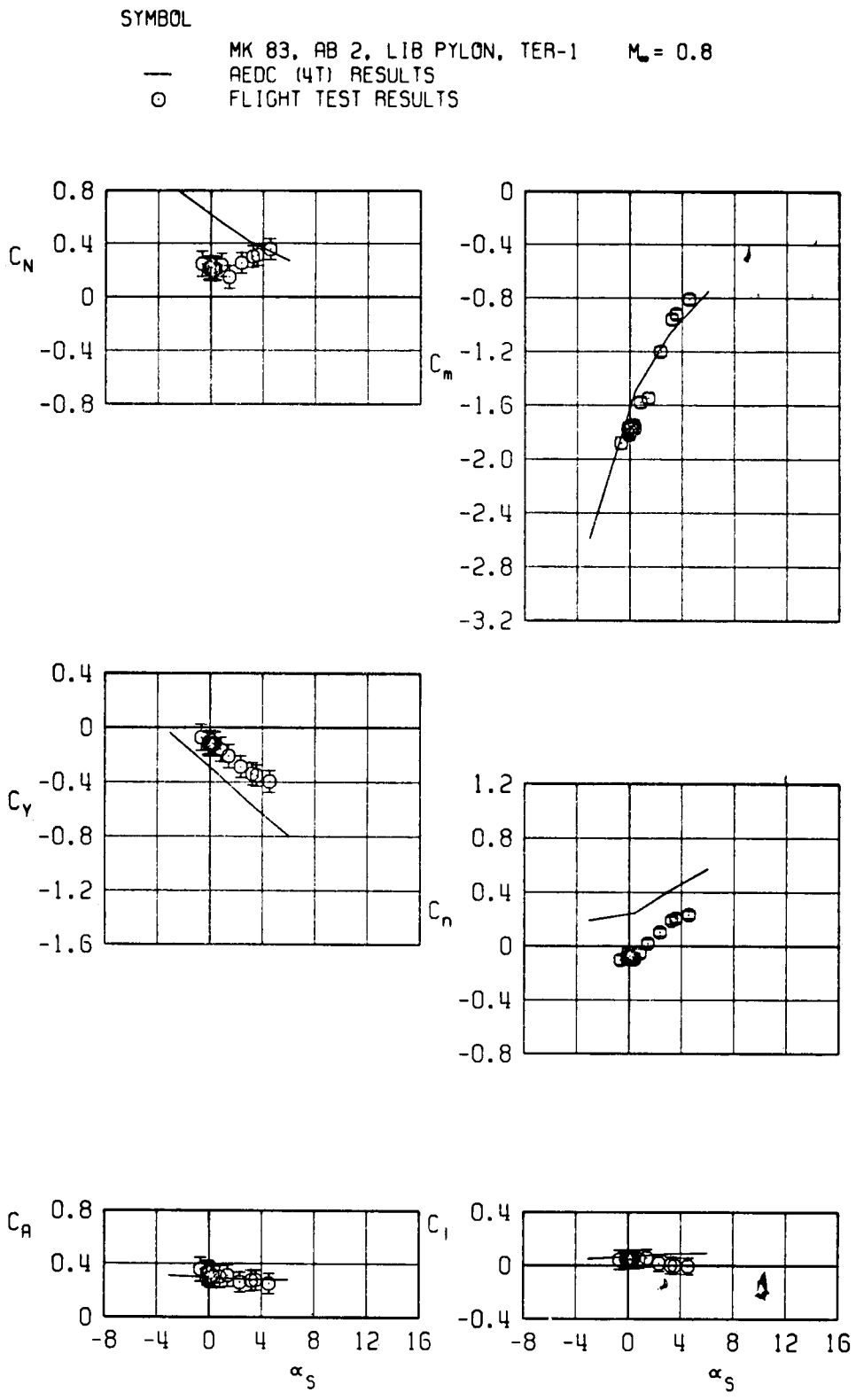

c. $M_\infty = 0.8$

Figure 21. (Continued)

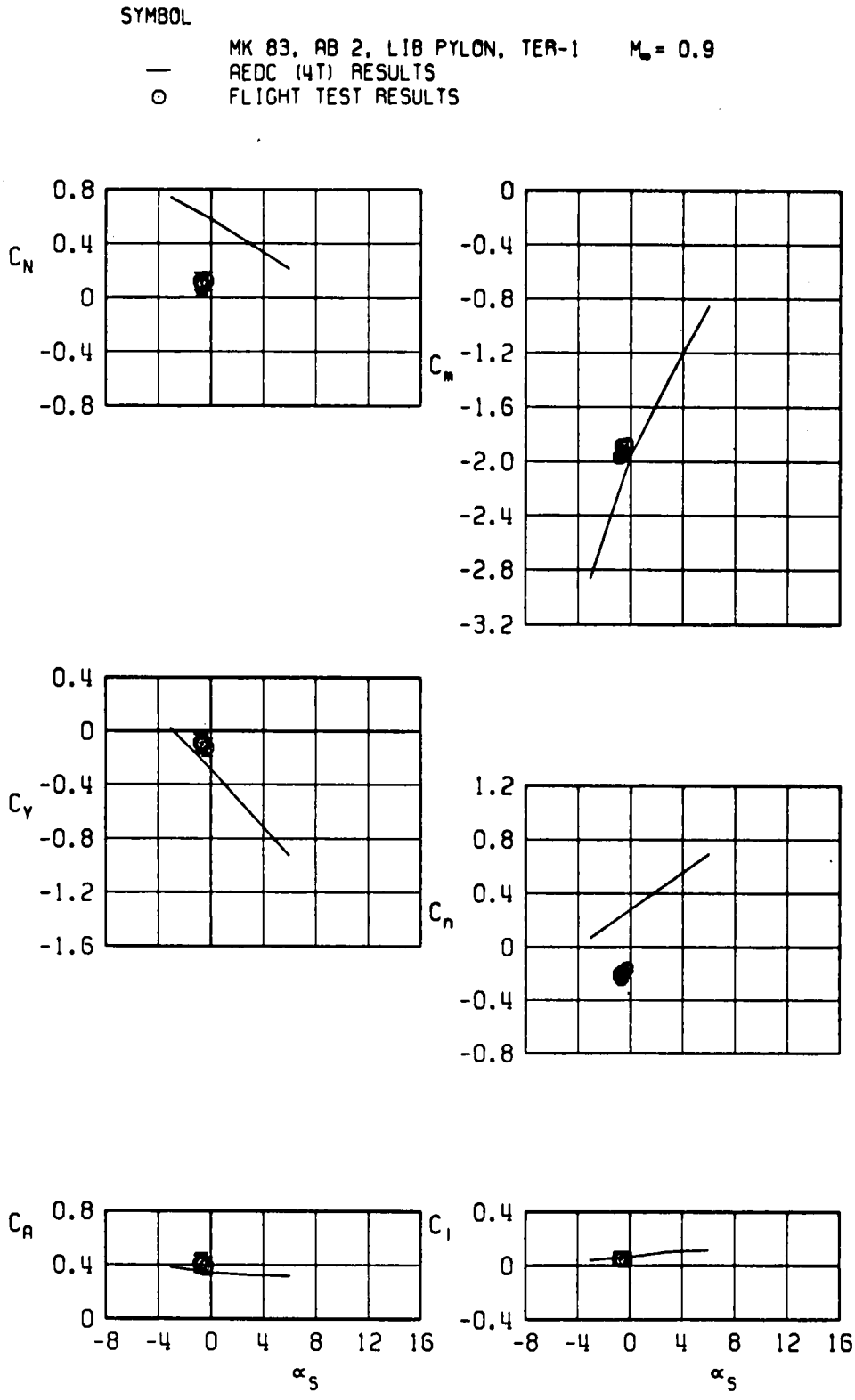

d. $M_\infty = 0.9$

Figure 21. (Continued)

as a function of store angle of attack. The wind tunnel coefficient curves shown in Figure 20 were obtained using the internal bracket support (IBS) data acquisition technique. The wind tunnel coefficient curves shown in Figure 21 were obtained using the captive trajectory support (CTS) data acquisition technique. The flight test coefficient uncertainties are represented by the uncertainty bars. At Mach numbers of 0.6 and 0.7, data obtained using both acquisition techniques show positive normal-force and pitching-moment coefficient increments when compared to the flight test data and indicate that the center of pressure shifts aft. A positive increment indicates that the wind tunnel results are more positive or less negative than the flight test results. A positive yawing-moment coefficient increment is shown at all Mach numbers for data obtained using the CTS technique. The large discontinuity in the wind tunnel yawing-moment coefficient curve, Figure 21a, is believed to be largely a result of CTS positioning errors.[1] However, the discontinuity does not effect the comparison. At a Mach number of 0.8, the slope of the flight test normal-force coefficient curve changes sign at a store angle of attack of two degrees; wind tunnel data do not follow this trend. It is not known whether the slope change occurs at a Mach number of 0.9 because of the limited amount of flight test data that were

---

[1] CTS positioning errors are discussed on page 83.

obtained. Agreement between wind tunnel and flight test side-force coefficients generally deteriorates with increasing Mach number and angle of attack. Axial-force and rolling-moment coefficients are in good agreement. There are then four major areas of concern: disagreement between normal-force coefficients coupled with a center of pressure shift; yawing-moment coefficient disagreement between the CTS technique and the flight test data; failure to simulate the aerodynamic phenomenon responsible for the reversal of the normal-force coefficient slope at a Mach number of 0.8; and the deterioration of agreement between side-force coefficients. A more detailed set of wind tunnel data was clearly needed if the differences were to be resolved.

Following the preliminary comparison of flight and wind tunnel data, a detailed investigation of carriage position airloads was conducted in 4T. Data were obtained in order to assess the effects of the TER geometric details, data acquisition techniques, bomb afterbody configuration, Reynolds number, wind tunnel wall porosity, and CTS sting interference. Trajectory data were also obtained in order to assess the effects of TER geometry. Wind tunnel data were obtained using one-twentieth-scale models of the F-4C aircraft, MK-83 bomb, and associated aircraft hardware.

Perhaps one of the more overlooked aspects of wind tunnel model design has been the geometric details of the TER. The details are very expensive if not physically impossible to fabricate at the 5-percent scale. However, for this

investigation a detailed TER was built. Venting slots and sway brace arms were simulated. The venting slots simulated spacings between the ejector units and the main body of the TER.

Data obtained in order to assess the effects of TER geometric details on the aerodynamic coefficients of the MK-83 model are presented in Figures 22 and 23. Data were obtained for both bomb afterbody configurations using the IBS data acquisition technique. An approximation of the coefficient uncertainties is indicated by the symbol size. The effect of venting slots and sway brace arms on the aerodynamic coefficient of the MK-83 model is typified by reduced normal-force and pitching-moment coefficients as well as increased yawing-moment coefficients. Data were obtained in order to separate the effect of venting slots and sway brace arms on the aerodynamic coefficients of the MK-83 model; the results are shown in Figure 24. The results are typical of the effects observed at all Mach numbers and for both bomb afterbody configurations. For this carriage configuration, the data clearly show that the sway braces are primarily responsible for inducing the change in coefficient data. Although no pressure data were obtained, the reduction in normal-force coefficients is most likely due to an increase in the pressure over the upper surface of the bomb. The pressure increase would be a direct result of flow deceleration at and near the sway braces. Since the forward sway brace arm is ahead of the moment reference point (the bomb center of gravity) and

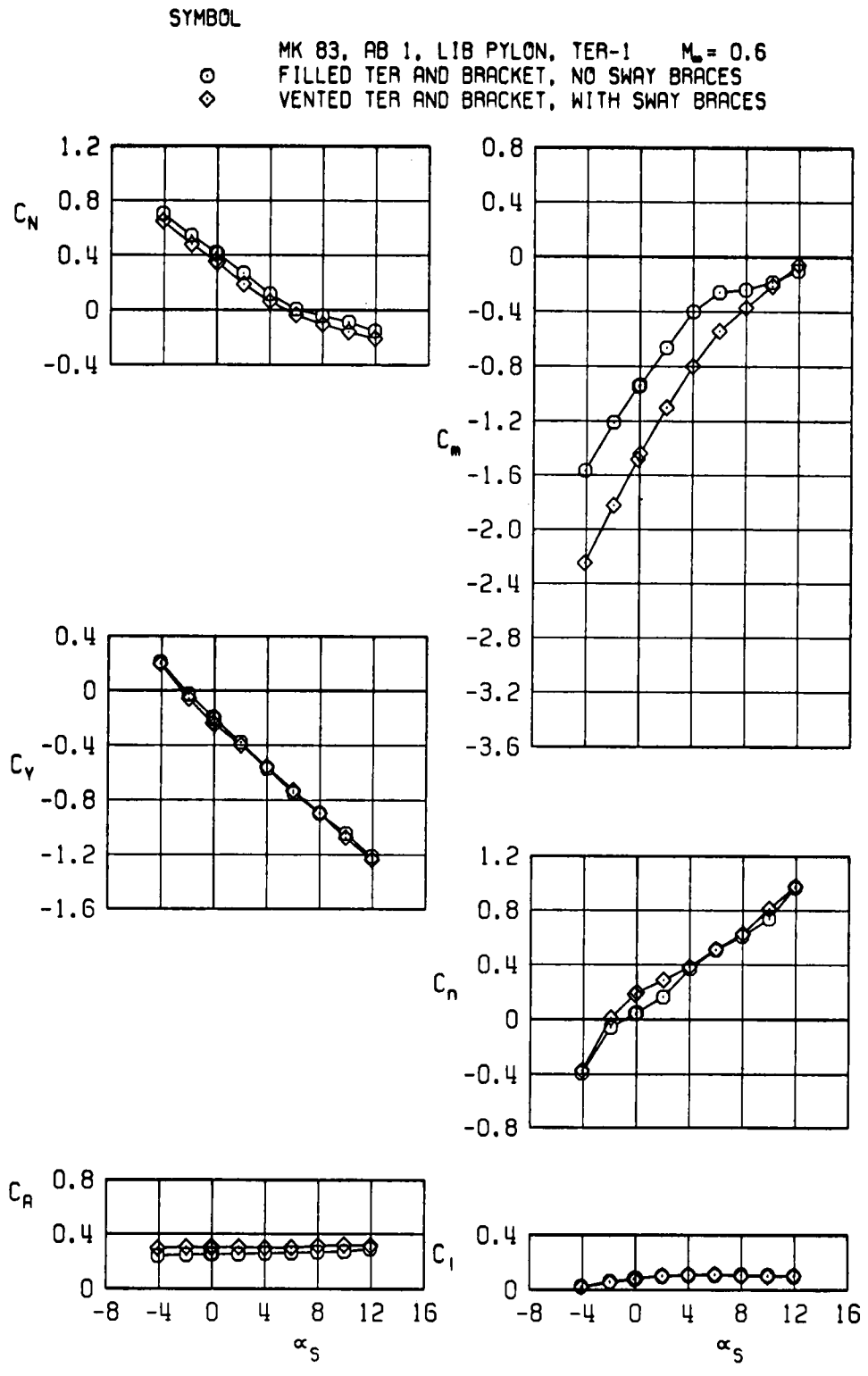

a. $M_\infty = 0.6$

Figure 22. The effect of TER geometric details on the aerodynamic coefficients of the MK-83 model, standard afterbody.

SYMBOL

MK 83, AB 1, LIB PYLON, TER-1 M_∞ = 0.8
⊙ FILLED TER AND BRACKET, NO SWAY BRACES
◇ VENTED TER AND BRACKET, WITH SWAY BRACES

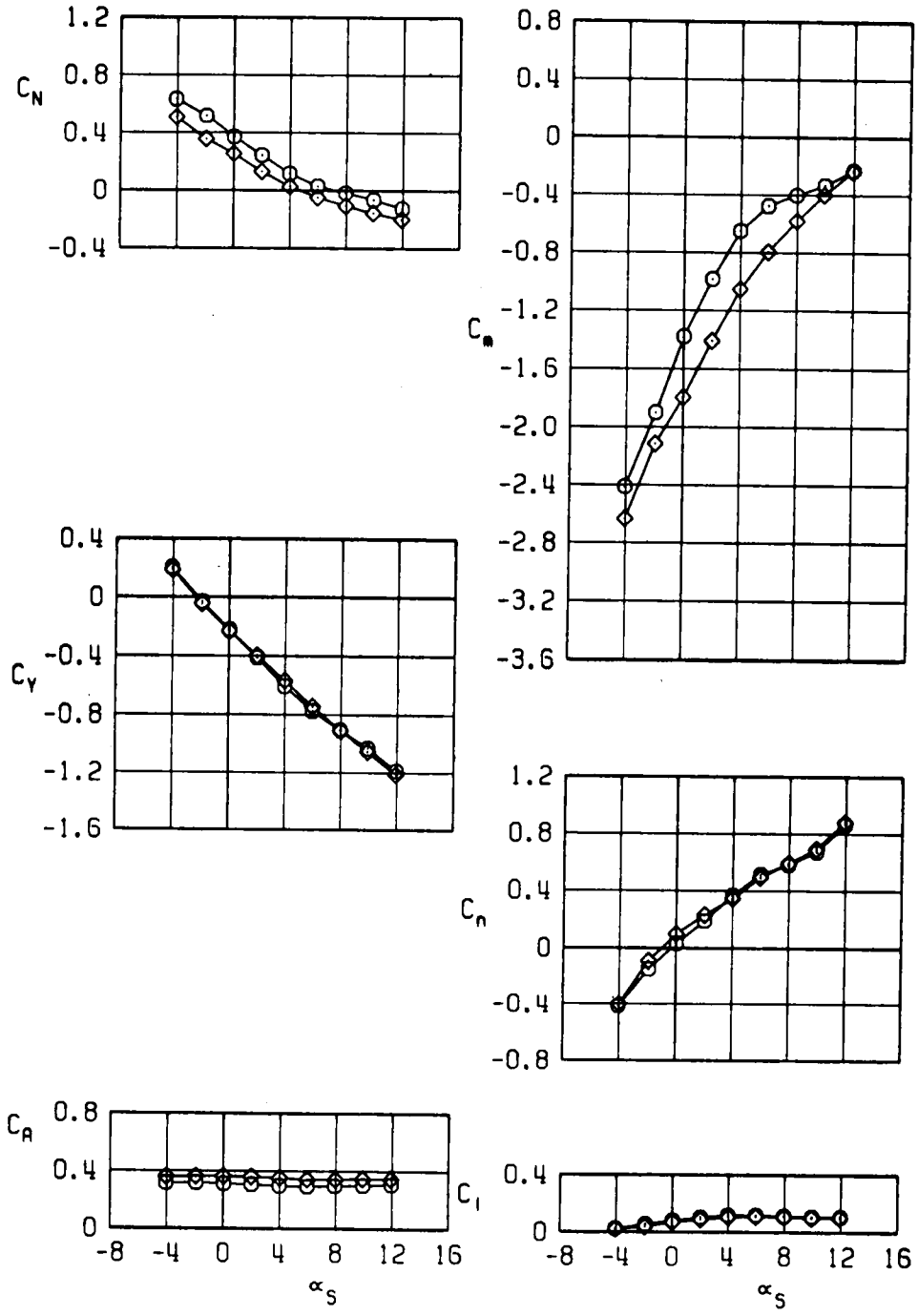

b. M_∞ = 0.8

Figure 22. (Continued)

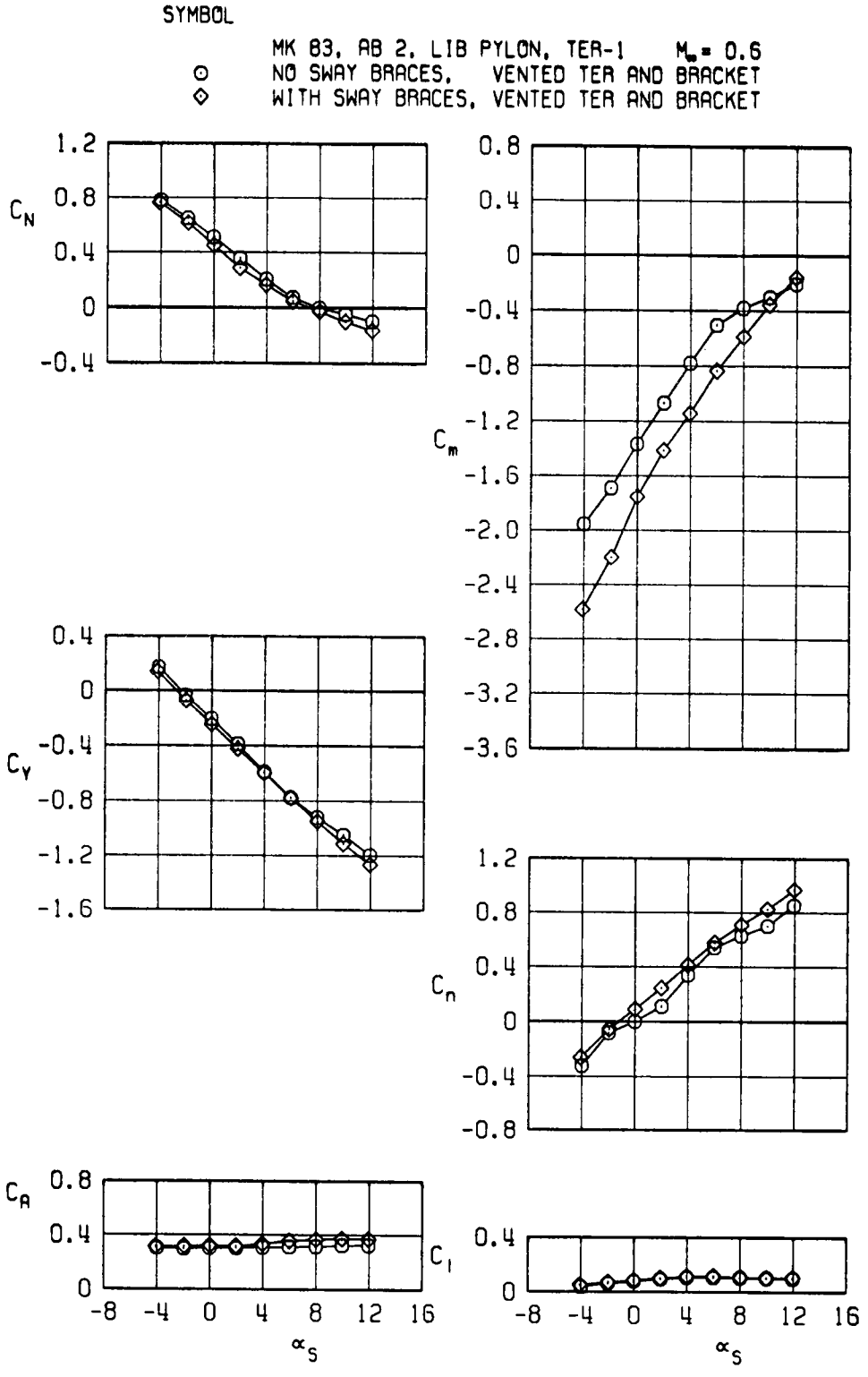

a. M_∞ = 0.6

Figure 23. The effect of TER geometric details on the aerodynamic coefficients of the MK-83 model, modified afterbody.

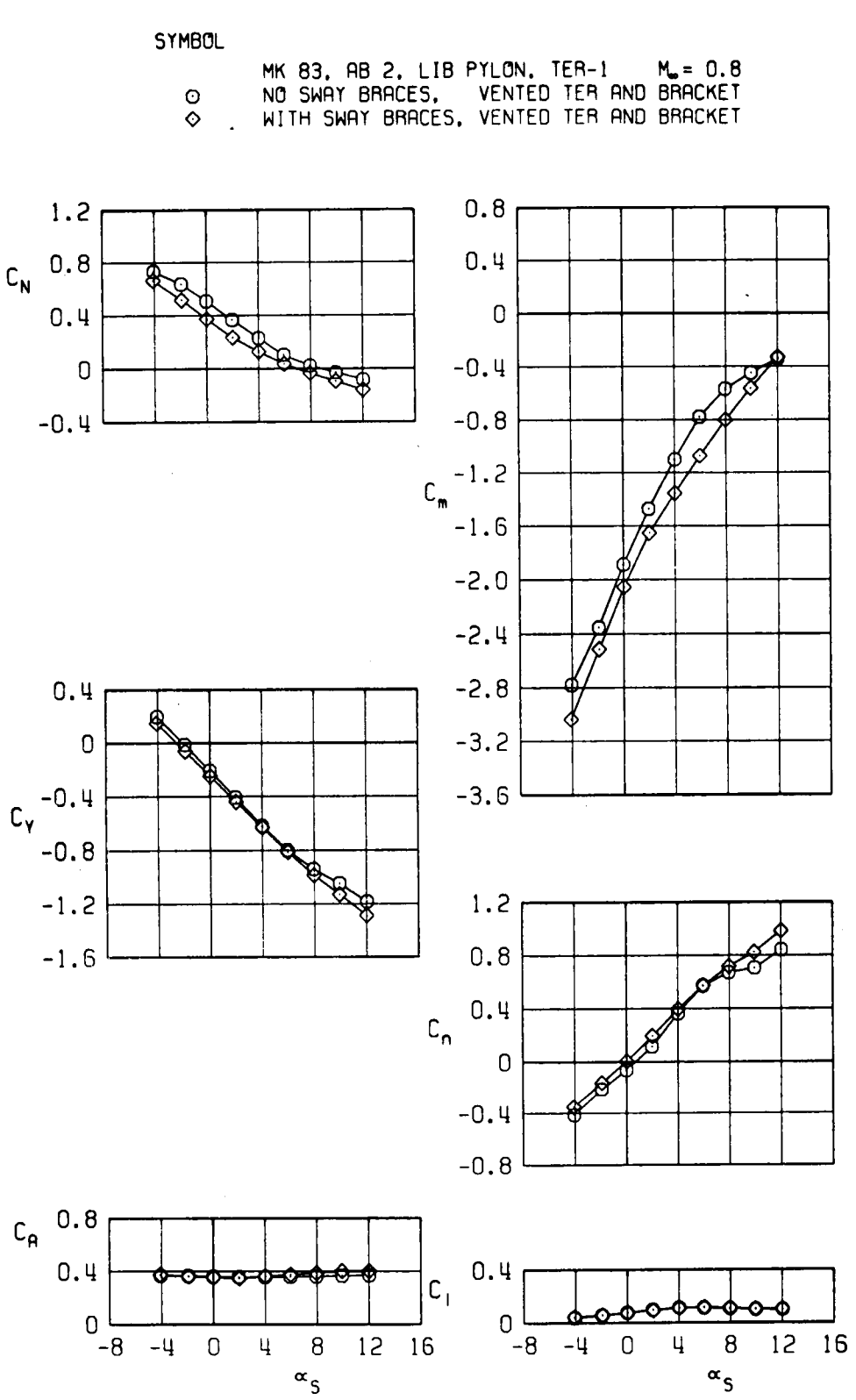

b. $M_\infty = 0.8$

Figure 23. (Continued)

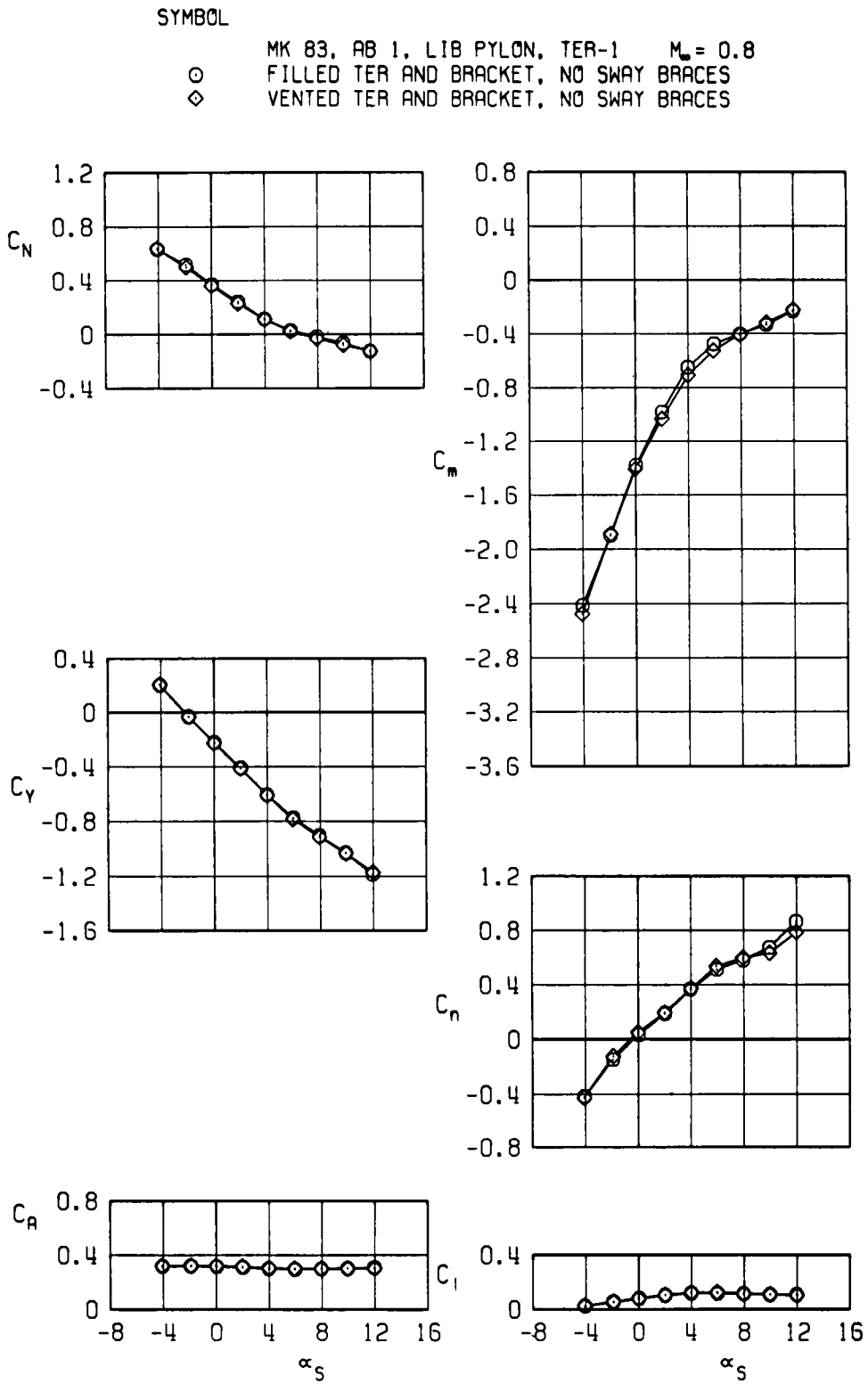

a. Venting slots without sway braces

Figure 24. The effect of venting slots and sway brace arms on the aerodynamic coefficients of the MK-83 model.

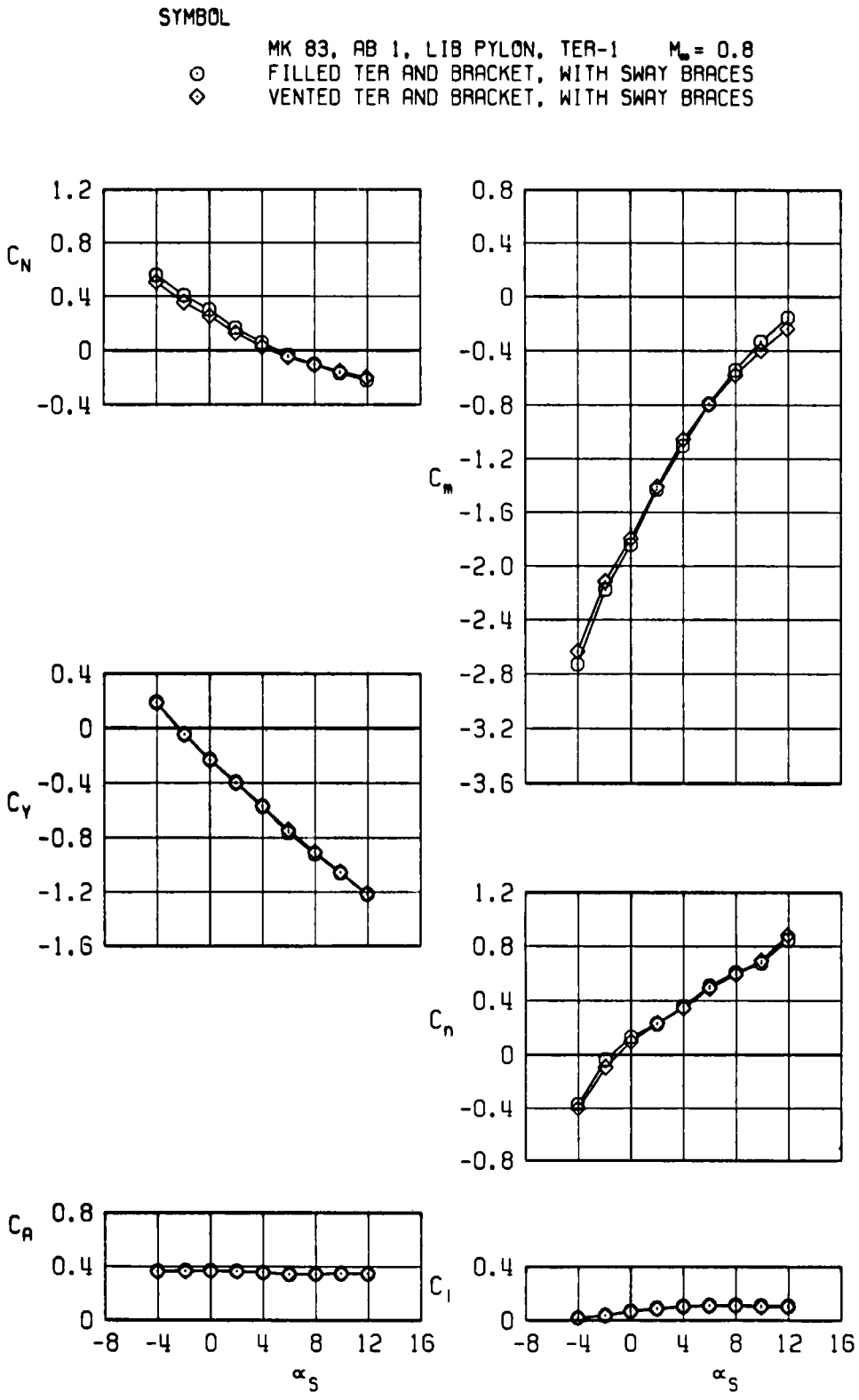

b. Venting slots with sway braces

Figure 24. (Continued)

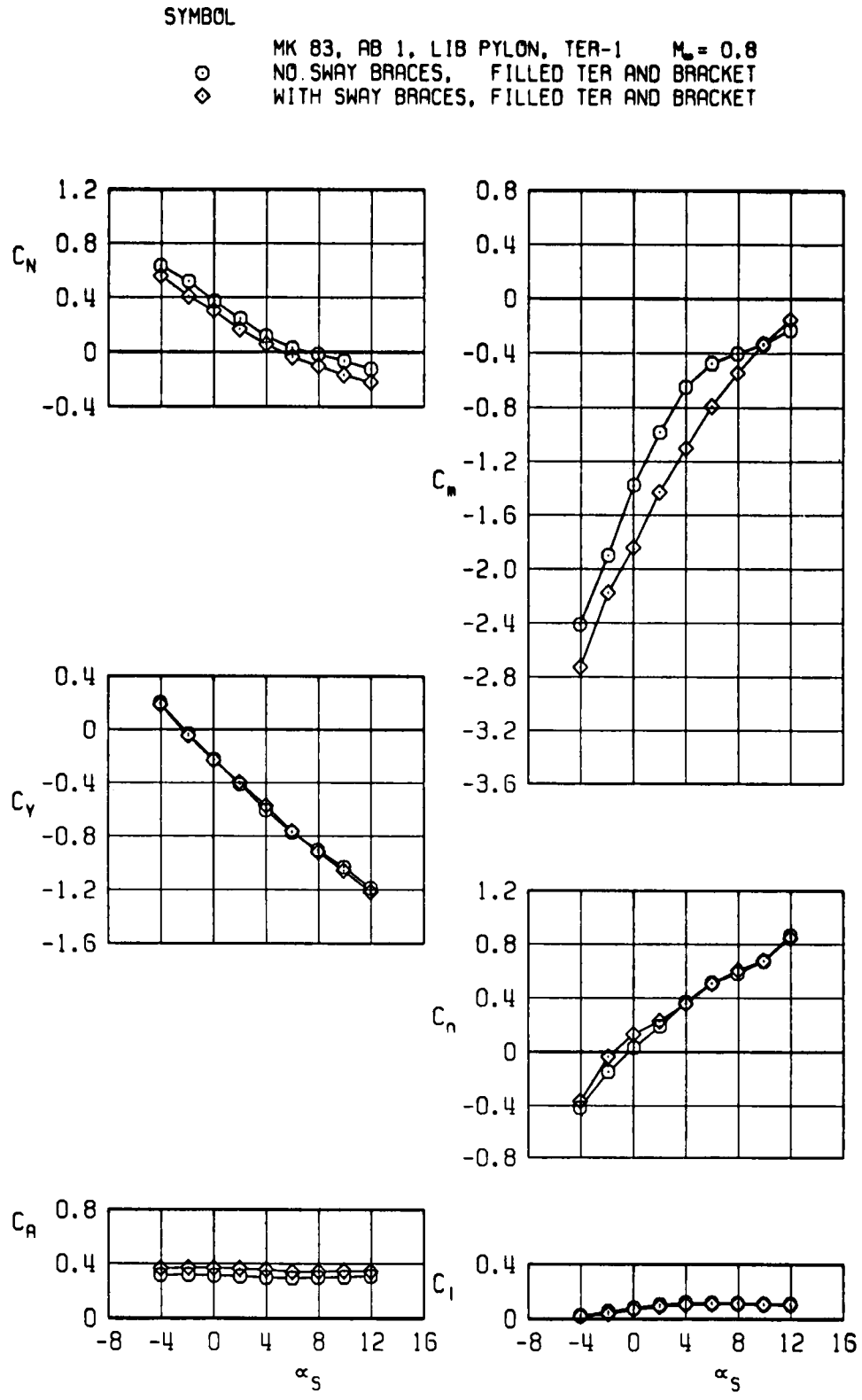

c. Sway braces without venting slots

Figure 24. (Continued)

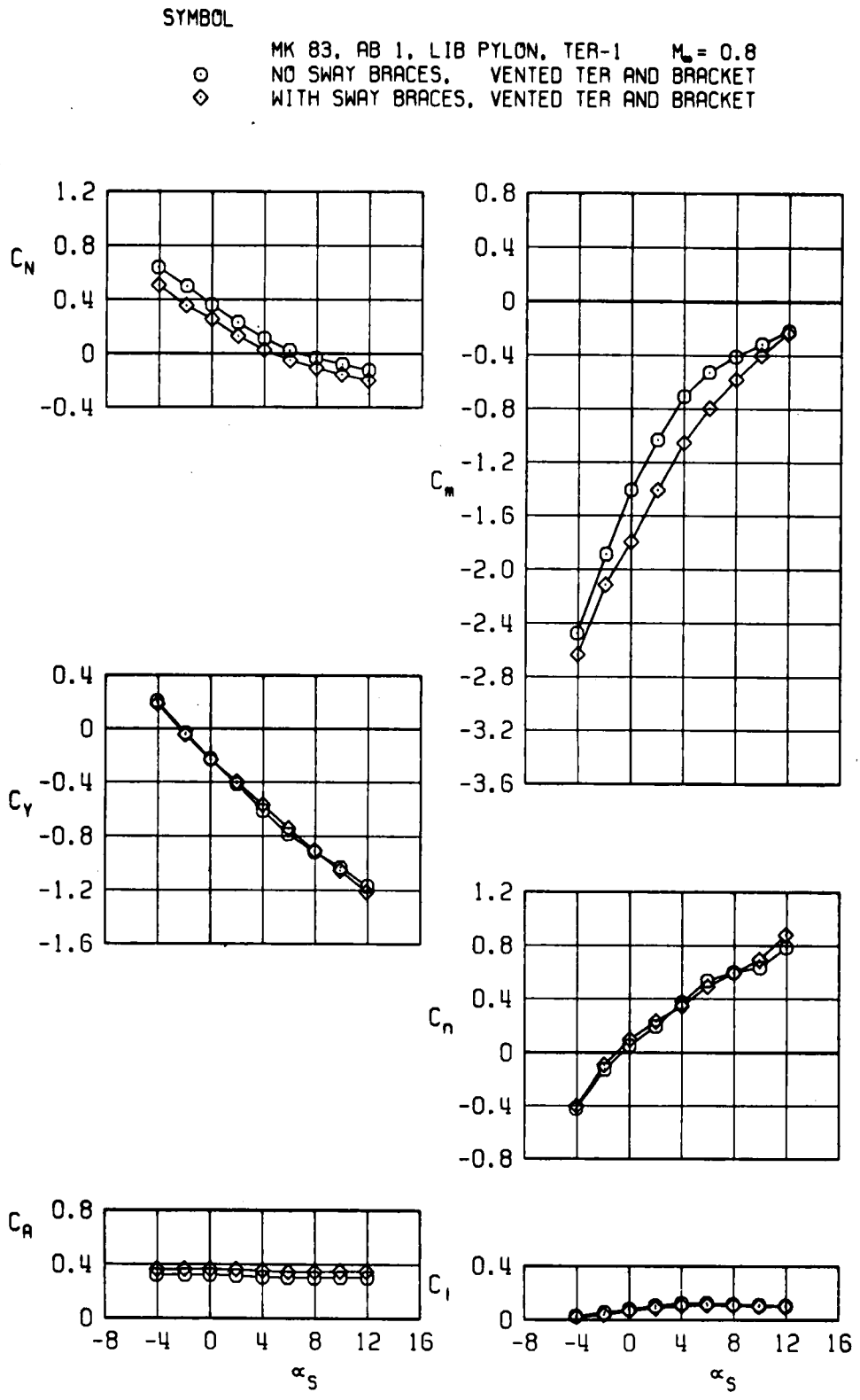

d. Sway braces with venting slots

Figure 24. (Continued)

venting slots, the pressure increase at and upstream (in local subsonic flow) of the sway braces would result in a negative pitching-moment increment or a center of pressure shift. An added means of relieving a buildup or reduction in local pressures within the cavity formed between the TER and attached weapons was provided by the venting slots. However, it is apparent that for this configuration the added ventilation has little or no effect on the aerodynamic coefficients. The effect of venting slots in wind tunnels using larger scale models is not known. Presented in Figures 25 and 26 are comparisons of IBS data obtained in the flow field of the detailed TER model and flight test data. Data for both afterbody configurations are shown. A comparison between the normal-force coefficient data presented in Figure 20, page 55, and Figure 25 shows that better agreement between wind tunnel data and the flight test data was obtained when the geometric details of the TER were simulated. Agreement between pitching-moment coefficient data improved at a Mach number of 0.6 but worsened at a Mach number of 0.8. Perhaps the failure to accurately simulate local shock wave formations and their interactions with the boundary layer (a strong function of the wind tunnel unit Reynolds number, wall porosity, and acoustics) was responsible for the disagreement at the transonic Mach numbers. Agreement between yawing-moment coefficients deteriorates at the lower Mach numbers. Normal-force coefficients obtained in the flow field of the detailed TER model at a Mach number of 0.8 still show no evidence of a

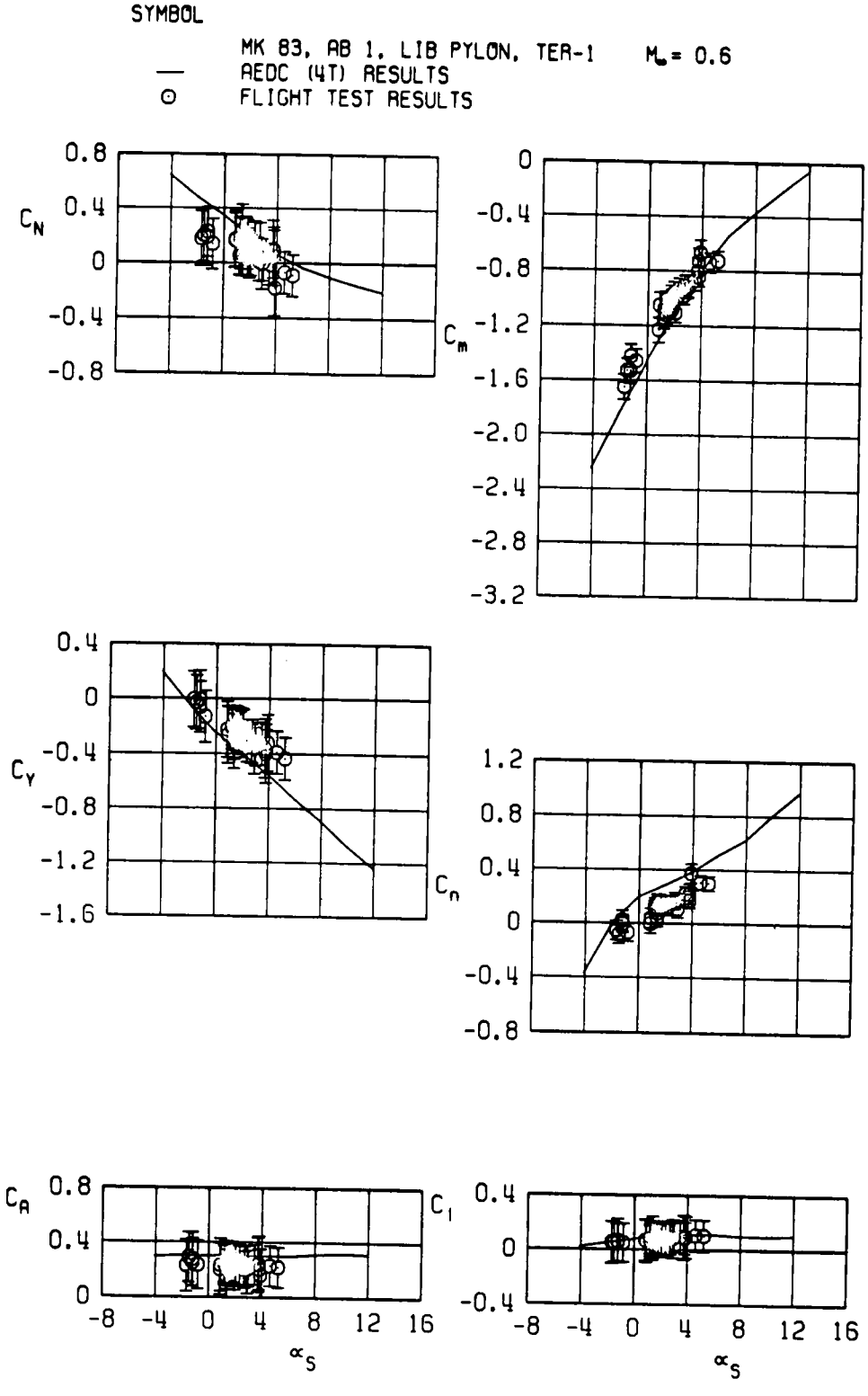

a. $M_\infty = 0.6$

Figure 25. Comparisons of IBS data obtained in the flow field of the detailed TER model and flight test data, standard afterbody.

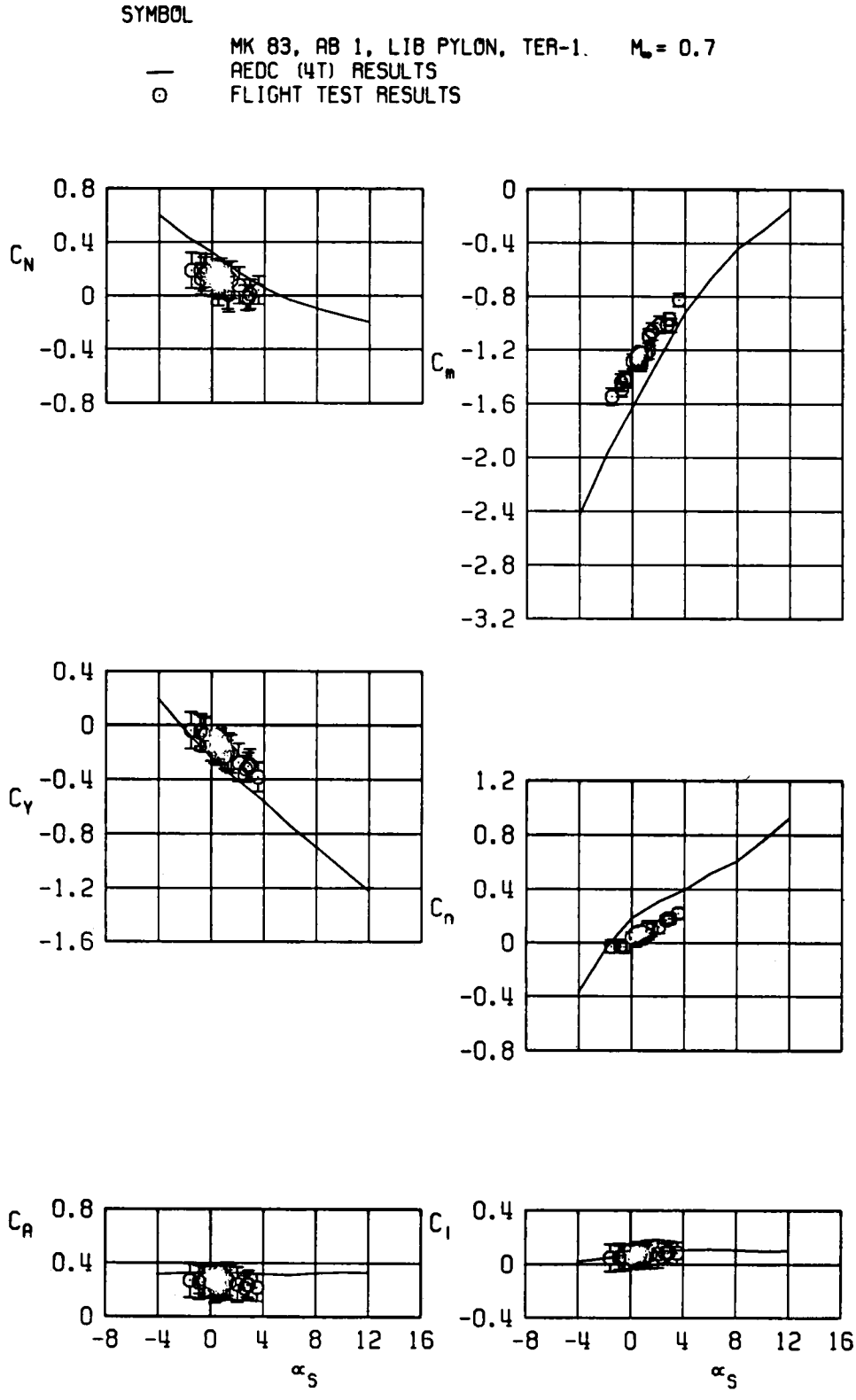

b. $M_\infty = 0.7$

Figure 25. (Continued)

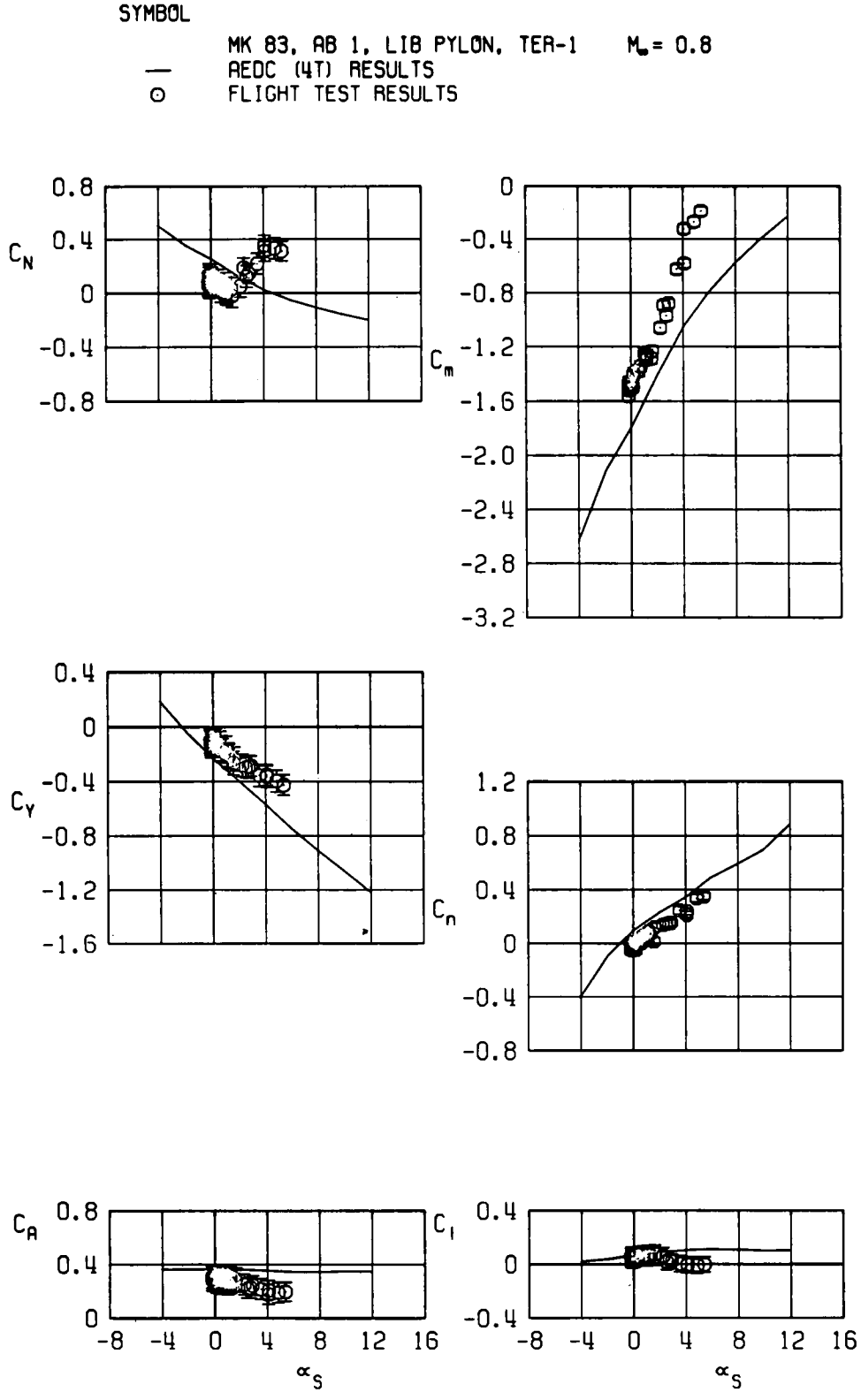

c. $M_\infty = 0.8$

Figure 25. (Continued)

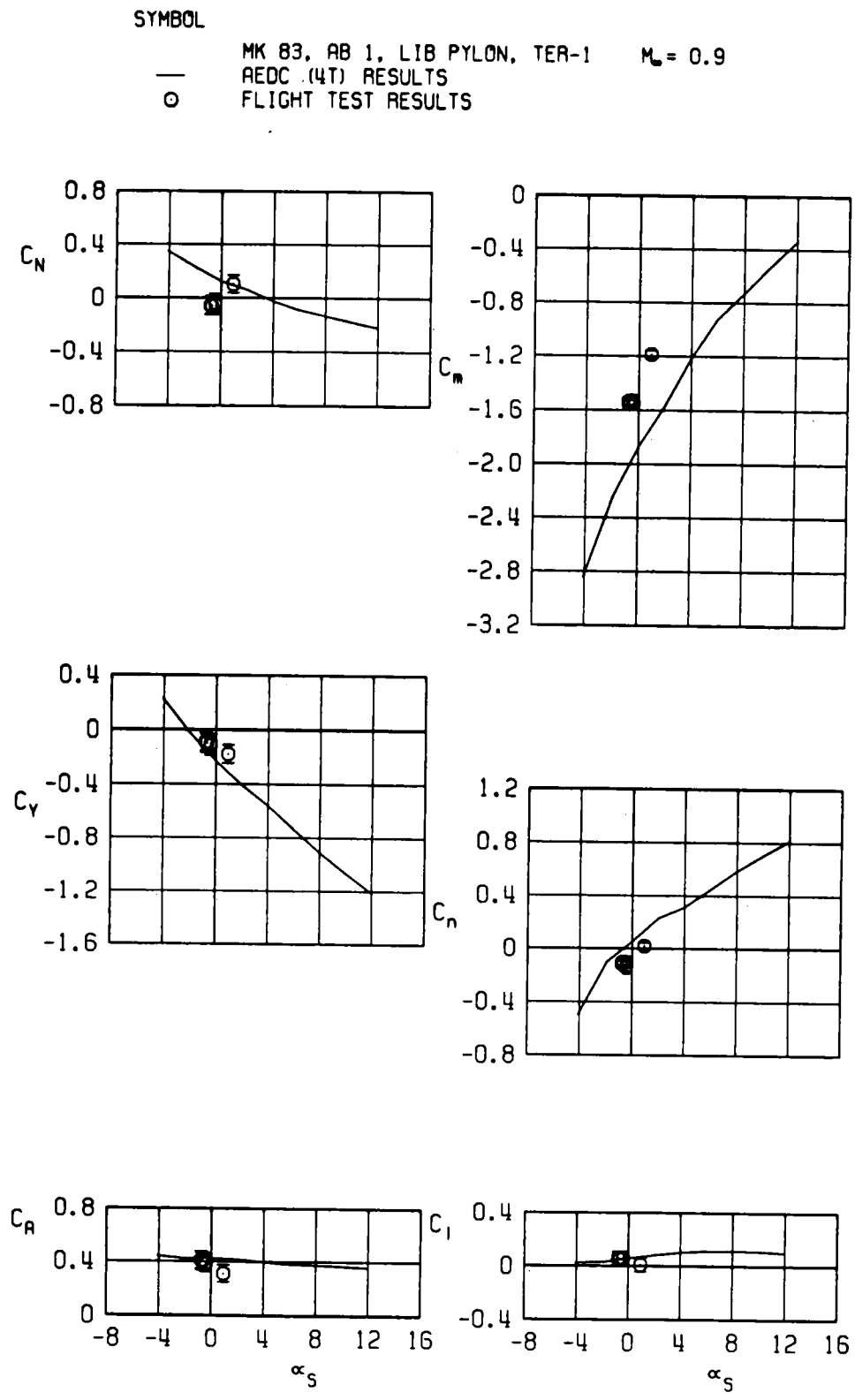

d. $M_\infty = 0.9$

Figure 25. (Continued)

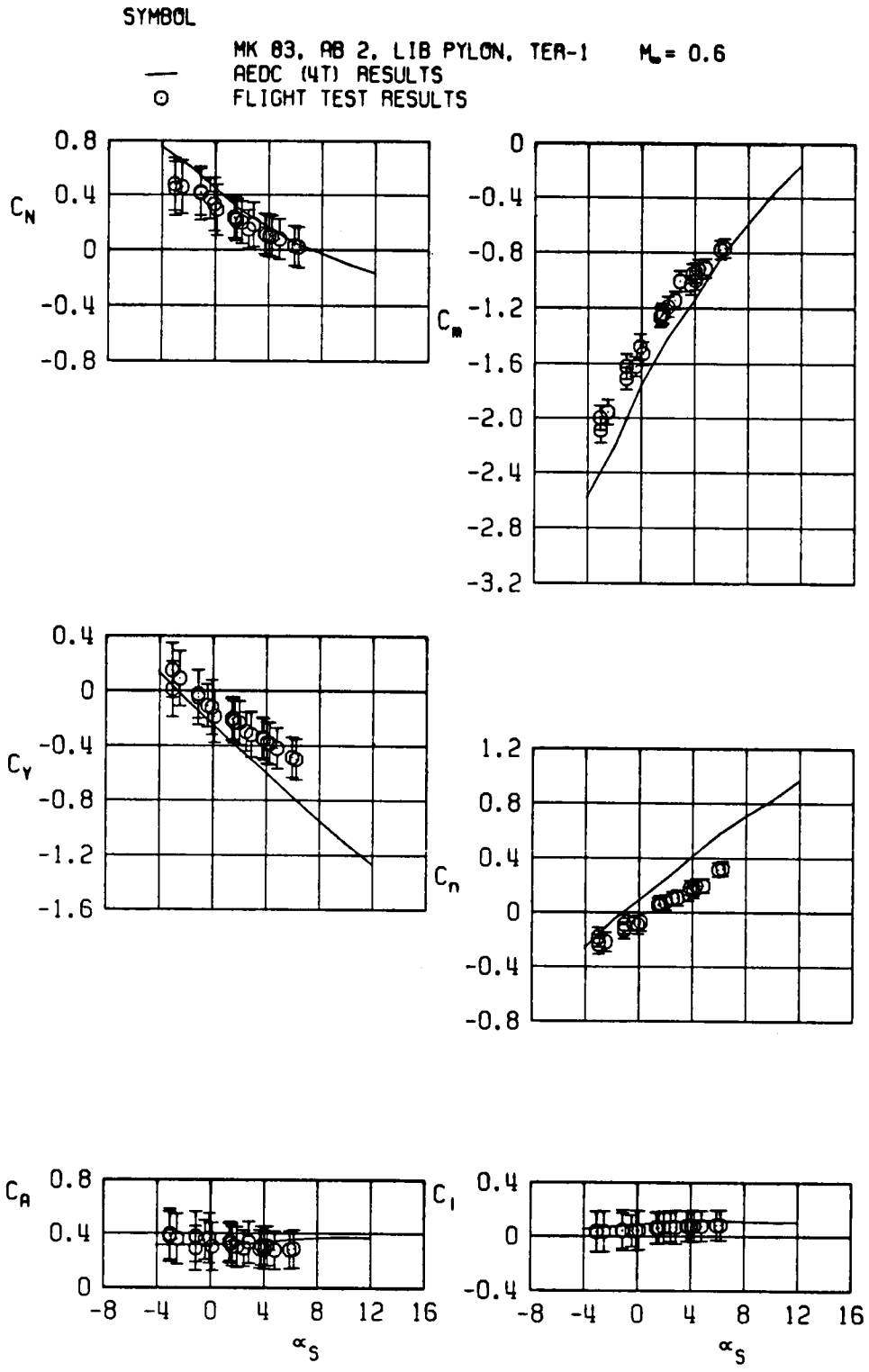

a. $M_\infty = 0.6$

Figure 26. Comparisons of IBS data obtained in the flow field of the detailed TER model and flight test data, modified afterbody.

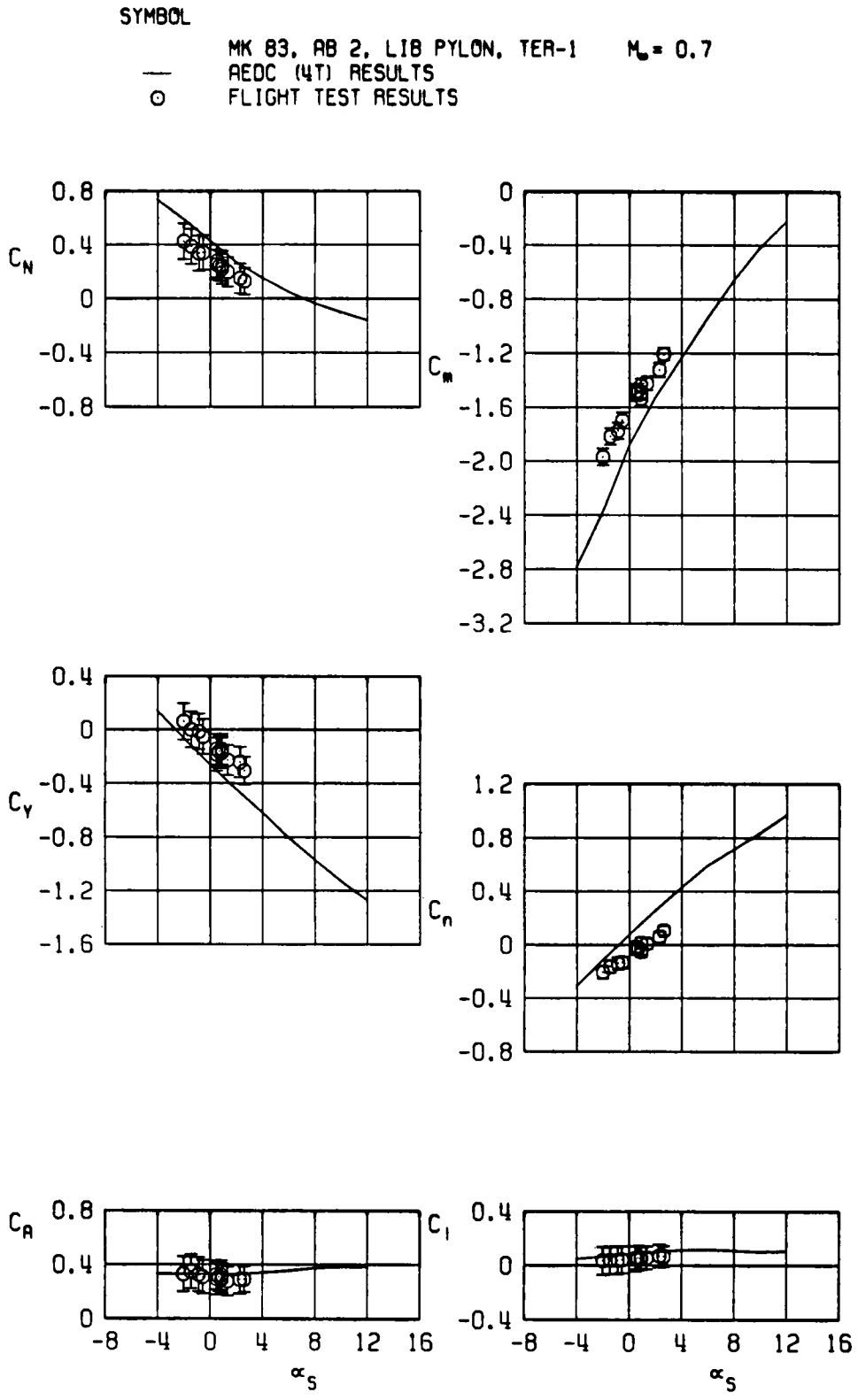

b. $M_\infty = 0.7$

Figure 26. (Continued)

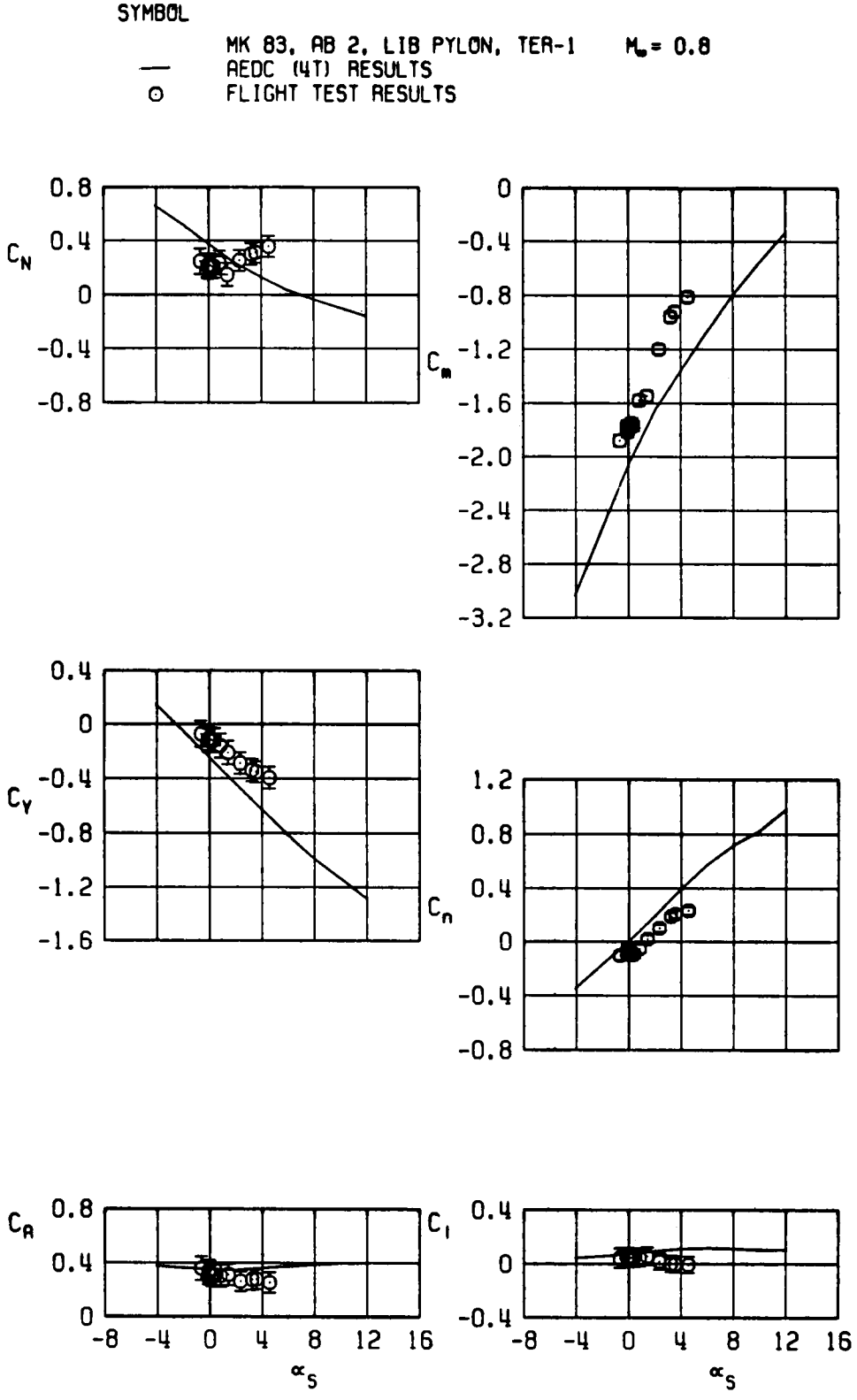

c. $M_\infty = 0.8$

Figure 26. (Continued)

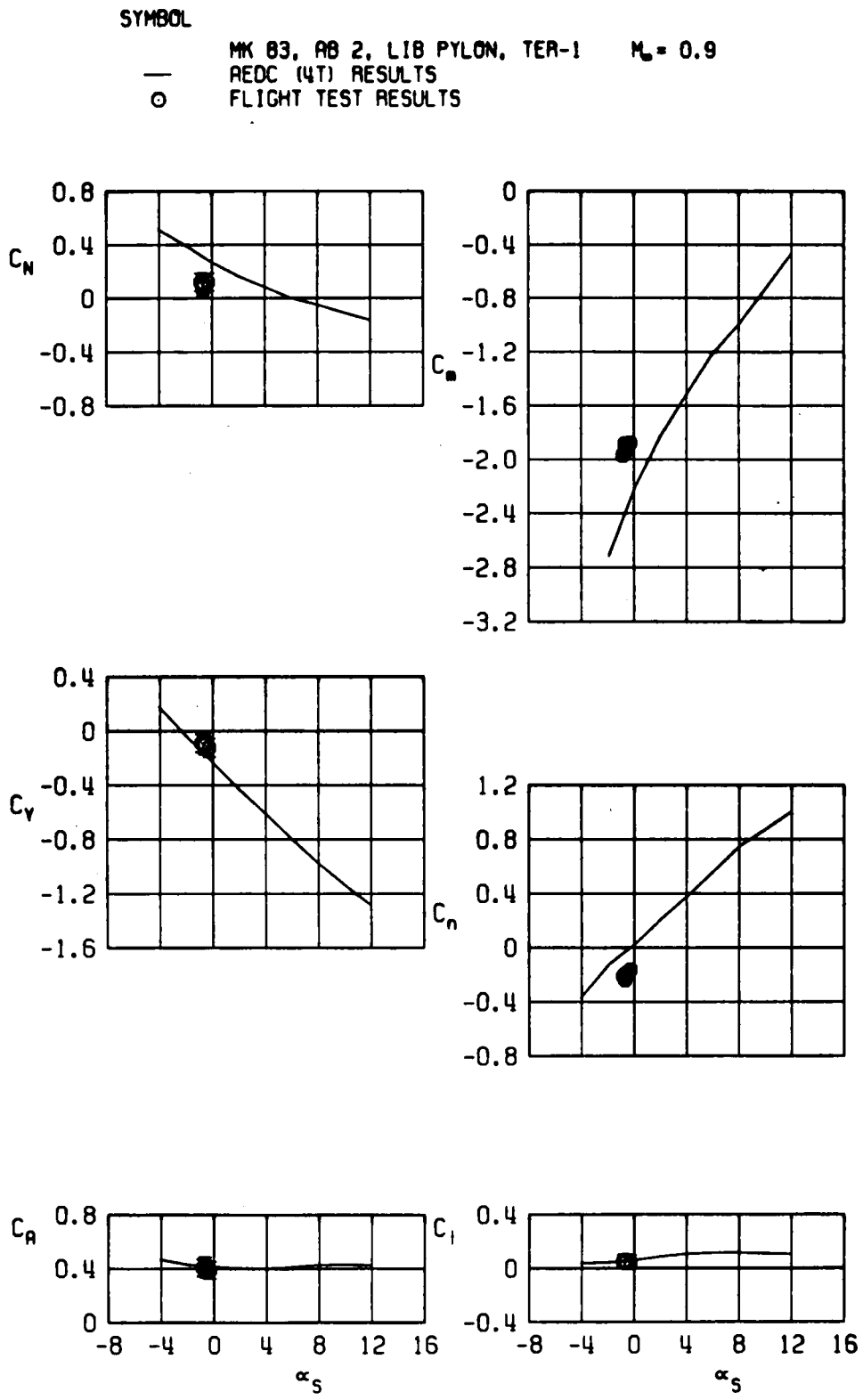

d. $M_\infty = 0.9$

Figure 26. (Continued)

slope reversal as do the flight test data. At store angles of attack greater than two degrees, flight test data at a Mach number of 0.8 were obtained during high "g" maneuvers. An example of aircraft load factors at various Mach numbers and store angles of attack is presented in Figure 27. Aerodynamic loads were determined from the difference between gross and inertial load measurements and therefore were strongly dependent on the accuracy of the accelerometer measurements. The sudden reversal of the normal-force coefficient slope at store angles of attack corresponding to aircraft load factors of approximately three, indicates a strong possibility of accelerometer divergence. The divergence of accelerometer output from output obtained during the laboratory calibration would invalidate the calculation of inertial loads and the subsequent calculation of the aerodynamic coefficients.

The effects of venting slots and sway brace arms on the aerodynamic coefficient data obtained by the CTS data acquisition technique were also investigated. The effects are similar to those obtained using the IBS technique. A comparison of CTS data obtained in the flow field of the detailed TER model and the flight test data is shown in Figure 28. With the exception of the pitching-moment coefficients at a Mach number of 0.6, CTS data do not match the flight test data as well as the IBS data (see Figure 26). Perhaps a large part of the discrepancies can be attributed

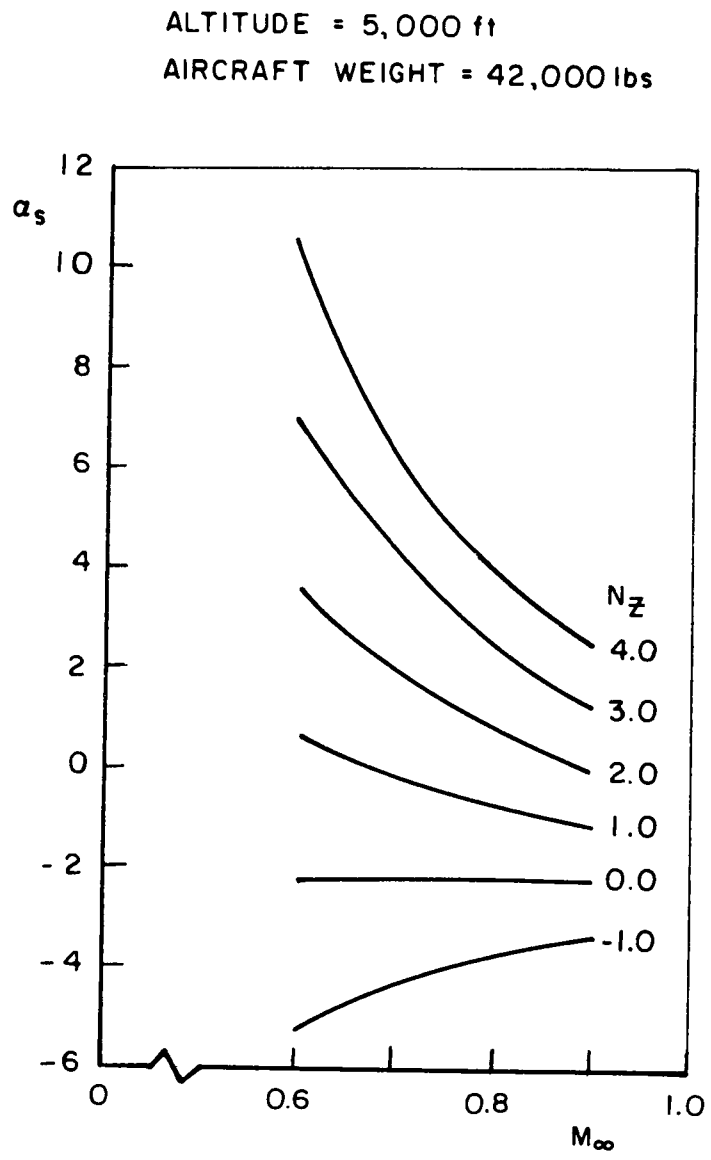

Figure 27. An example of aircraft load factors at various Mach numbers and store angles of attack.

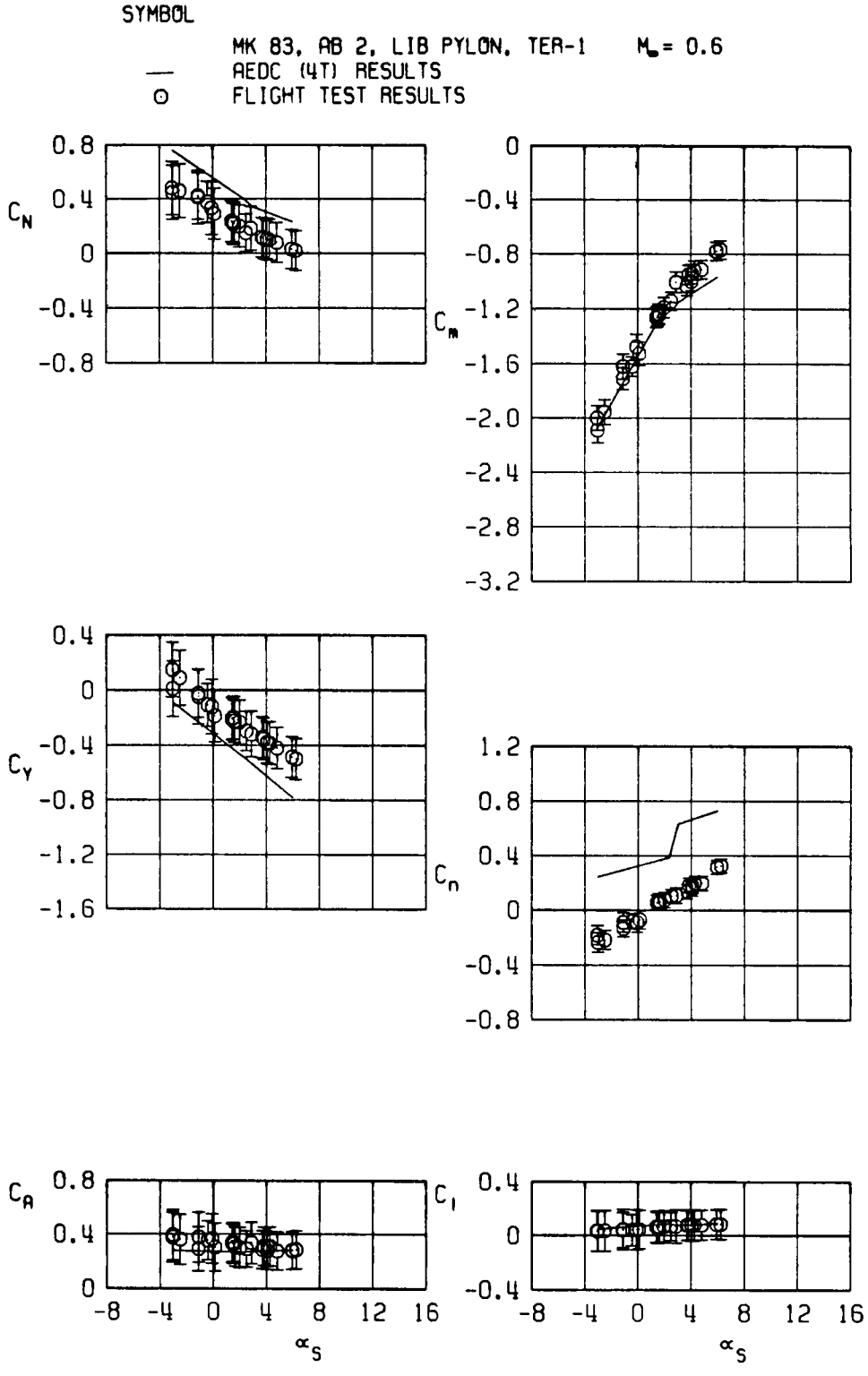

a. $M_\infty = 0.6$

Figure 28. A comparison of CTS data obtained in the flow field of the detailed TER model and the flight test data.

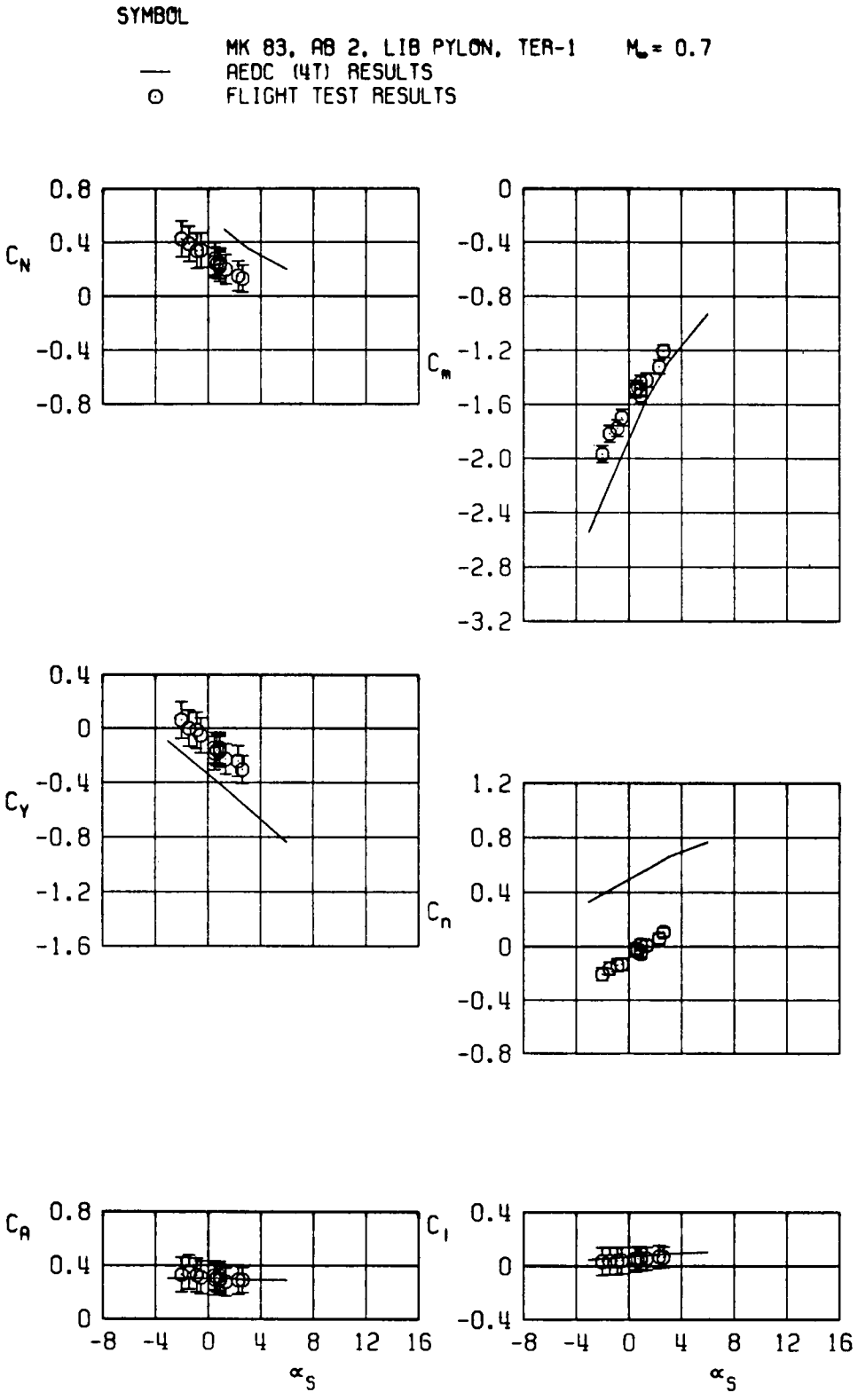

b. $M_\infty = 0.7$

Figure 28. (Continued)

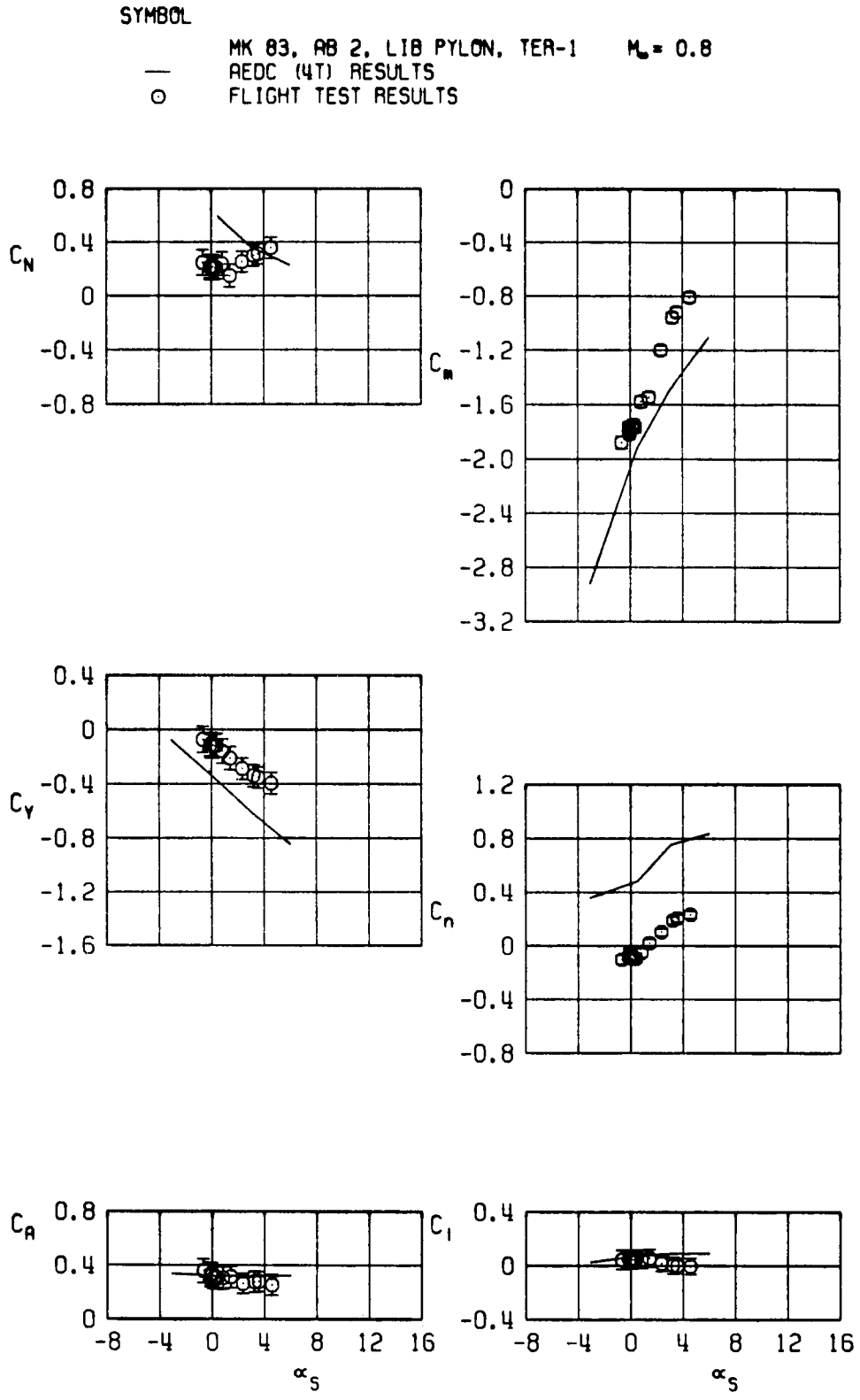

c. $M_\infty = 0.8$

Figure 28. (Continued)

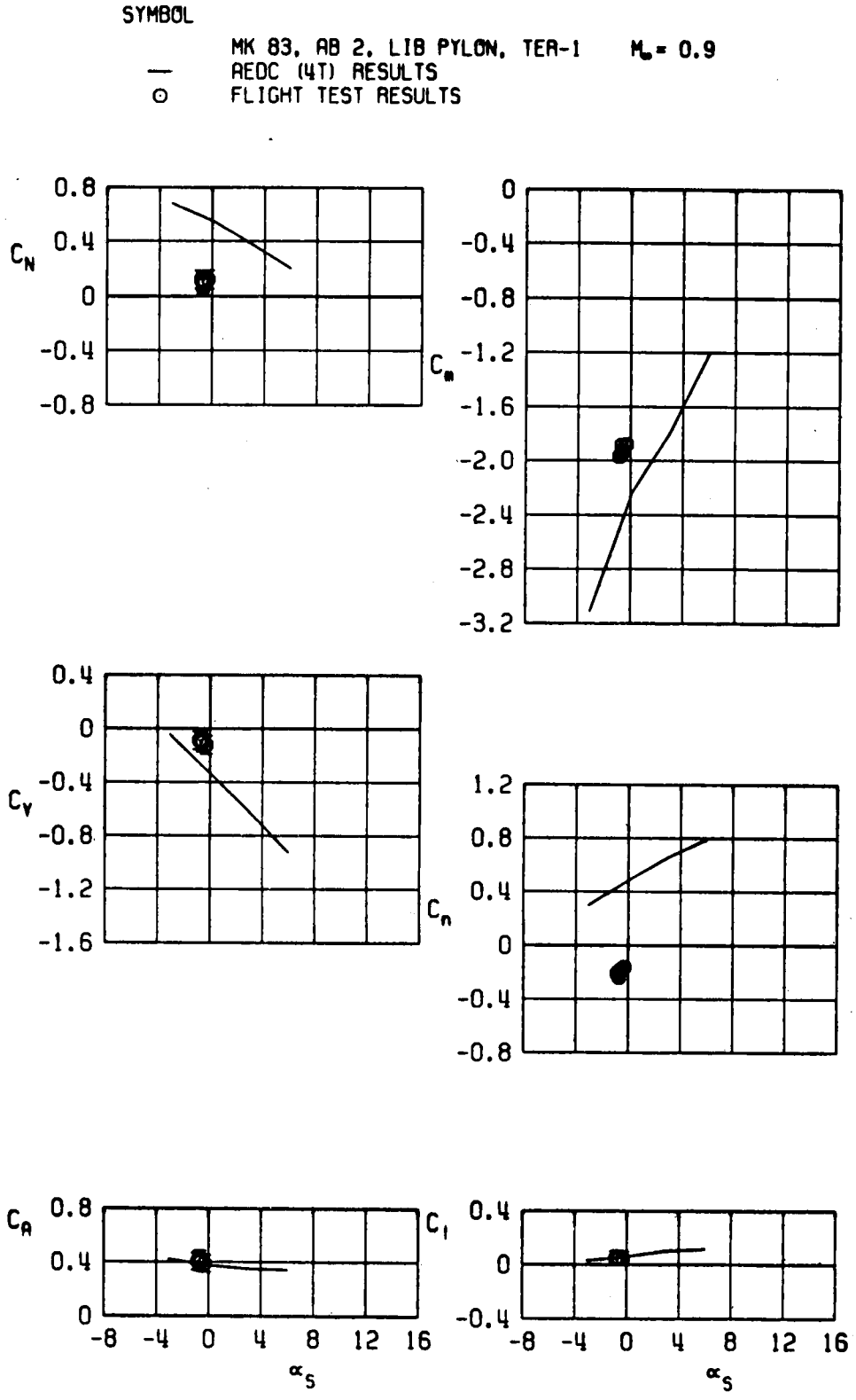

d. $M_\infty = 0.9$

Figure 28. (Continued)

to CTS positioning errors.[2] Before aerodynamic loads data were obtained, the CTS was positioned to a "wind off" reference location, determined prior to establishing airflow in the tunnel. At this reference location, the store model was at the "wind off" carriage position. However, once airflow is established, aerodynamic loads cause the store and aircraft model to deflect. As a result of aerodynamic deflections, the store model was manually repositioned to an estimated "wind on" carriage position. However, once operational control of the CTS was switched to the digital computer to initiate the data acquisition cycle, CTS deflections were automatically calculated. Thus the repositioning of the store model at the "wind on" carriage position results in positioning errors. Although positioning errors were estimated to be small, such errors particularly in the complex flow field associated with a TER, can have large effects on aerodynamic coefficients. Such effects are discussed in Reference 7. Another source of error inherent to CTS testing is the relative dynamic motion of the CTS store model to the aircraft model. In most instances, as in this test, small adjustments to the wind tunnel diffuser flaps minimize this dynamic effect.

The influence of the store model support sting on the aerodynamic coefficients of the MK-83 model was

---

[2] CTS positioning errors have subsequently been minimized.

investigated during an IBS test described in Reference 8. The CTS was equipped with a dummy sting which could be positioned at the store model base. The effects of the CTS sting on the aerodynamic coefficients of the MK-83 are given in Figure 29. The sting induces a small positive pitching-moment coefficient increment. The remaining coefficients are virtually insensitive to the presence of the sting. Correcting CTS data for sting effects would give slightly better correlation between wind tunnel and flight test results. However, better overall agreement was still obtained by the IBS test technique.

The alteration made to the store model afterbody in order to accommodate the CTS sting was also investigated during IBS testing. Presented in Figure 30 are the effects of the afterbody modification on the aerodynamic coefficients of the MK-83 model. Should the results be applied to the CTS data shown in Figure 28, page 85, agreement with the flight test data would deteriorate.

A nominal wind tunnel unit Reynolds number of three and one-half million per foot and a nominal wind tunnel wall porosity of 5-percent open were maintained during the wind tunnel test. Although very limited in scope, the effect of Reynolds number and wall porosity was investigated. The effect of Reynolds number on the aerodynamic coefficients of the MK-83 model is given in Figure 31. Negative yawing-moment and pitching-moment coefficient increments are shown at the lower Reynolds number. Application of the yawing-

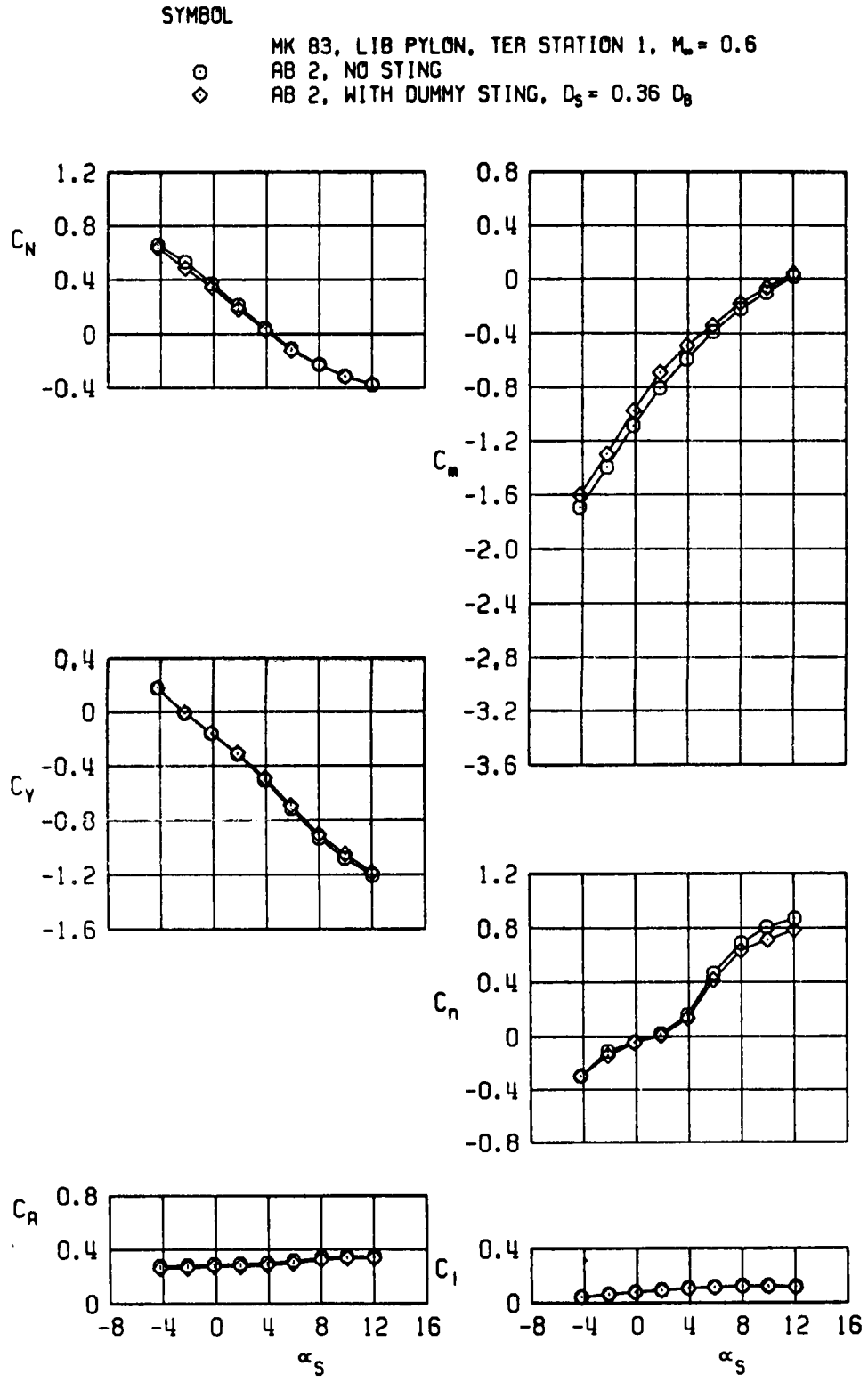

a. $M_\infty = 0.6$

Figure 29. The effects of the CTS sting on the aerodynamic coefficients of the MK-83 model.

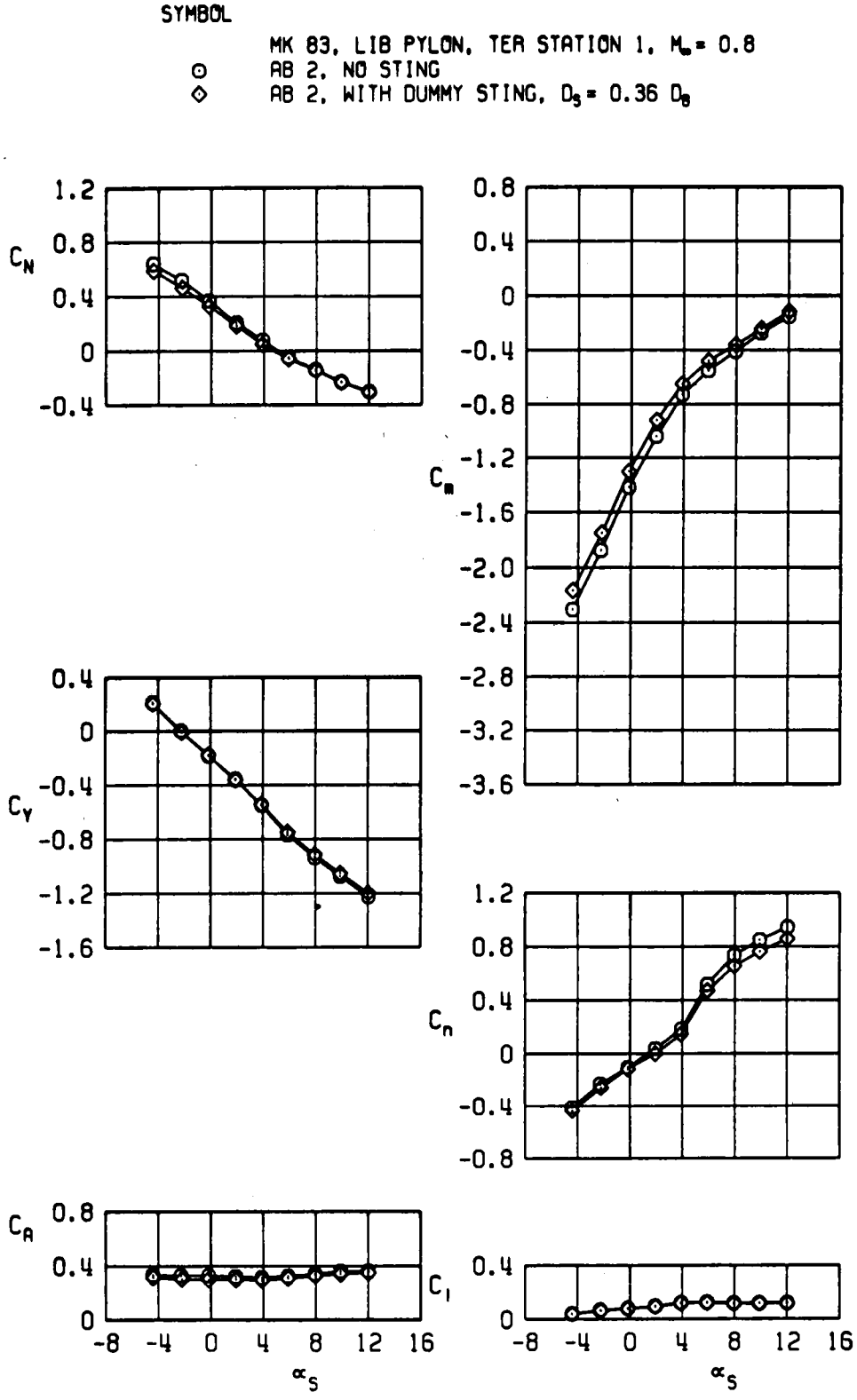

b. $M_\infty = 0.8$

Figure 29. (Continued)

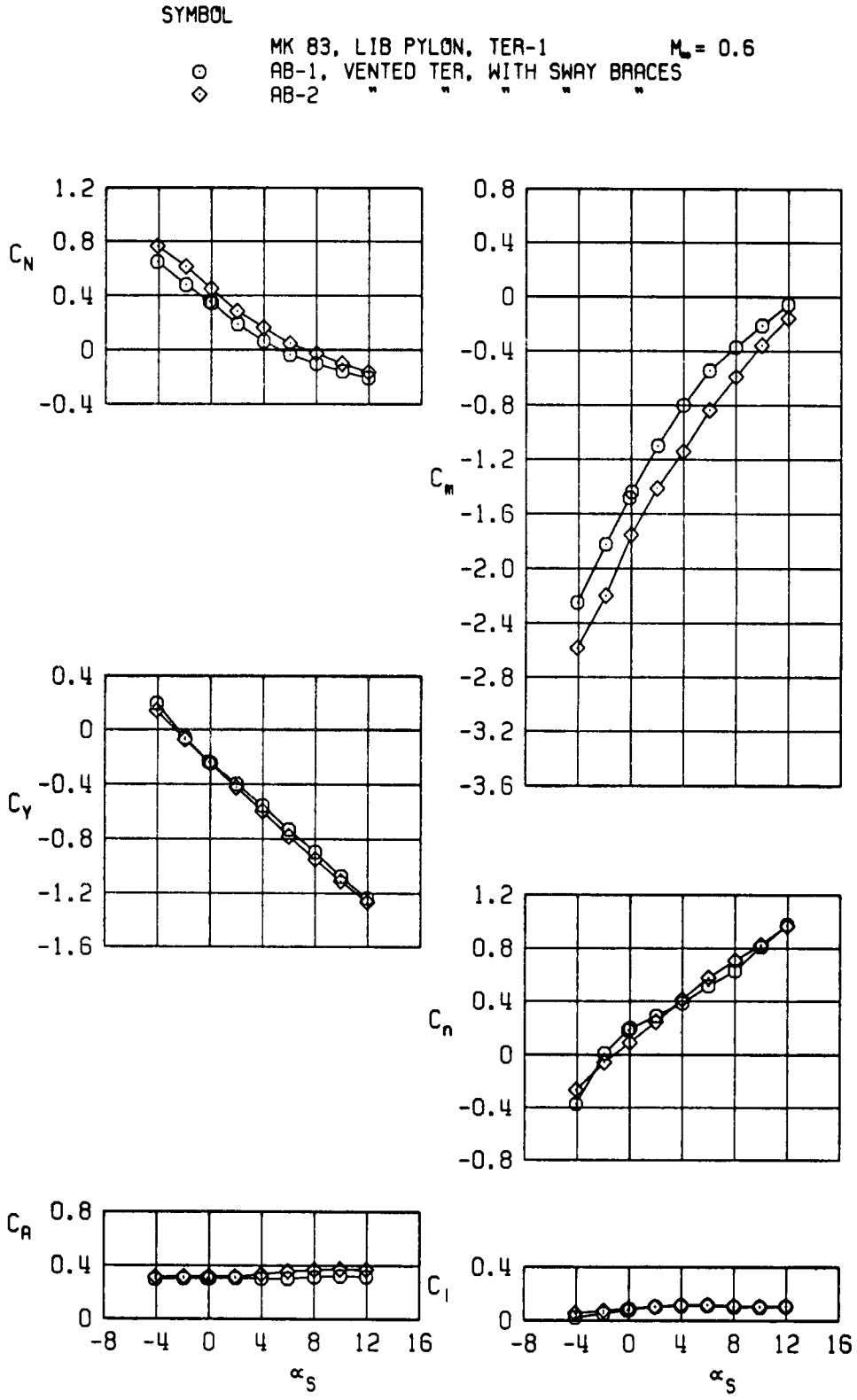

a. $M_\infty = 0.6$

Figure 30. The effects of afterbody modification on the aerodynamic coefficients of the MK-83 model.

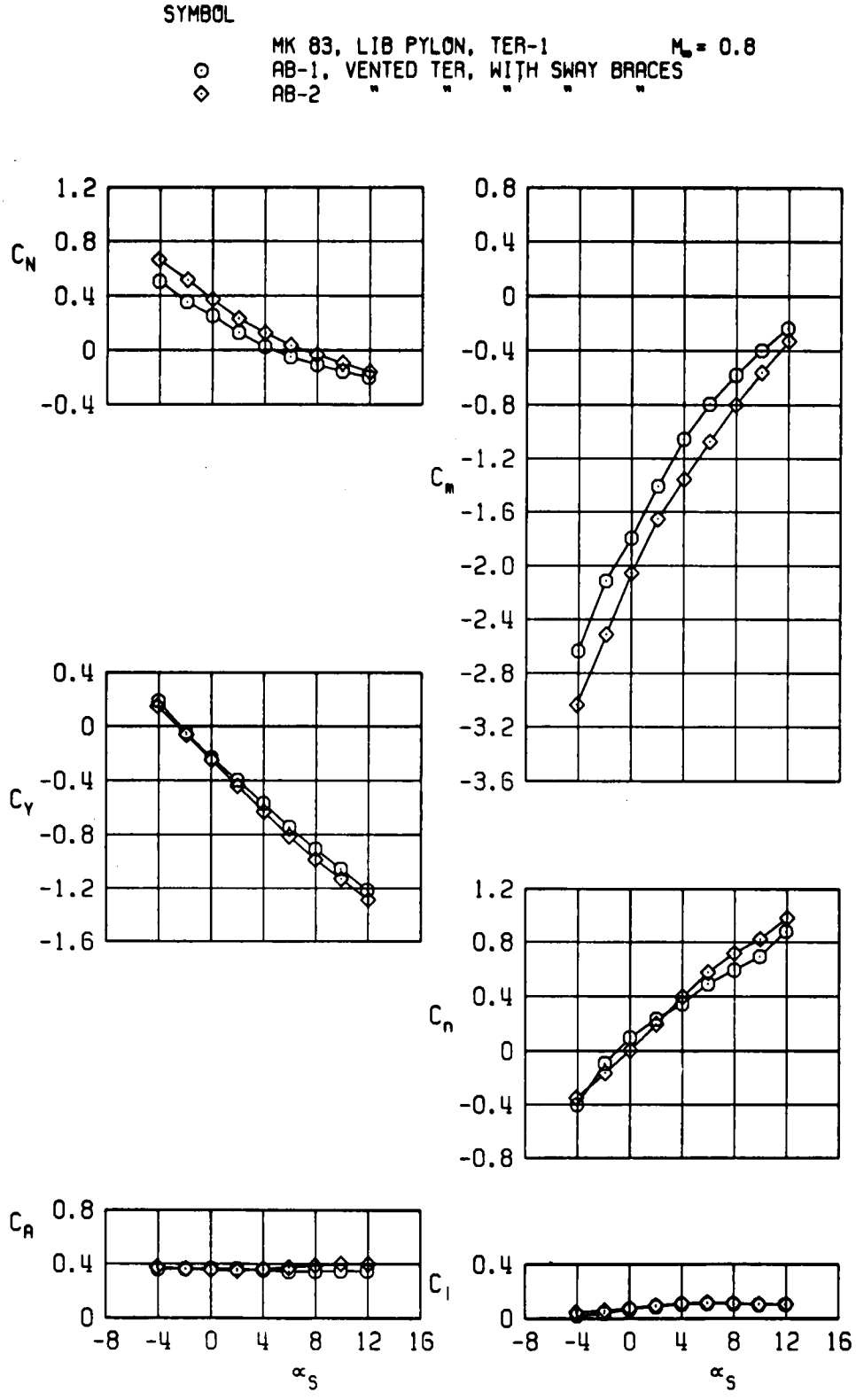

b. $M_\infty = 0.8$

Figure 30. (Continued)

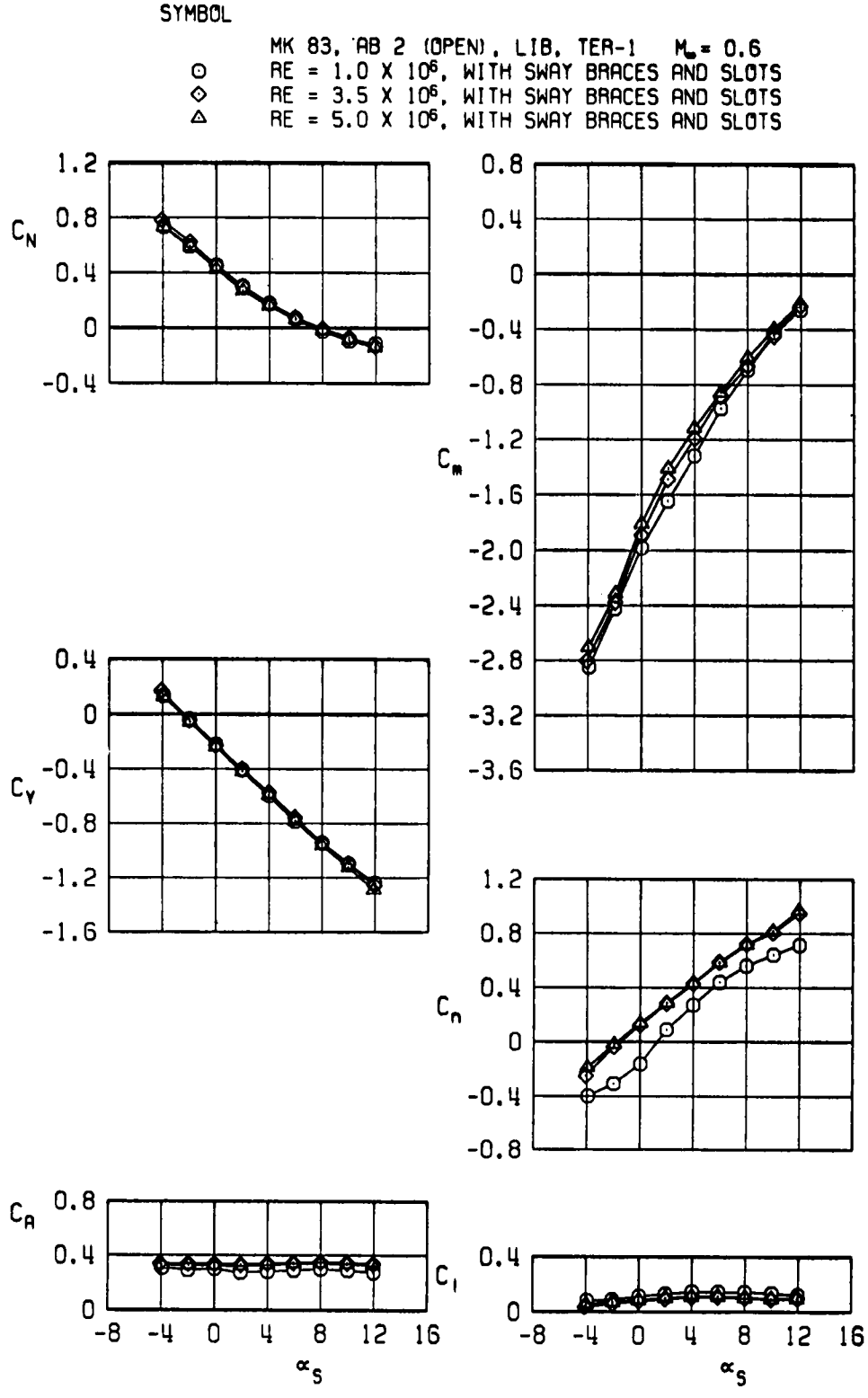

a. $M_\infty = 0.6$

Figure 31. The effect of Reynolds number on the aerodynamic coefficients of the MK-83 model.

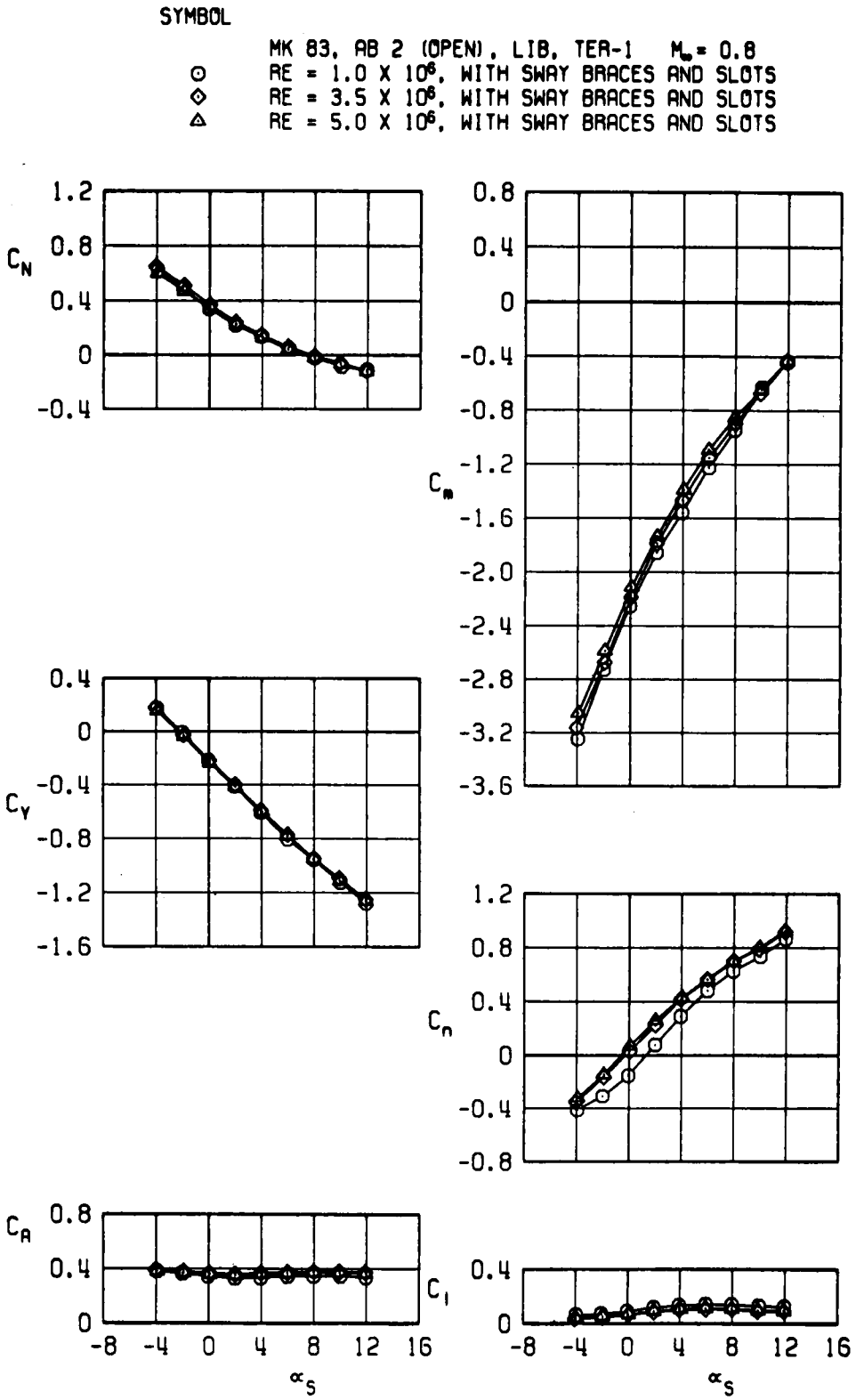

b. M_∞ = 0.8

Figure 31. (Continued)

moment coefficient increment to wind tunnel data obtained in the flow field of the detailed TER model would result in data that more closely match the flight test data. However, application of the pitching-moment coefficient would only worsen the comparison of wind tunnel and flight test data. A slightly positive pitching-moment coefficient increment can be seen at the higher Reynolds number. A positive pitching-moment coefficient increment would aid the correlation of wind tunnel and flight test data. The remaining coefficient data are relatively insensitive to Reynolds number variation. The effects of wind tunnel wall porosity on the aerodynamic coefficients of the MK-83 are presented in Figure 32. Porosity effects are noticeable only at a Mach number of 0.6. While better correlation between wind tunnel normal-force and yawing-moment coefficients and the flight test data would be achieved at the lower porosity setting, agreement between the pitching-moment coefficients would deteriorate.

Wind tunnel data were obtained in order to investigate carriage position airloads. The results were compared to flight test data. Wind tunnel data obtained using the IBS data acquisition technique generally correlate better with flight test data than do wind tunnel data obtained using the CTS data acquisition technique. Data obtained by the latter technique were subject to positioning errors. Wind tunnel data were obtained in the flow field induced by a simple and a detailed TER model. IBS data obtained at a Mach number of 0.6 in the flow field of the detailed TER model have shown

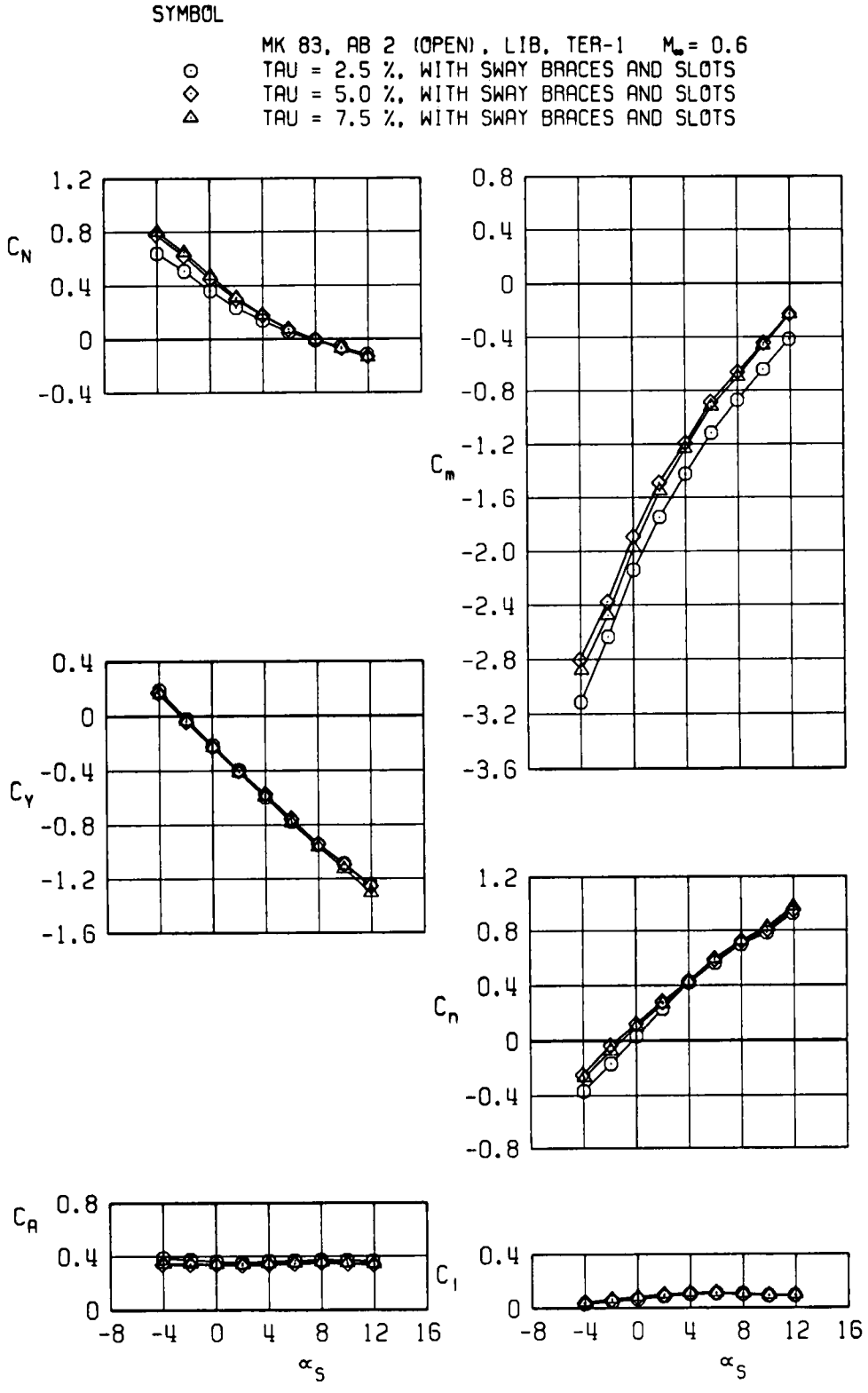

a. $M_\infty = 0.6$

Figure 32. The effects of wind tunnel wall porosity on the aerodynamic coefficients of the MK-83 model.

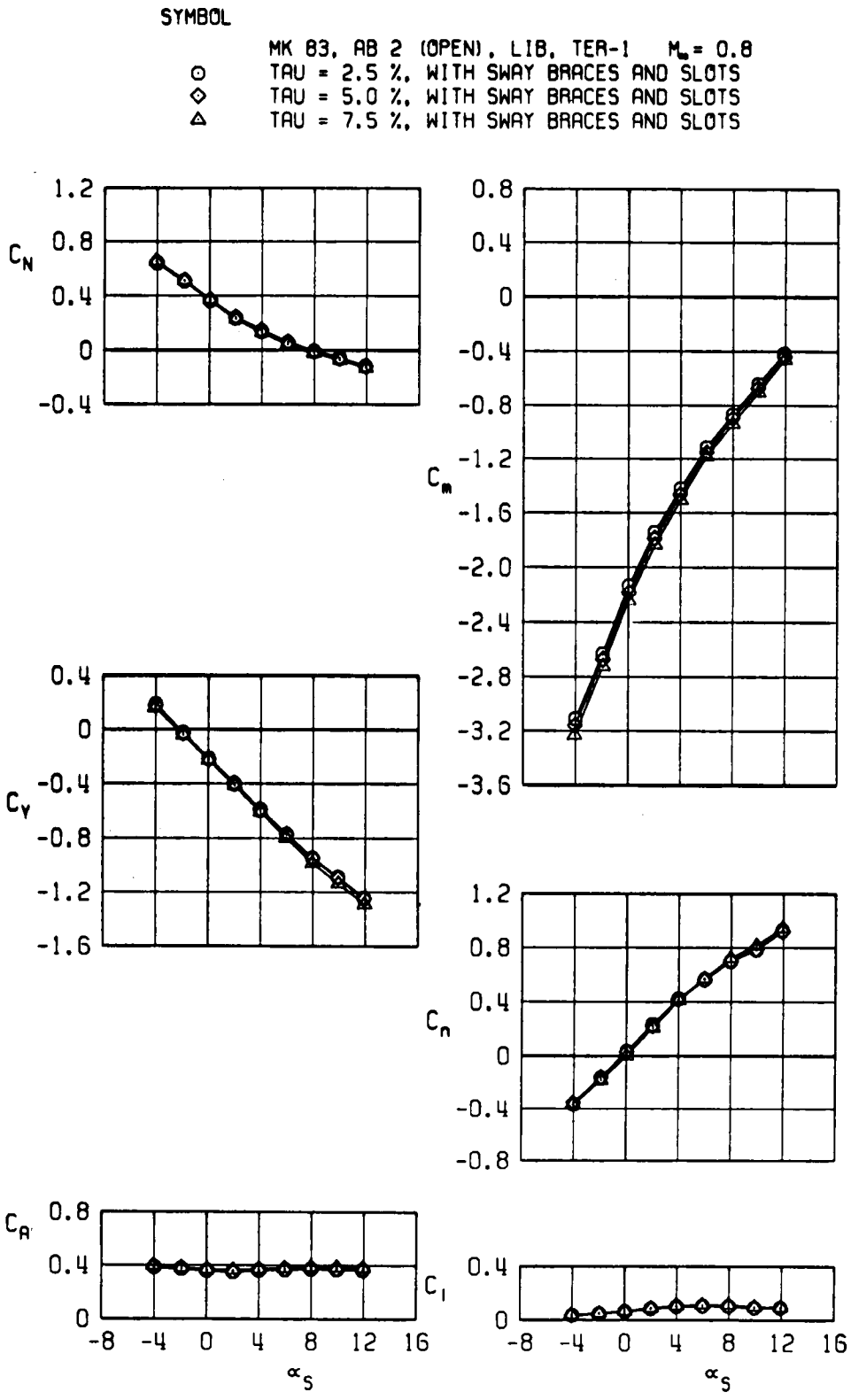

b. $M_\infty = 0.8$

Figure 32. (Continued)

better agreement with flight test data than data obtained in the flow field of the simple TER model. At Mach numbers above 0.6, comparisons of wind tunnel and flight test data did not clearly favor either TER model configuration. Variations in wind tunnel unit Reynolds number and wall porosity did not help the overall comparison of wind tunnel and flight test data. Further analyses of the flight and wind tunnel test data may be found in References 9 and 10.

Discrepancies between wind tunnel data and the flight test data base have been discussed. The effect of such discrepancies on the separation characteristics of the MK-83 bomb from the F-4 aircraft were investigated experimentally in the wind tunnel and analytically using a six-degree-of-freedom trajectory prediction program.

The effects of TER geometry on wind tunnel trajectory simulation are shown in Figure 33 as a function of flight time. The detailed TER model induced larger nose down pitch and outboard yaw rates than did the simple TER model design. The larger angular rates correlate well with trends observed during carriage position airloads testing. Except at a Mach number of 0.6, the increased nose down pitch rate caused contact between the MK-83 model support sting and the aircraft thus terminating the trajectory.

Analytical trajectories were computed using the Fojt six-degree-of-freedom trajectory prediction program described in Reference 11. The equations of motion used in the program are based on those defined in Reference 12,

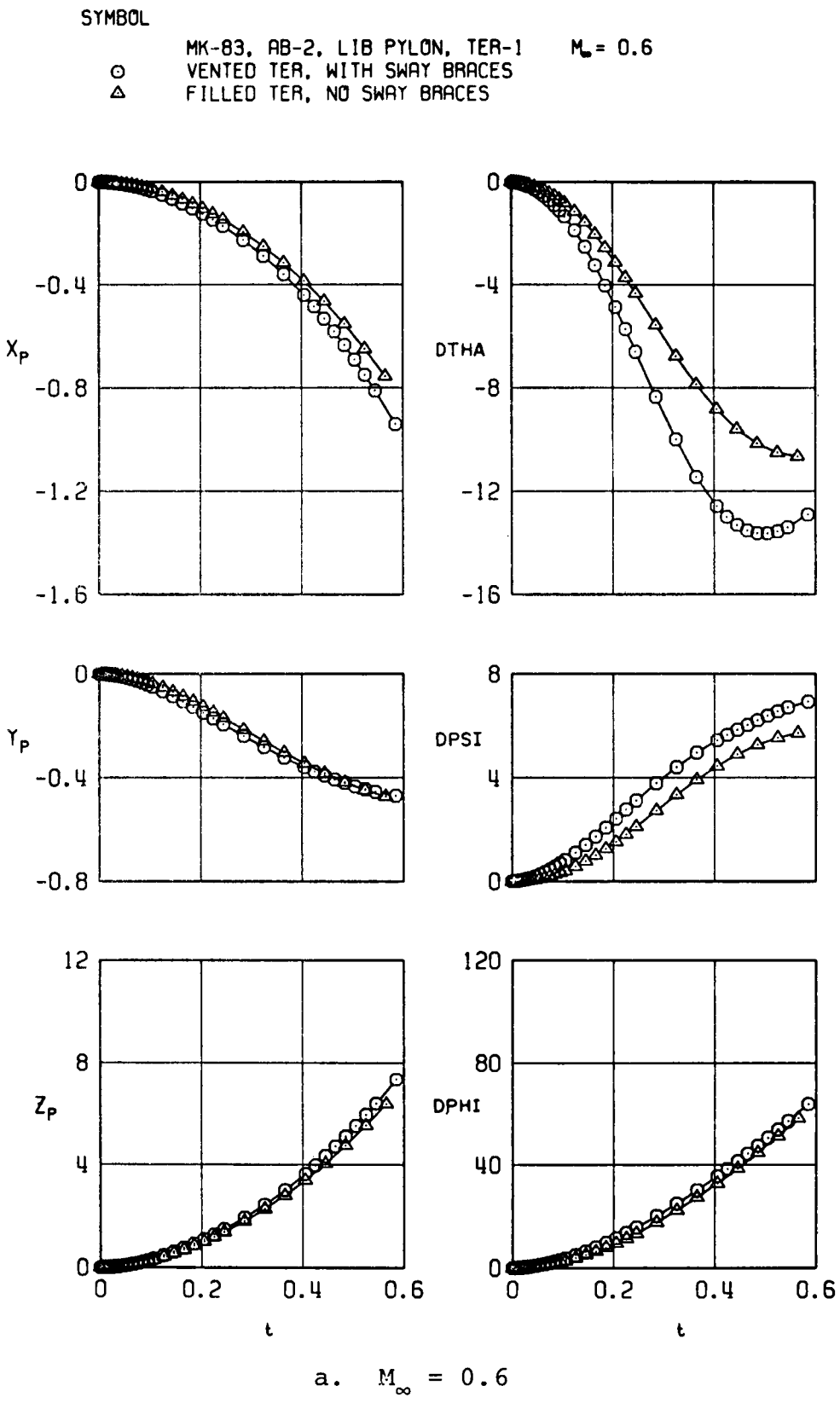

a. $M_\infty = 0.6$

Figure 33. The effects of TER geometry on wind tunnel trajectory simulations.

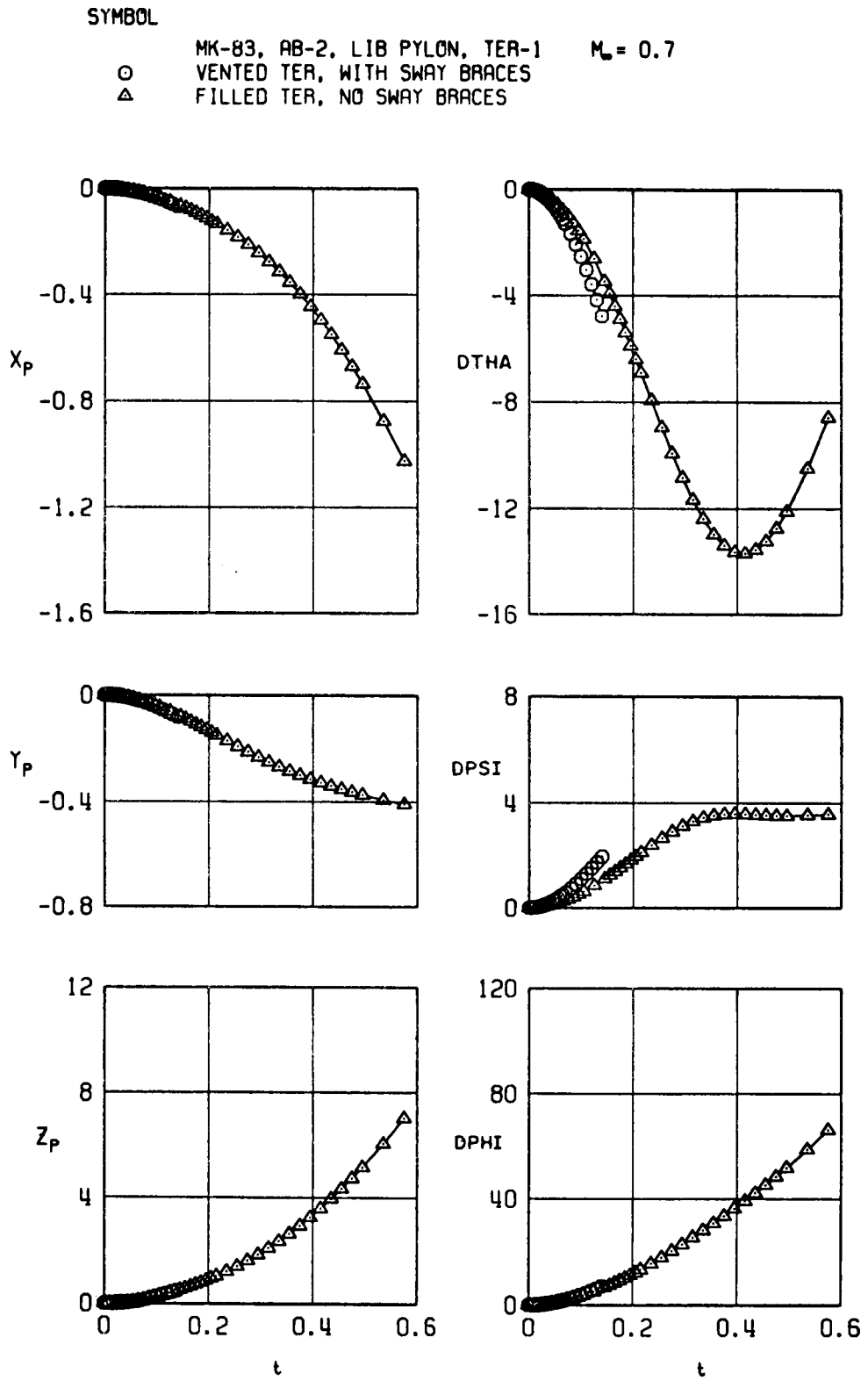

b. $M_\infty = 0.7$

Figure 33. (Continued)

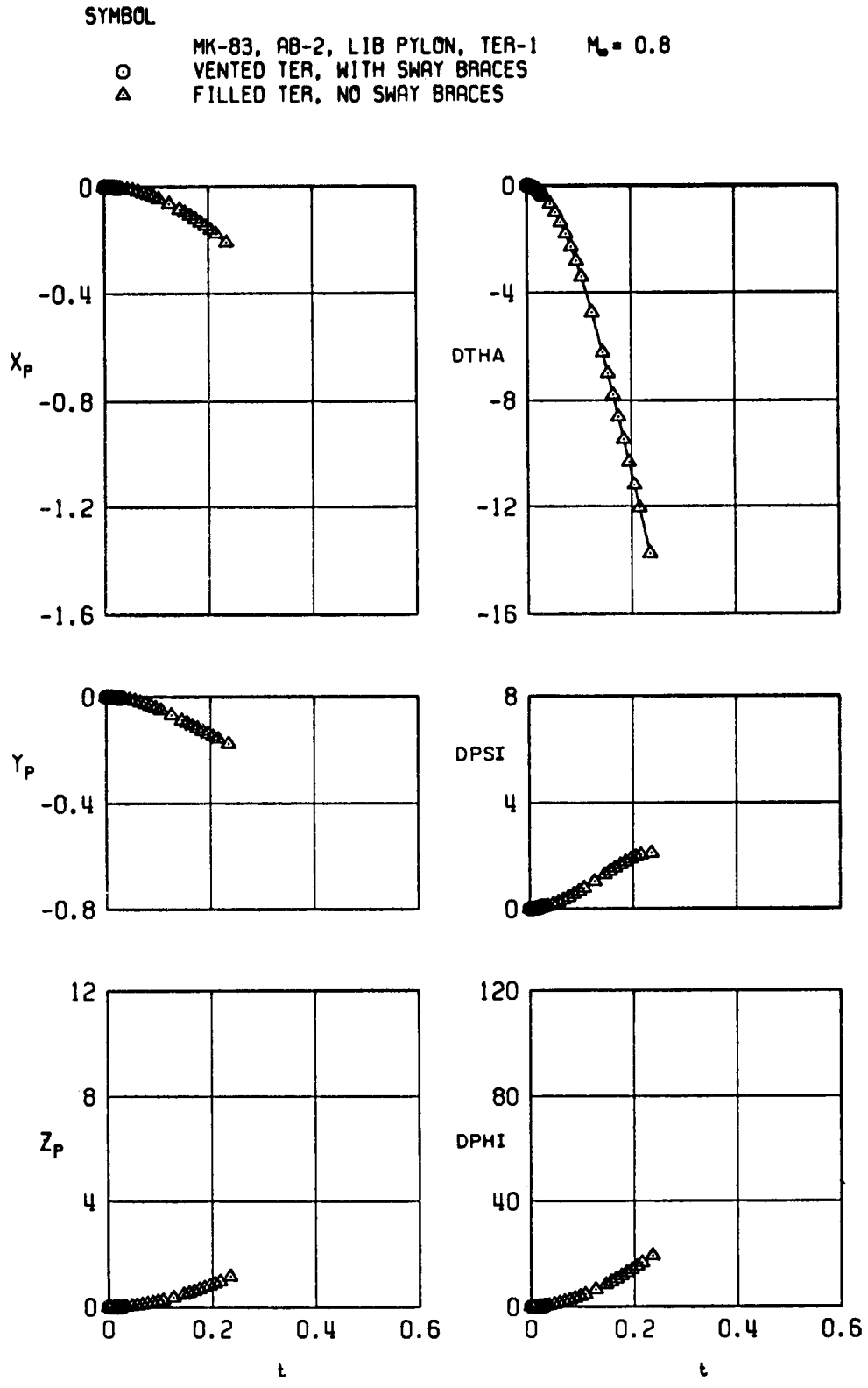

c. $M_\infty = 0.8$

Figure 33. (Continued)

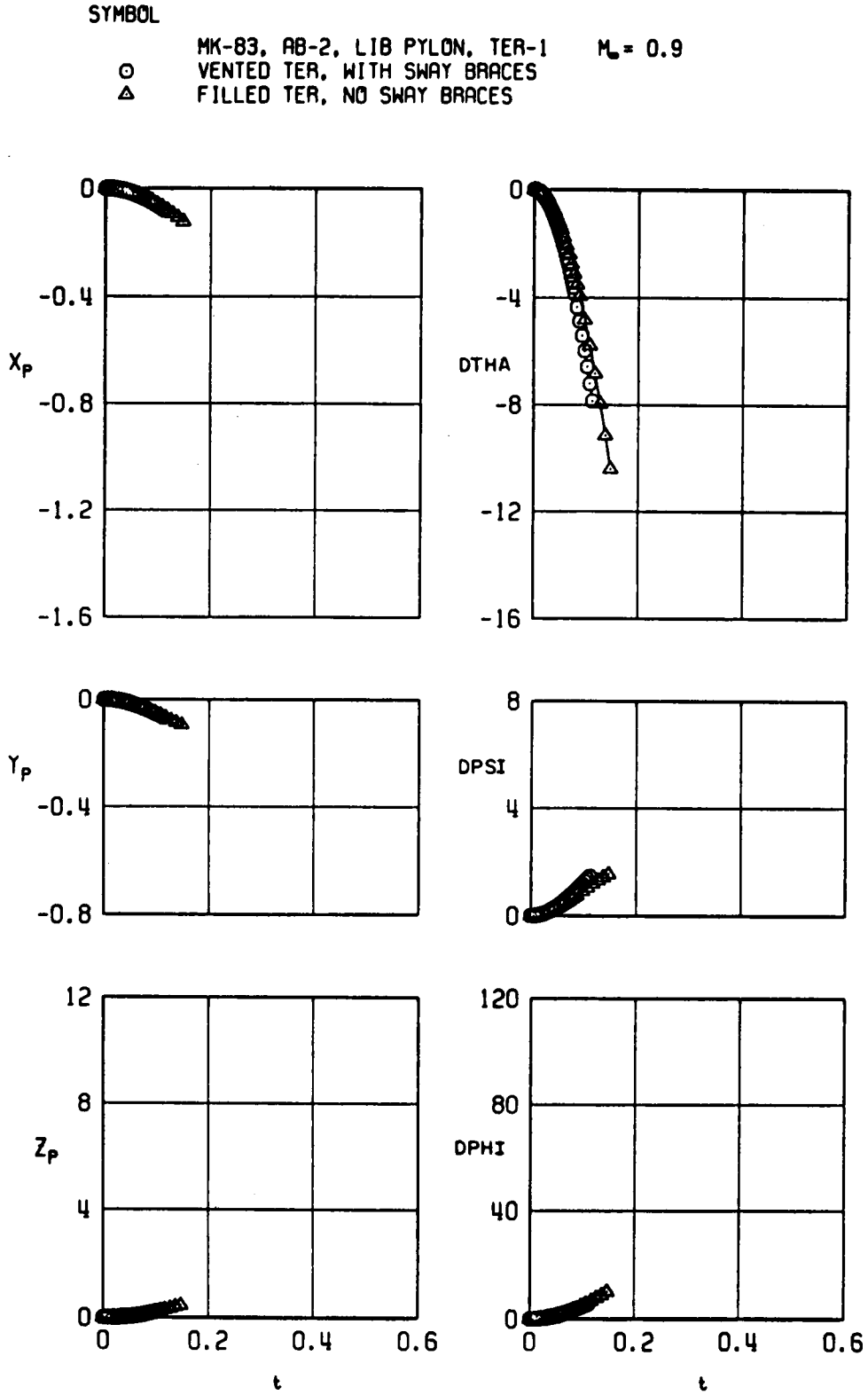

d. $M_\infty = 0.9$

Figure 33. (Continued)

Chapter IV. The equations of motion were integrated by a fourth-order Runge-Kutta method. Store related inputs included mass properties, free-stream aerodynamic coefficients, and interference aerodynamic coefficients. Interference coefficients, at various vertical displacements perpendicular to TER station one, were calculated by subtracting free-stream coefficient data from coefficient data obtained in the flow field of the F-4 aircraft model at the same store model angle of attack. The free-stream and flow field coefficient data were obtained in the wind tunnel using the CTS data acquisition technique.

Trajectories were computed in order to assess differences between flight and wind tunnel carriage position airloads data. Flight and wind tunnel coefficient data obtained at the carriage position were graphically faired to CTS wind tunnel coefficient data obtained in the flow field of the aircraft model. The results were a family of interference coefficient data curves. One example of a family of interference coefficient data curves is shown in Figure 34 as a function of vertical displacement. Interference coefficients thus calculated were used in the trajectory prediction program. Trajectories were calculated for Mach numbers of 0.6 and 0.8 at various aircraft angles of attack. The trajectories were initiated at an altitude of five-thousand feet. The results are meant only to show the incremental effects of carriage position airloads.

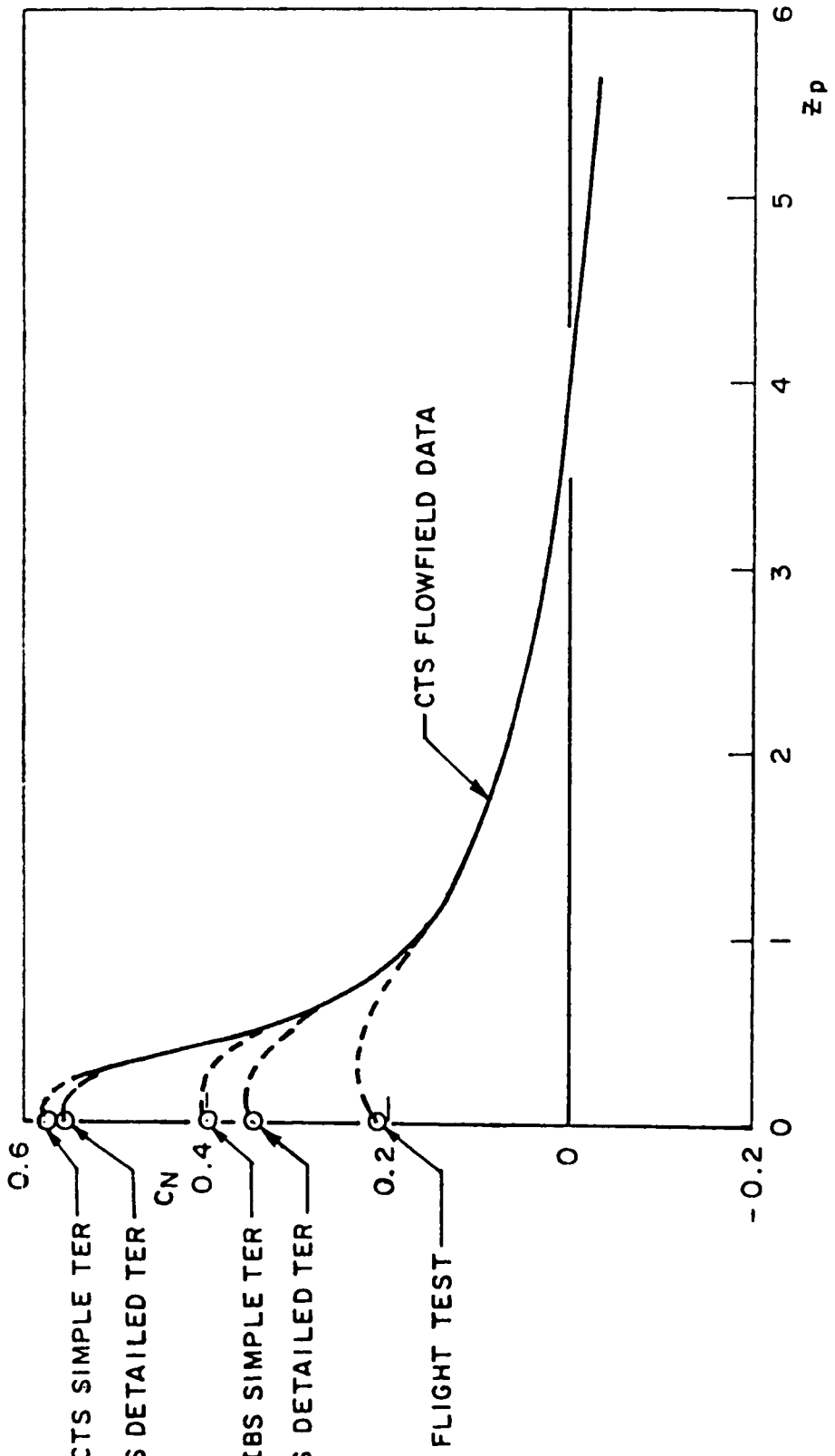

Figure 34. One example of a family of interference coefficient data curves.

Computer predicted trajectories were examined for trends which could cause store-aircraft collisions and for store ground dispersion effects. The effects of experimental carriage position airloads on the predicted pitch orientation of the MK-83 bomb are presented in Figures 35 and 36 as a function of vertical displacement. The nose down pitch orientation rate increases with increasing Mach number and angle of attack as do wind tunnel trajectory simulations. Carriage position airloads, as measured by the various techniques, do not significantly alter the trajectory of the MK-83 bomb at a Mach number of 0.6. However, the importance of accurate carriage position airload measurements is evident at a Mach number of 0.8. Normal-force and pitching-moment coefficients measured during CTS testing caused the trajectory of the MK-83 bomb to prematurely cross the collision boundary at a store angle of attack of minus two degrees and caused an erroneous collision indication at a store angle of attack of 0.15 degrees. Better trajectory comparisons near the aircraft were obtained from using IBS carriage position airloads data. At vertical displacements greater than five feet, the trajectory of the MK-83 bomb is no longer significantly effected by initial carriage position airloads.

The effect of experimental carriage position airloads on the predicted ground dispersion of the MK-83 bomb at various angles of attack is shown in Figure 37. At discrete angles of attack, trajectory impact points obtained using interference coefficient curves derived from wind

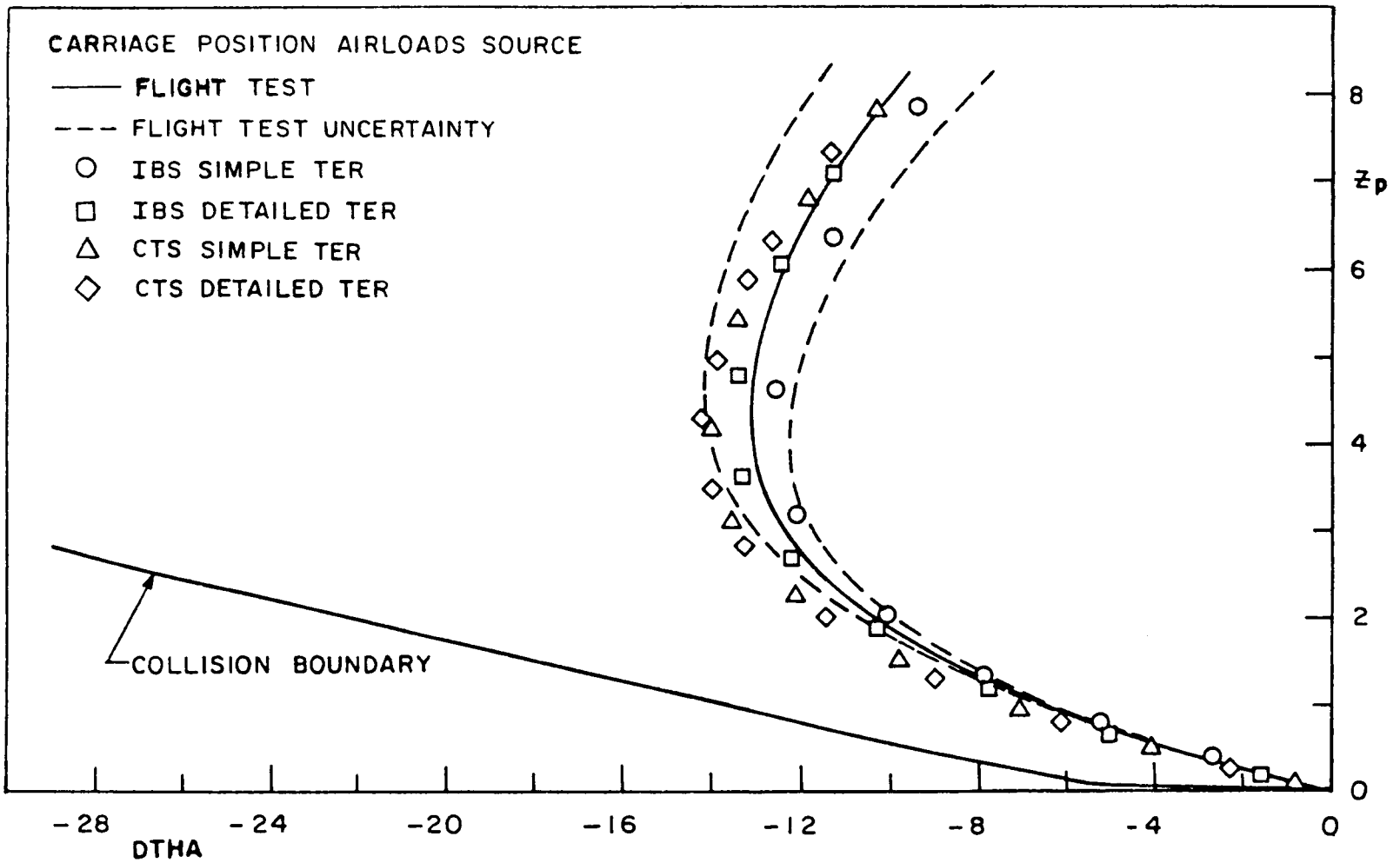

a. $\alpha_s = -1.9°$

Figure 35. The effects of experimental carriage position airloads on the predicted pitch orientation of the MK-83 bomb, $M_\infty = 0.6$.

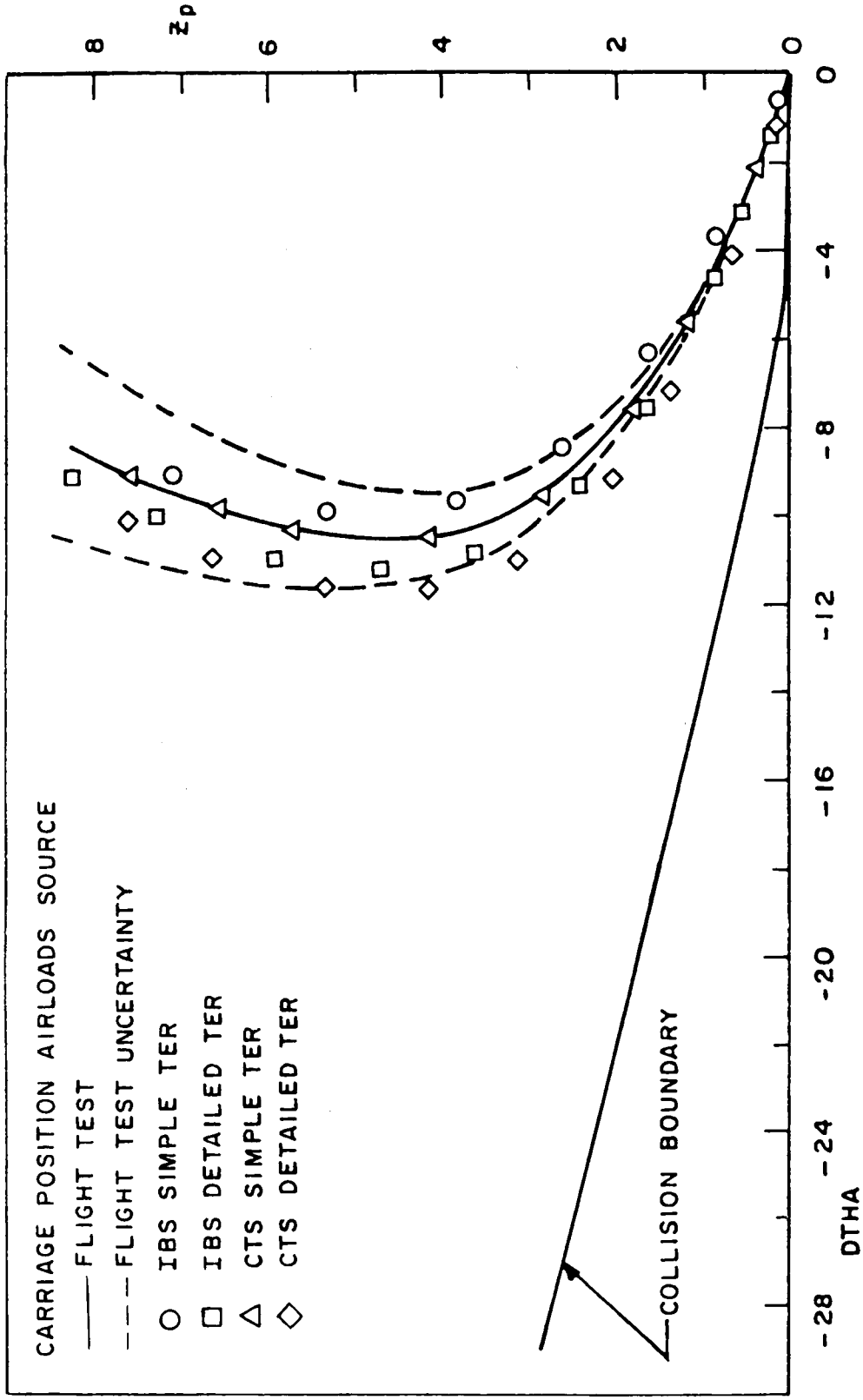

b. $\alpha_s = 2.2°$

Figure 35. (Continued)

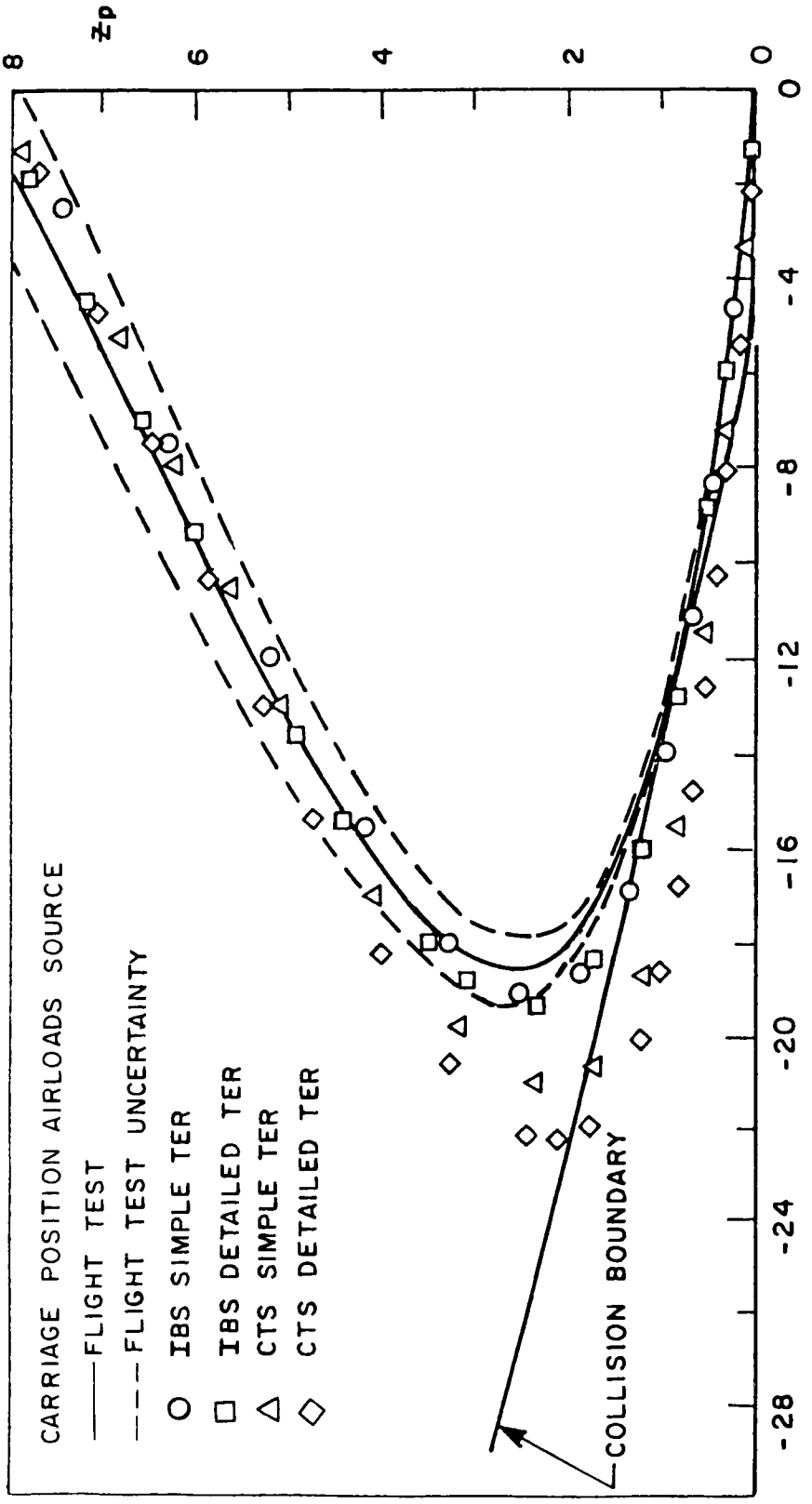

a. $\alpha_s = -2.0°$

Figure 36. The effects of experimental carriage position airloads on the predicted pitch orientation of the MK-83 bomb, $M_\infty = 0.8$.

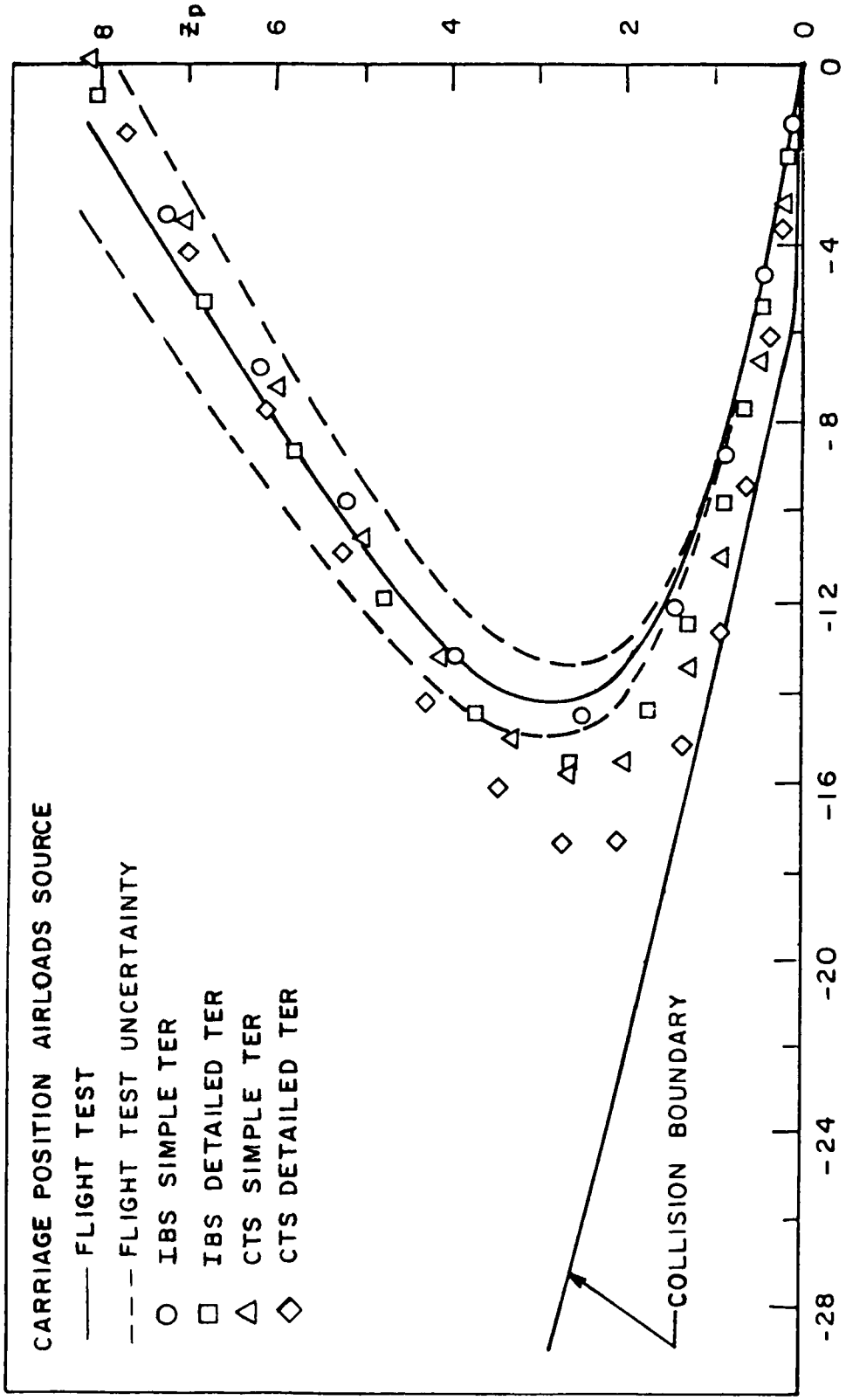

b. $\alpha_s = 0.15°$

Figure 36. (Continued)

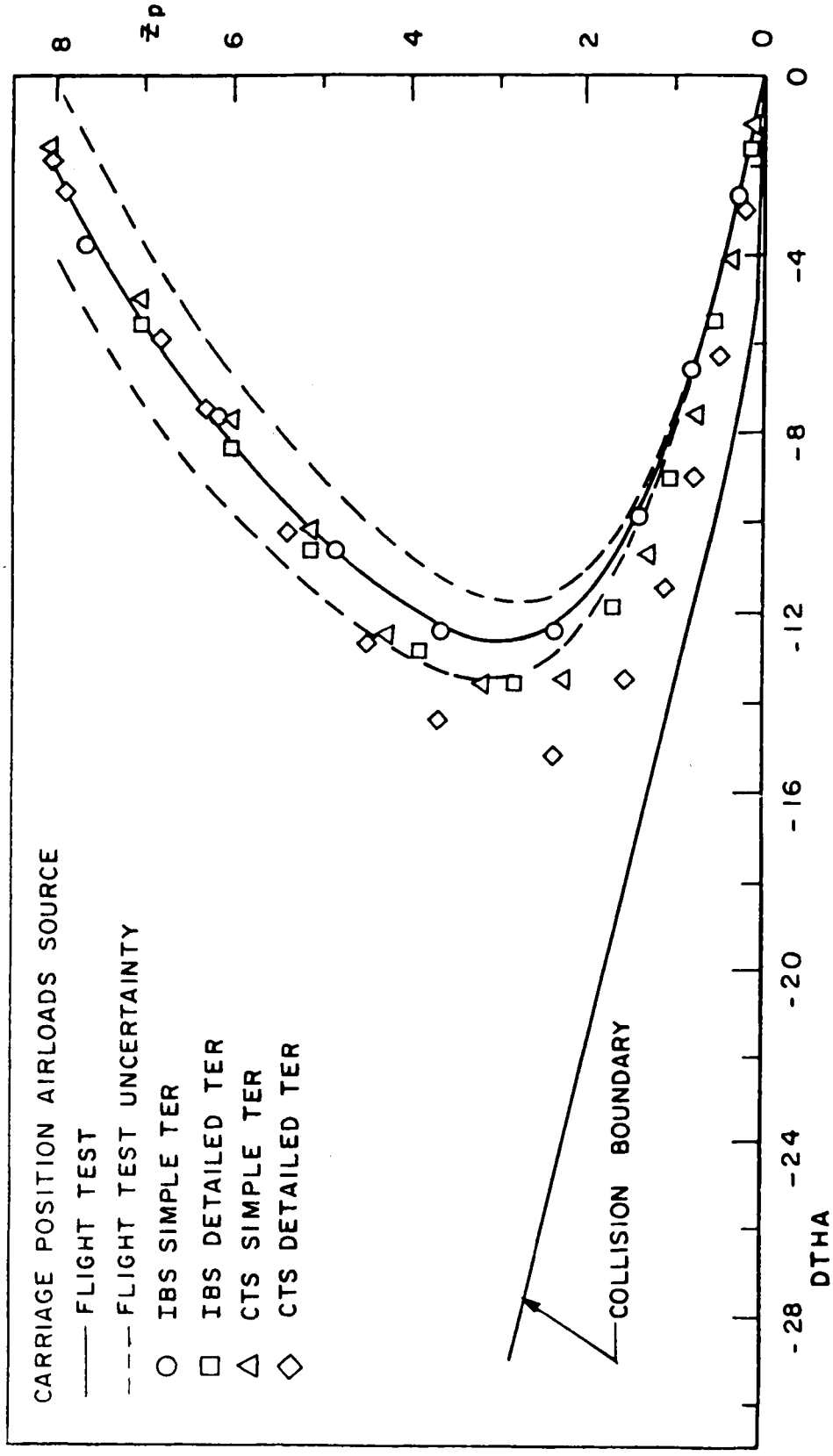

c. $\alpha_s = 2.2°$

Figure 36. (Continued)

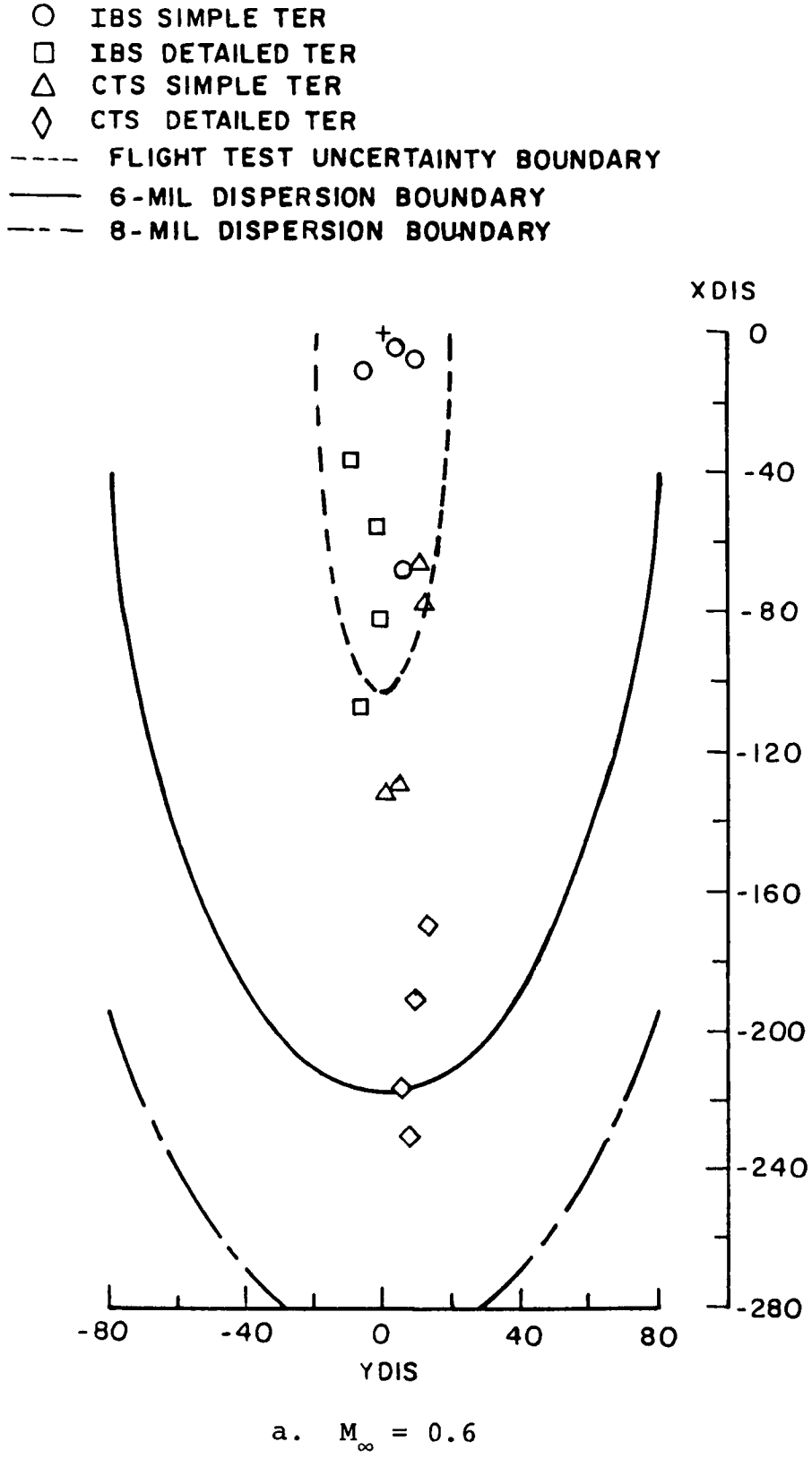

a. $M_\infty = 0.6$

Figure 37. The effect of experimental carriage position airloads on the predicted ground dispersion of the MK-83 bomb at various angles of attack.

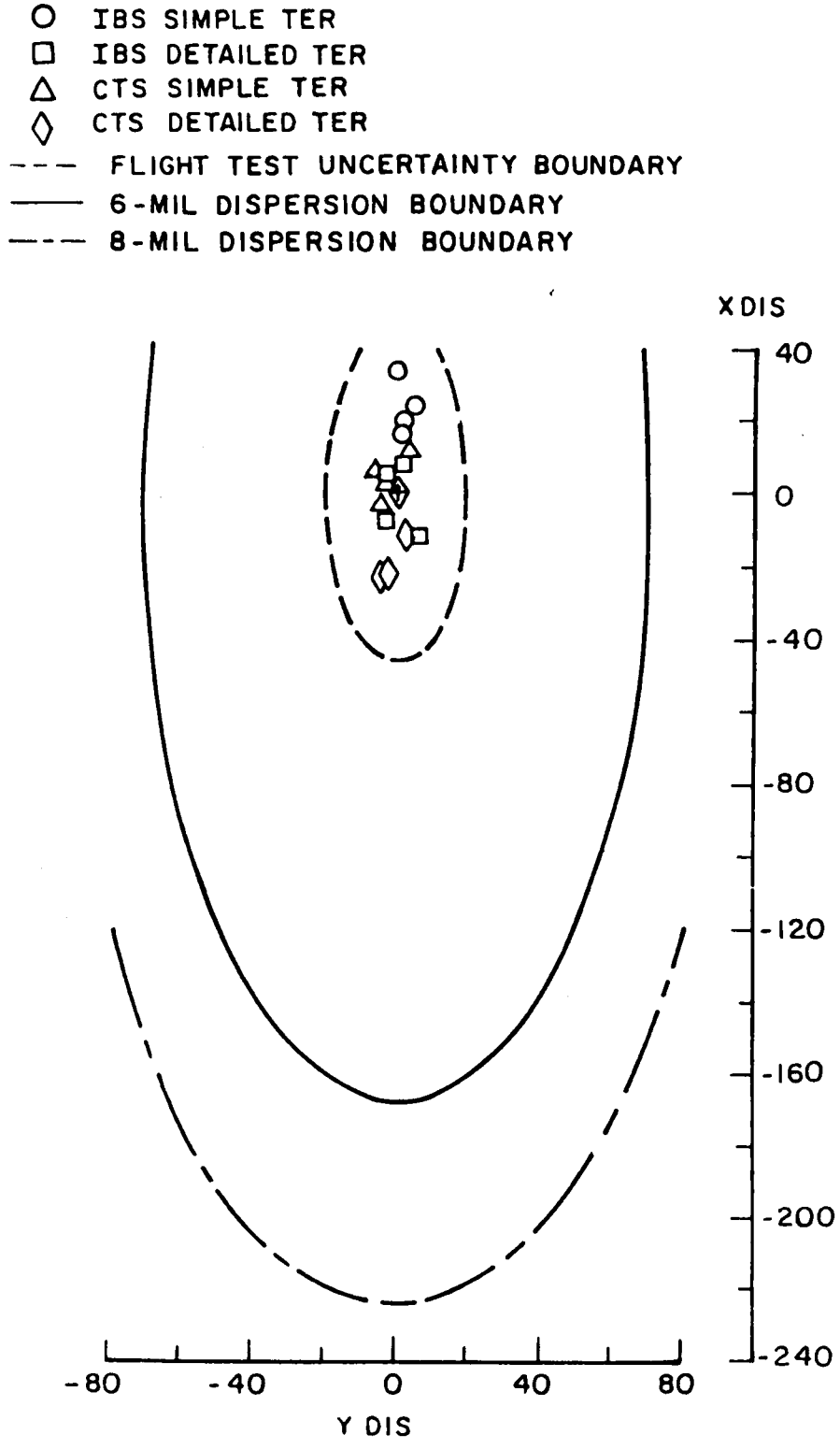

b. $M_\infty = 0.8$

Figure 37. (Continued)

tunnel carriage position airloads were referenced to the impact point obtained from interference coefficient curves from flight test data. Hence, individual angles of attack are not identified. A flight test uncertainty boundary was calculated by adding coefficient uncertainties to the interference coefficient curves derived from flight test data; no uncertainties were added to the free-stream coefficient data. The resulting boundaries are shown in Figure 37. Even though the axial dispersion of some impact points fall outside the flight test uncertainty boundary at a Mach number of 0.8, the maximum axial dispersion was less than 2 percent of the axial distance traveled from release to impact and was within the typical six to eight mil dispersion area quoted for this type of weapon. The typical dispersion area is a primary result of aircraft flight dynamics, ejector force variations, atmospheric turbulence, and weapon production tolerances.

The effect of carriage position airloads on the trajectory of the MK-83 bomb from TER station one has been shown to influence the initial portion of each trajectory. The trajectory became critical as the product of the positive normal-force and the negative pitching-moment coefficient approached -1.5. The positive normal force reduced the vertical displacement rate while the negative pitching moment increased the nose down pitch rate. Both combine to yield possible store-aircraft collisions. The effect of carriage position airloads on ground dispersion was found to be insignificant.

CHAPTER V

CONCLUSIONS

A study of carriage position airloads has been conducted. Meaningful comparisons between flight and wind tunnel data can be made when extreme care is taken in setting up the experimental investigations. In particular, since store aerodynamics are a strong function of the local flow environment, store positioning is critical. The acquisition of flight test data must be made during transient flight maneuvers during which aerodynamic loads are small in comparison to inertial loads. Hence, every effort should be made to minimize store mass and accelerometer uncertainties.

A detailed investigation of carriage position airloads and their effect on trajectory simulations was made for a MK-83 bomb mounted to the number one TER station on the inboard pylon of an F-4 aircraft. The results are as follows:

1. Flight test data obtained during high "g" maneuvers indicated a strong possibility of accelerometer divergence. Data obtained during such aircraft maneuvers were questionable.

2. The extreme weight of the instrumented MK-83 bomb combined with accelerometer uncertainties resulted in large aerodynamic flight test coefficient uncertainties.

3. Normal-force and pitching-moment coefficient data obtained in the wind tunnel at TER station one, dummy

stores on TER stations two and three, were significantly influenced by simulating TER sway brace arms. Venting slots had little or no effect on coefficient data for this aircraft-store configuration.

4. Better correlation between flight and wind tunnel carriage position airloads was obtained using the IBS rather than the CTS wind tunnel data acquisition technique. The latter technique was subject to CTS positioning errors. The subsequent minimization of these positioning errors should improve future data correlation.

5. The detailed TER model improved the correlation between IBS wind tunnel data and flight test data at a Mach number of 0.6. However, at Mach numbers above 0.6, comparisons did not clearly favor either TER model configuration.

6. Coefficient increments induced by varying the wind tunnel wall porosity and Reynolds number did little to improve the overall comparisons between wind tunnel and flight test data.

7. Correcting CTS carriage position coefficients to account for the presence of the store model sting support and the store model afterbody modification did little to improve wind tunnel and flight test data comparisons.

8. Trajectories computed using IBS carriage position airloads compared favorably with trajectories computed using flight test carriage position airloads, especially at a Mach number of 0.8. Trajectories computed using CTS carriage position airloads generally resulted in larger nose

down pitch rates than those computed using IBS data. In some instances, the larger nose down pitch rate caused the store to cross the collision boundary.

9. Trajectories computed in order to evaluate the TER model geometry indicate that neither TER configuration is favored at a Mach number of 0.6 but that the simple TER configuration is favored at a Mach number of 0.8.

10. The trajectory of the MK-83 bomb was not significantly effected by carriage position airloads beyond vertical displacements of five feet.

LIST OF REFERENCES

LIST OF REFERENCES

1. Schindel, L. H. "Store Separation," Advisory Group for Aerospace Research and Development, AGARD-AG-202, June 1975.

2. Mattasits, G. R. Experimental data in the flow field of a transonic wing configuration. Private communication.

3. Dix, R. E. Methods for measuring aerodynamic forces and moments acting on captive stores in the wind tunnel. Private communication.

4. Test Facilities Handbook (Tenth Edition). "Propulsion Wind Tunnel Facility, Vol. 4." Arnold Engineering Development Center, May 1974.

5. Hill, D. W., Jr. Experimental data on factors affecting the wind tunnel measurements of carriage-position airloads. Private communication.

6. Marsden, P. "Design Study for the Installation of a Two-Sting Rig for Captive Store Trajectory Simulation." Aircraft Research Association Limited, January 1976.

7. Dix, R. E. "Comparison of Two Methods Used to Measure Aerodynamic Loads Acting on Captive Store Models in Wind Tunnel Tests." Arnold Engineering Development Center AEDC-TR-76-122, September 1976.

8. Dix, R. E. "Influences of Sting Support on Aerodynamic Loads Acting on Captive Store Models." Arnold Engineering Development Center AEDC-TR-76-1, March 1976.

9. Maddox, A. R., Dix, R. E., and Mattasits, G. R. "In-Flight Measurements of Captive Loads on a Store as Compared with Wind Tunnel and Mathematical Simulations." Naval Weapons Center NWC TP 6026, April 1978.

10. Dix, R. E. Comparison of wind tunnel and flight test measurements of static aerodynamic loading of a captive store. Private communication.

11. Rogers, R. M. Six-degree-of-freedom store trajectory program. Private communication.

12. Etkin, B. "Dynamics of Flight: Stability and Control." John Wiley & Sons, Inc., New York, 1959.

13. Summers, W. E. Experimental data in the flow field of the F-4C aircraft. Private communication.

14. Roberts, R. H. Experimental data in the flow field of the Nielsen aircraft model. Private communication.

APPENDIXES

APPENDIX A

ESTIMATION OF INERT SHELL ELEMENT EFFECTS

Elements of the MK-83 bomb shell were isolated to provide attachment points and bearing surfaces for the TER suspension hooks and sway brace pads, respectively. Aerodynamic loads acting on the inert elements were not sensed by the balance. Coefficient data obtained during the flight test were, therefore, subject to a bias error. An estimation of this error was made using pressure data obtained in the four-foot wind tunnel at AEDC.

Circumferential pressure coefficient data were obtained for a tangent-ogive-cylinder model mounted at the number one TER station on the left wind inboard pylon of an F-4C aircraft model (Reference 13) and on the Nielsen transonic wing-body model (Reference 14). Details and dimensions of the pressure model and the Nielsen model are given in Figures A-1 and A-2, respectively.

Local normal-force coefficients were first calculated for the pressure model assuming no inert elements. The coefficients were obtained by integrating the circumferential pressure coefficient distribution at each longitudinal pressure orifice location. Circumferential pressure coefficient distributions obtained for the pressure model in the flow field of the Nielsen model are shown in Figure A-3 and were obtained at a Mach number of 0.7 at an angle of attack of six

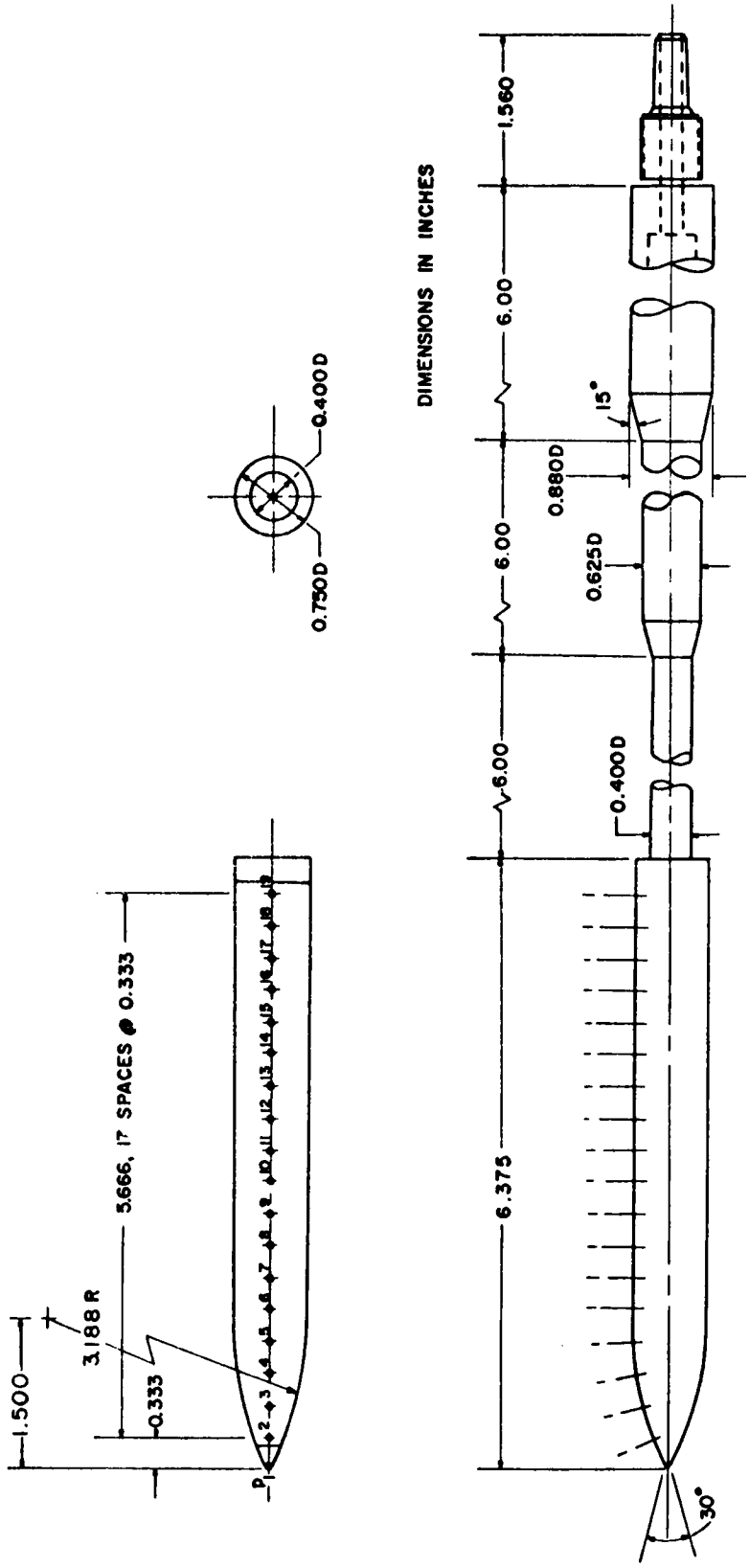

Figure A-1. Details and dimensions of the pressure model.

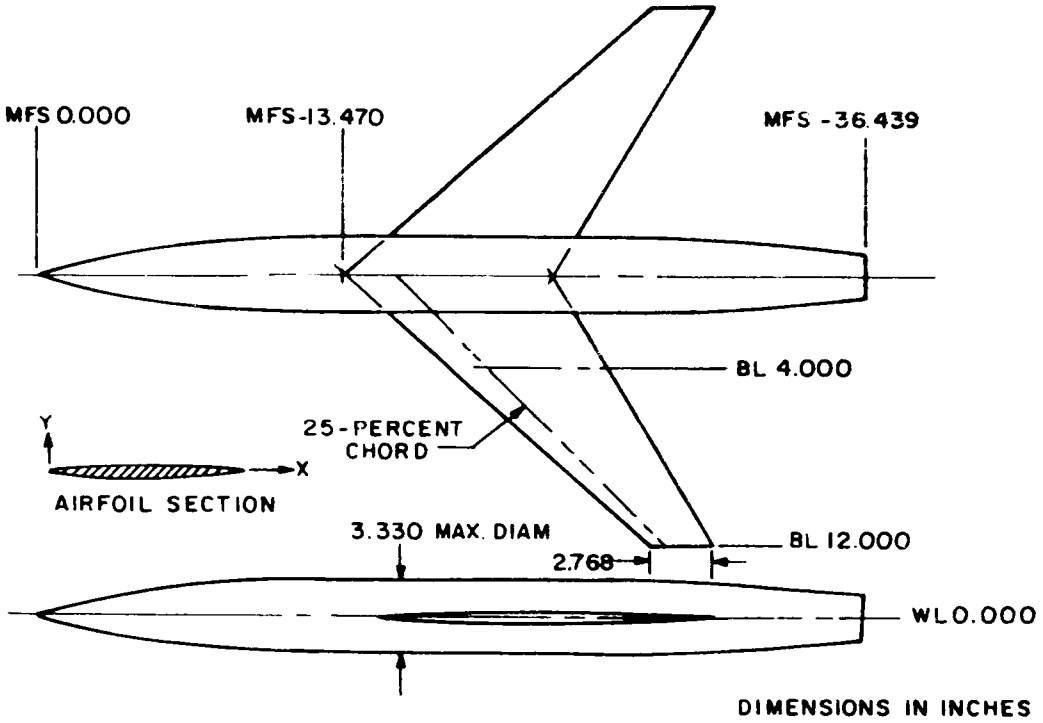

BODY COORDINATES

STATION PERCENT LENGTH	RADIUS PERCENT LENGTH
0.00	0.00
3.28	0.91
6.57	1.71
9.86	2.41
13.15	3.00
16.43	3.50
19.72	3.90
23.01	4.21
26.29	4.43
29.58	4.53
32.00	4.57
75.34	4.57
76.69	4.54
79.98	4.38
83.26	4.18
86.55	3.95
89.84	3.72
93.13	3.49
96.41	3.26
100.00	3.02

AIRFOIL COORDINATES

X, % CHORD SEE SEC.	Y, % CHORD SEE SEC.
0.00	0.000
0.50	0.464
0.75	0.563
1.25	0.718
2.50	0.981
5.00	1.313
7.50	1.591
10.00	1.824
15.00	2.194
20.00	2.474
25.00	2.687
30.00	2.842
35.00	2.945
40.00	2.996
45.00	2.992
50.00	2.925
55.00	2.793
60.00	2.602
65.00	2.364
70.00	2.087
75.00	1.775
80.00	1.437
85.00	1.083
90.00	0.727
95.00	0.370
100.00	0.013
L.E. RADIUS 0.229 % CHD	
T.E. RADIUS 0.014 % CHD	

Figure A-2. Details and dimensions of the Nielsen model.

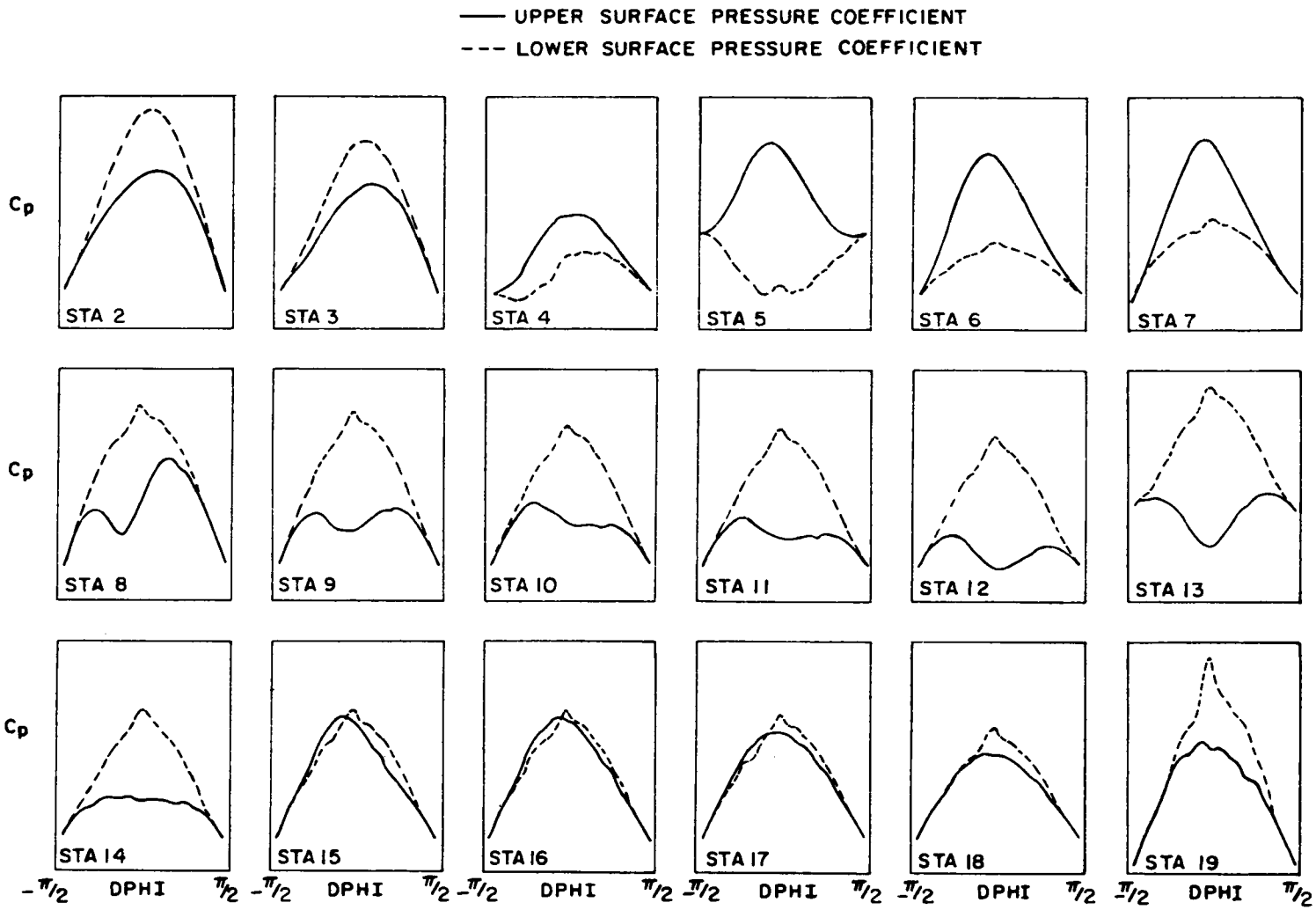

Figure A-3. Circumferential pressure coefficient distributions.

degrees. Local normal-force coefficients were then calculated for the pressure model with inert elements. The elements were simulated by substituting a cavity pressure coefficient for the surface pressure coefficient associated with each element. The cavity pressure coefficient was a weighted average of the model surface pressure coefficients at the perimeters of the simulated elements.[1] Examples of circumferential pressure coefficient distributions associated with the various inert elements are shown in Figure A-4.

The total normal-force coefficient was calculated by integrating the local normal-force coefficients over the model length. The pitching-moment coefficient was obtained by multiplying each local normal-force coefficient by its distance to the moment reference point and then integrating the results over the model length. Examples of local normal-force and pitching-moment coefficient distributions with and without simulated inert-shell elements are presented in Figure A-5.

Three sets of calculated normal-force and pitching-moment coefficients were obtained for the pressure model. The ratios of the coefficients calculated for the pressure model with simulated elements to those calculated for the model without simulated elements are given below:

---

[1]Although not measured, the cavity pressure of the MK-83 bomb was believed to have been a major function of the surface pressures acting at the isolation gaps.

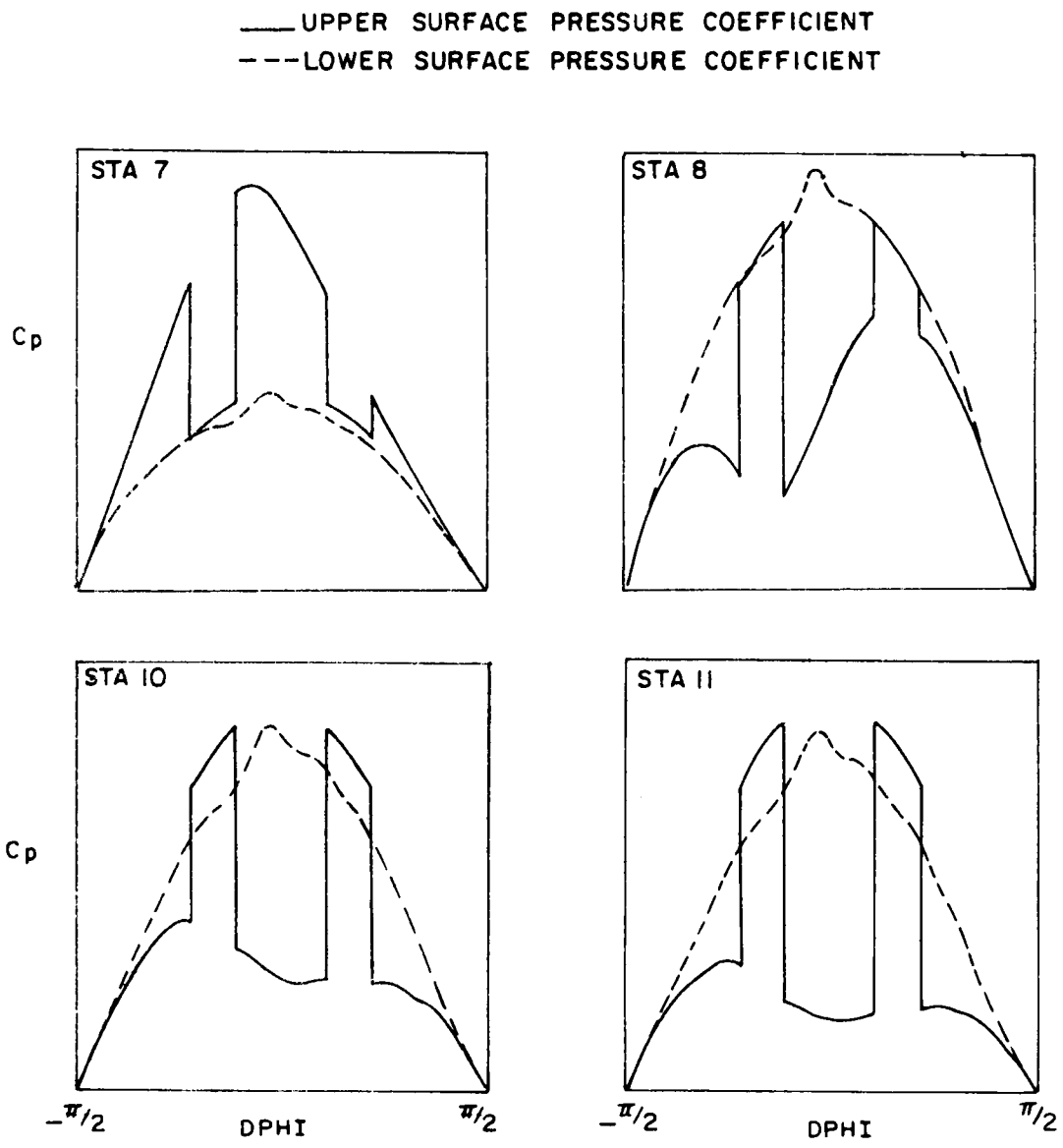

a. Circular elements

Figure A-4. Circumferential pressure coefficient distributions associated with various inert elements.

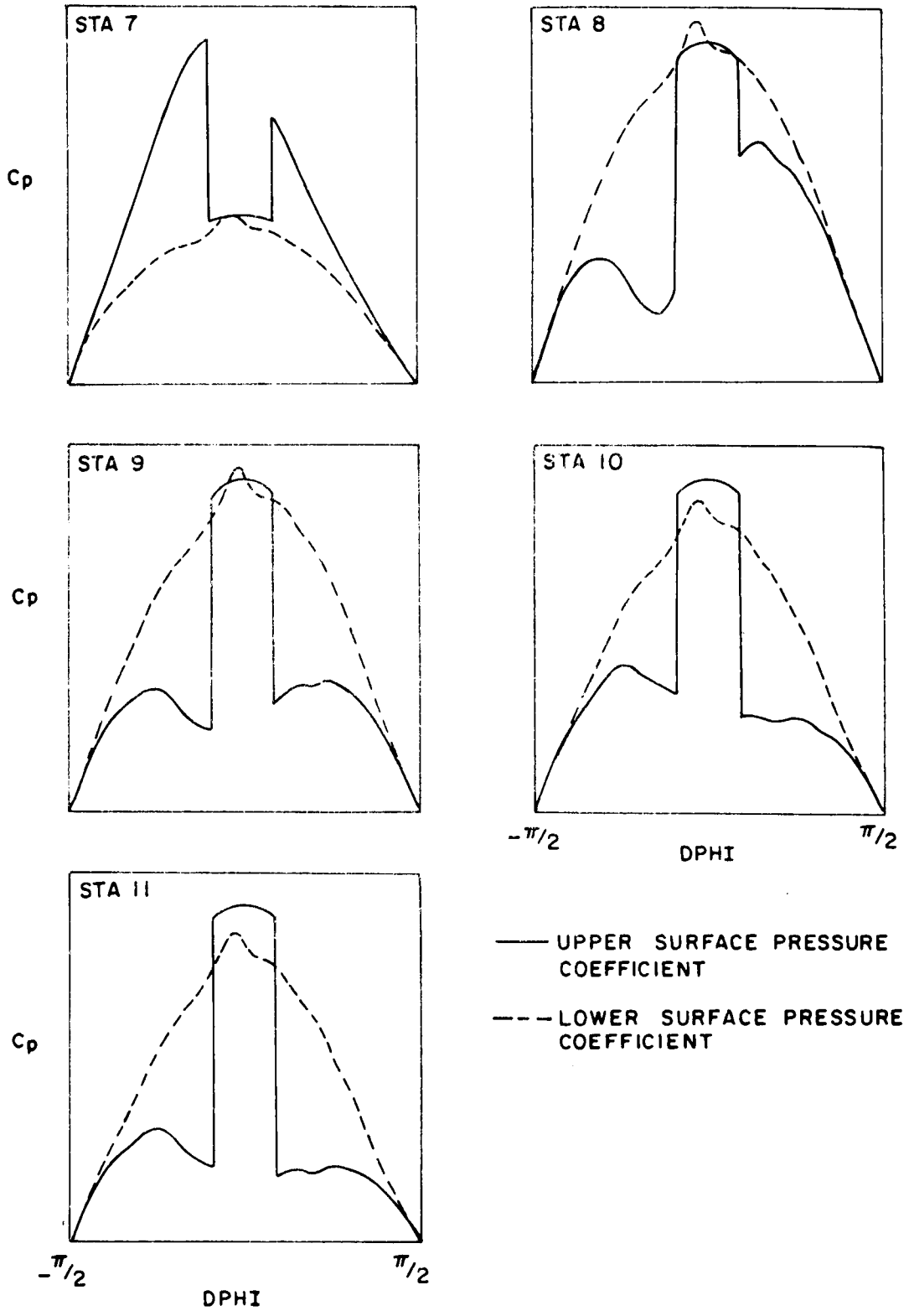

b. Rectangular elements

Figure A-4. (Continued)

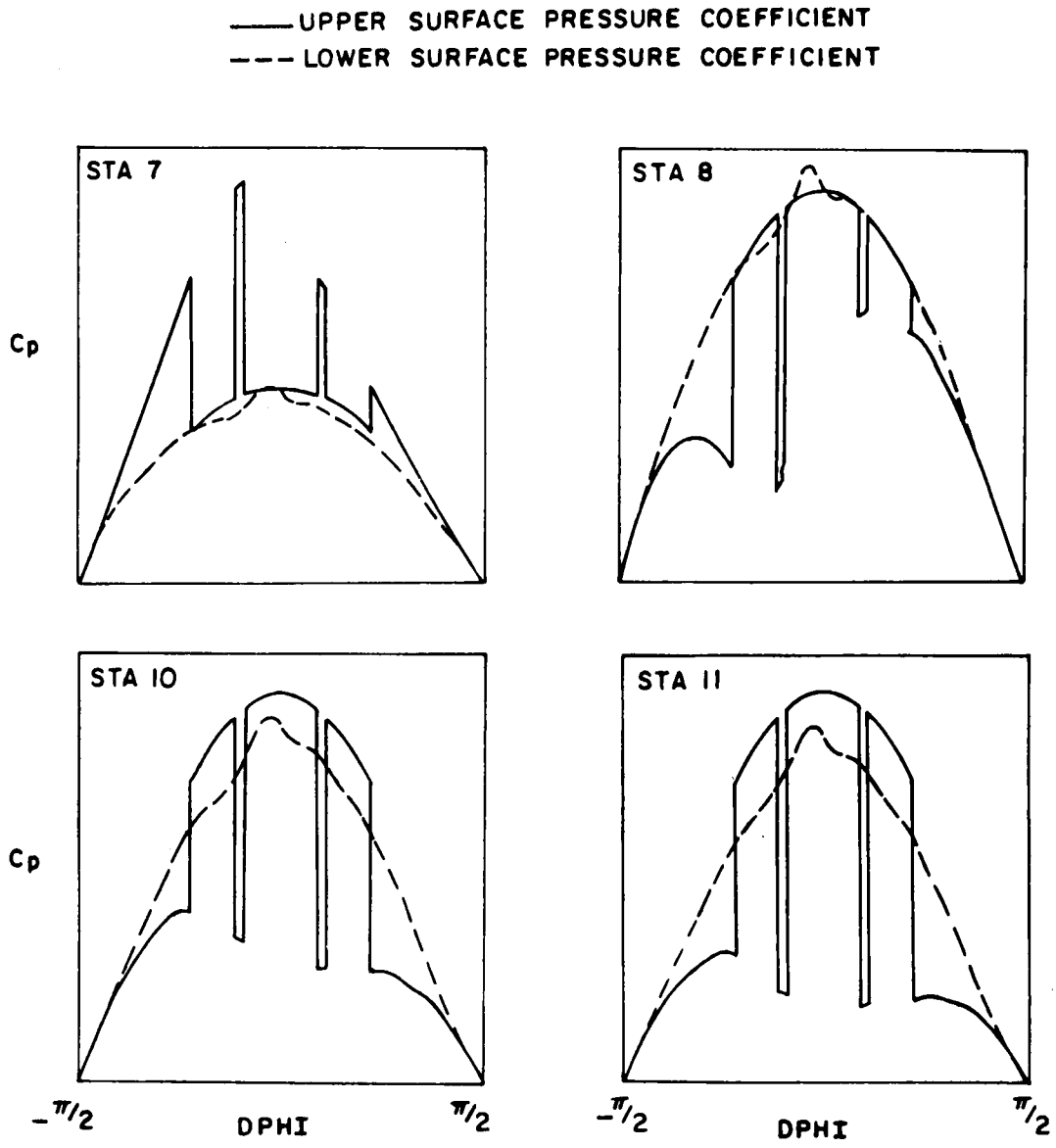

c. Circular and rectangular elements

Figure A-4. (Continued)

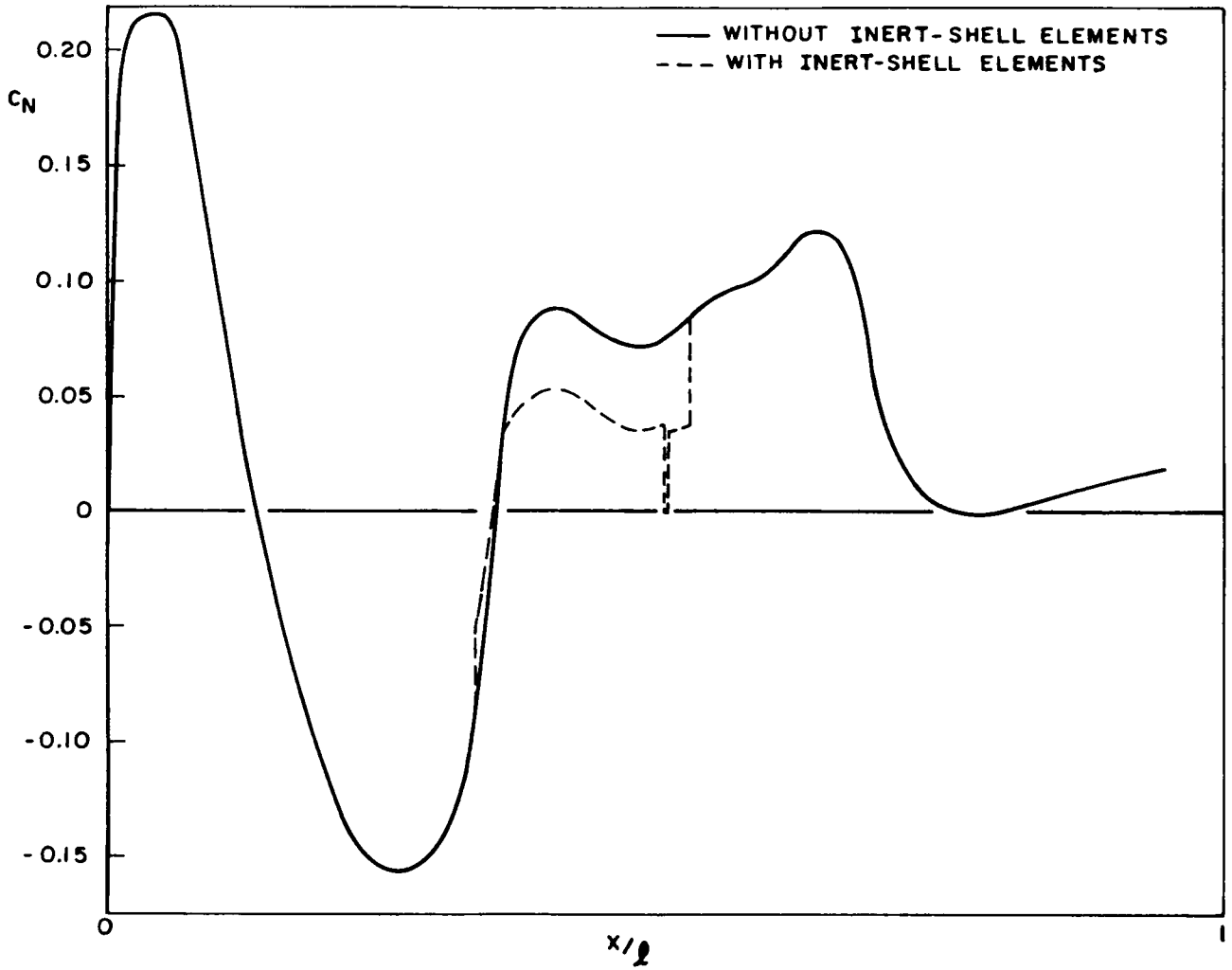

a. Local normal-force coefficient

Figure A-5. Examples of local normal-force and pitching-moment coefficient distributions with and without simulated inert-shell elements.

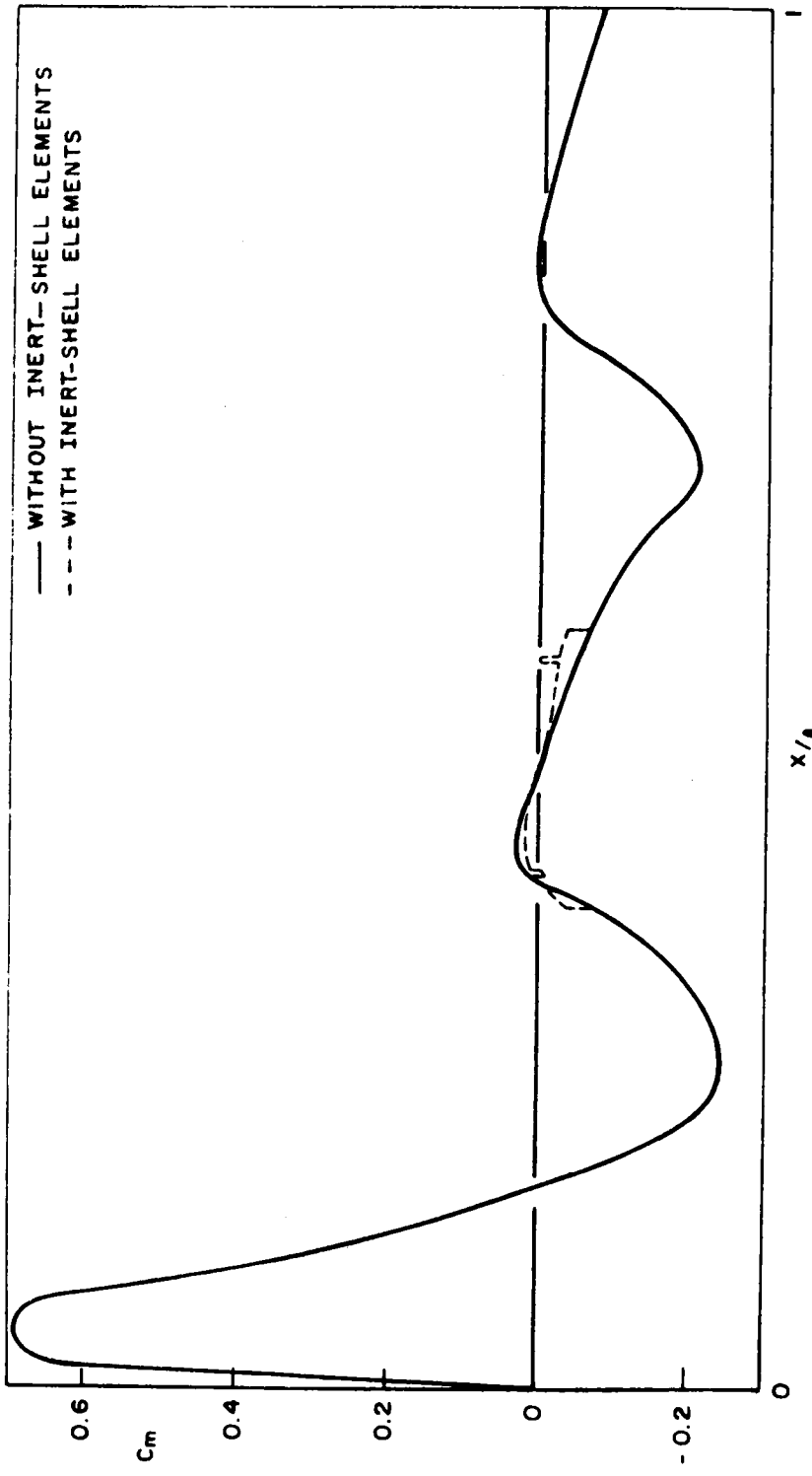

b. Local pitching-moment coefficient

Figure A-5. (Continued)

Aircraft Model	Mach Number	Aircraft Angle of Attack	$\frac{C_{N_w}}{C_{N_{wo}}}$	$\frac{C_{m_w}}{C_{m_{wo}}}$
Nielsen	0.7	0	0.83	1.02
Nielsen	0.7	6	0.81	0.98
F-4C	0.9	0	0.90	0.99

Clearly, normal-force coefficients decreased by approximately 15 percent as a result of simulating inert-shell elements; pitching-moment coefficients were virtually unchanged. Although the results were obtained for a simple tangent-ogive-cylinder model, similar results could be expected for the MK-83 flight test weapon.

APPENDIX B

AN OUTLINE OF THE DATA REDUCTION PROGRAM

1. Calculation of Bridge Power Shunt Ratios:

$$K_{BP_i} = S_{o,i} + S_{1,i}\, B_i \qquad i = 1 \text{ through } 9$$

2. Calculation of Differential Balance Outputs:

$$DR_1 = 19.99\left[\left(\frac{R_1}{K_{BP_1}}\right) - R_{1,o}\right] \Big/ K_{S1}$$

$$DR_2 = 19.62\left[\left(\frac{R_2}{K_{BP_2}}\right) - R_{2,o}\right] \Big/ K_{S2}$$

$$DR_3 = 19.97\left[\left(\frac{R_3}{K_{BP_3}}\right) - R_{3,o}\right] \Big/ K_{S3}$$

$$DR_4 = 19.58\left[\left(\frac{R_4}{K_{BP_4}}\right) - R_{4,o}\right] \Big/ K_{S4}$$

$$- 19.92\left[\left(\frac{R_5}{K_{BP_5}}\right) - R_{5,o}\right] \Big/ K_{S5}$$

$$DR_5 = \frac{1}{2}\left\{19.58\left[\left(\frac{R_4}{K_{BP_4}}\right) - R_{4,o}\right] \Big/ K_{S4}\right.$$

$$\left. + 19.92\left[\left(\frac{R_5}{K_{BP_5}}\right) - R_{5,o}\right] \Big/ K_{S5}\right\}$$

$$DR_6 = 19.81\left[\left(\frac{R_6}{K_{BP_6}}\right) - R_{6,o}\right] \Big/ K_{S6}$$

3. Calculation of Accelerometer Outputs:

$$A_x = 1.33 \left\{ \left[\left(\frac{R_{AX}}{K_{BP_7}} \right) - R_{AX,o} \right] \Big/ K_{SX} \right\} \times 10^{-2}$$

$$A_y = 1.29 \left\{ \left[\left(\frac{R_{AY}}{K_{BP_8}} \right) - R_{AY,o} \right] \Big/ K_{SY} \right\} \times 10^{-2}$$

$$A_z = 2.00 \left\{ \left[\left(\frac{R_{AZ}}{K_{BP_9}} \right) - R_{AZ,o} \right] \Big/ K_{SZ} \right\} \times 10^{-2}$$

4. Calculation of Balance Outputs:

$$[L_i] = [\pm K_{i,j}] [\pm DR_i] \qquad i = 1 \text{ through } 6$$

$$j = 1 \text{ through } 6$$

use $[+K_{i,j}]$ with $[+DR_i]$

use $[-K_{i,j}]$ with $[-DR_i]$

5. Calculation of Gross Forces and Moments:

$$F_{N_g} = (L_5 - L_1)/X_1$$

$$F_{Y_g} = (L_6 - L_2)/X_7$$

$$F_{A_g} = L_3$$

$$M_{\ell_g} = L_4$$

$$M_{m_g} = (L_1 + L_5)/2$$

$$M_{n_g} = (L_2 + L_6)/2$$

6. Calculation of Inertial Forces and Moments:

$$F_{N_{st}} = W_N A_z$$

$$F_{Y_{st}} = -W_y A_y$$

$$F_{A_{st}} = -W_A A_x$$

$$M_{\ell_{st}} = -W_N \bar{Y} A_z + W_y \bar{Z} A_y$$

$$M_{m_{st}} = W_A \bar{Z} A_y + W_N \bar{X}_m A_z$$

$$M_{n_{st}} = -W_y \bar{X}_n A_y - W_A \bar{Y} A_x$$

7. Calculation of Aerodynamic Forces and Moments:

$$F_N = F_{N_g} - F_{N_{st}}$$

$$F_Y = F_{Y_g} - F_{Y_{st}}$$

$$F_A = F_{A_g} - F_{A_{st}}$$

$$M_\ell = M_{\ell_g} - M_{\ell_{st}}$$

$$M_m = M_{m_g} - M_{m_{st}} - X_{m_T} F_N$$

$$M_n = M_{n_g} - M_{n_{st}} - X_{n_T} F_y$$

8. Calculation of Aircraft Boom Parameters:

$$P = 78.05 + 2.92 R_P$$

$$V_{CAL} = 64.456 + 1.546 R_{V_{CAL}}$$

$$H = 83058.4 - 83.885 R_H$$

$$T_T = 309.45 + 0.3389 R_{T_T}$$

$$\alpha = -9.26 + 0.0198 R_\alpha$$

$$\beta = -10.63 + 0.020\ R_{\beta}$$

$$\theta = 47.74 - 0.094\ R_{\theta}$$

9. Calculation of Flight Conditions:

$$P_t = \left[\left(\frac{C_{CAL}{}^2(\gamma-1)}{2Va_o{}^2} + 1\right)^{\frac{\gamma}{\gamma-1}} - 1\right] P_o + P$$

$$M_\infty = \left[\left(\frac{P}{P_t}^{\frac{1-\gamma}{\gamma}} - 1\right)^{\frac{2}{\gamma-1}}\right]^{1/2}$$

$$q_\infty = \frac{1}{2}\ P\ M_\infty{}^2$$

$$Re/\ell \times 10^{-6} = \frac{1.798\ q_\infty\ (T+198.8)}{M_\infty T^2}$$

10. Calculation of Aerodynamic Coefficients:

$$C_N = F_N/q_\infty S$$

$$C_Y = F_y/q_\infty S$$

$$C_A = F_A/q_\infty S$$

$$C_\ell = M_\ell/q_\infty Sb$$

$$C_m = M_m/q_\infty Sb$$

$$C_n = M_n/q_\infty Sb$$

APPENDIX C

DERIVATION OF FLIGHT TEST UNCERTAINTY EQUATIONS

I. MACH NUMBER

The equation for Mach number is:

$$M_\infty = \left\{ \frac{2}{\gamma-1} \left[\left[\left(\frac{V_{CAL}^{\,2}(\gamma-1)}{2V_{a_o}^{\,2}} + 1 \right)^{\frac{\gamma}{\gamma-1}} - 1 \right] \frac{P_o}{P} + 1 \right]^{\frac{\gamma-1}{\gamma}} - 1 \right] \right\}^{1/2}$$

Differentiating the above equation with respect to the measured variables (V_{CAL} and P) yields:

$$\frac{\partial M_\infty}{\partial V_{CAL}} = \left\{ \frac{2}{\gamma-1} \left[\left[\left(\frac{V_{CAL}^{\,2}(\gamma-1)}{2V_{a_o}^{\,2}} + 1 \right)^{\frac{\gamma}{\gamma-1}} - 1 \right] \frac{P_o}{P} + 1 \right]^{\frac{\gamma-1}{\gamma}} - 1 \right] \right\}^{-1/2} \cdot$$

$$\left\{ \left[\left(\frac{V_{CAL}^{\,2}(\gamma-1)}{2V_{a_o}^{\,2}} + 1 \right)^{\frac{\gamma}{\gamma-1}} - 1 \right] \frac{P_o}{P} + 1 \right\}^{-\frac{1}{\gamma}} \cdot$$

$$\frac{P_o}{P} \left(\frac{V_{CAL}^{\,2}(\gamma-1)}{2V_{a_o}^{\,2}} + 1 \right)^{\frac{1}{\gamma-1}} \cdot \frac{V_{CAL}}{V_{a_o}^{\,2}}$$

$$\frac{\partial M_\infty}{\partial P} = \frac{2}{\gamma-1} \left[\left[\left(\frac{V_{CAL}^{\,2}(\gamma-1)}{2V_{a_o}^{\,2}} + 1 \right)^{\frac{\gamma}{\gamma-1}} - 1 \right] \frac{P_o}{P} + 1 \right]^{\frac{\gamma-1}{\gamma}} - 1 \right] \Bigg\}^{-1/2} \cdot$$

$$\frac{1}{\gamma} \left\{ \left[\left(\frac{V_{CAL}^{\,2}(\gamma-1)}{2V_{a_o}^{\,2}} + 1 \right)^{\frac{\gamma}{\gamma-1}} - 1 \right] \frac{P_o}{P} + 1 \right\}^{-\frac{1}{\gamma}} \cdot$$

$$\frac{P_o}{P^2} \left[\left(\frac{V_{CAL}^{\,2}(\gamma-1)}{2V_{a_o}^{\,2}} + 1 \right)^{\frac{\gamma}{\gamma-1}} - 1 \right]$$

The Mach number uncertainty equation is:

$$\Delta M_\infty = \left[\left(\frac{\partial M_\infty}{\partial V_{CAL}} \right)^2 \Delta V_{CAL}^{\,2} + \left(\frac{\partial M_\infty}{\partial P} \right)^2 \Delta P^2 \right]^{1/2}$$

II. DYNAMIC PRESSURE

The equation for dynamic pressure is:

$$q_\infty = \frac{1}{2} \gamma P M_\infty^{\,2}$$

Differentiating the above equation with respect to the measured variables (P and M_∞) yields:

$$\frac{\partial q_\infty}{\partial P} = \frac{1}{2} \gamma M_\infty^{\,2}$$

$$\frac{\partial q_\infty}{\partial M_\infty} = \gamma P M_\infty$$

The dynamic pressure uncertainty equation is:

$$\Delta q_\infty = \left[\left(\frac{\partial q_\infty}{\partial P} \right)^2 \Delta P^2 + \left(\frac{\partial q_\infty}{\partial M_\infty} \right)^2 \Delta M_\infty^{\,2} \right]^{1/2}$$

III. AERODYNAMIC COEFFICIENTS

The equations for balance gross forces and moments are:

$$F_{N,g} = \left[\frac{R_{11}}{C_{11}} + \frac{1}{2} \left(\frac{R_4}{C_{44}} + \frac{R_5}{C_{55}} \right) \right] \Big/ X_1$$

$$F_{y,g} = \left[\frac{R_2}{C_{22}} + \frac{R_6}{C_{66}} \right] \Big/ X_7$$

$$F_{A,g} = \frac{R_3}{C_{33}}$$

$$M_{\ell,g} = \left[\frac{R_4}{C_{44}} - \frac{R_5}{C_{55}}\right]$$

$$M_{m,g} = \left[\frac{R_1}{C_{11}} + \frac{1}{2}\left(\frac{R_4}{C_{44}} + \frac{R_5}{C_{55}}\right)\right] \Big/ 24$$

$$M_{n,g} = \left[\frac{R_2}{C_{22}} + \frac{R_6}{C_{66}}\right] \Big/ 24$$

Differentiating the gross force and moment equations with respect to the measured variables (R_1 through R_6) yields the following gross force and moment uncertainty equations:

$$\Delta F_{N,g} = \left[\left(\frac{\Delta R_1}{C_{11}}\right)^2 + \left(\frac{\Delta R_4}{2C_{44}}\right)^2 + \left(\frac{\Delta R_5}{2C_{55}}\right)^2\right]^{1/2} \Big/ X_1$$

$$\Delta F_{Y,g} = \left[\left(\frac{\Delta R_2}{C_{22}}\right)^2 + \left(\frac{\Delta R_6}{C_{66}}\right)^2\right]^{1/2} \Big/ X_7$$

$$\Delta F_{A,g} = \frac{\Delta R_{33}}{C_{33}}$$

$$\Delta M_{\ell,g} = \left[\left(\frac{\Delta R_4}{C_{44}}\right)^2 + \left(\frac{\Delta R_5}{C_{55}}\right)^2\right]^{1/2}$$

$$\Delta M_{m,g} = \left[\left(\frac{\Delta R_1}{C_{11}}\right)^2 + \left(\frac{\Delta R_4}{2C_{44}}\right)^2 + \left(\frac{\Delta R_5}{2C_{55}}\right)^2\right]^{1/2} \Big/ 24$$

$$\Delta M_{n,g} = \left[\left(\frac{\Delta R_2}{C_{22}}\right)^2 + \left(\frac{\Delta R_6}{C_{66}}\right)^2\right] \Big/ 24$$

The equations for the inertial forces and moments are:

$$F_{N,st} = W_N A_z$$

$$F_{Y,st} = -W_Y A_y$$

$$F_{A,st} = -W_A A_x$$

$$M_{\ell,st} = -W_N \bar{Y} A_z + W_Y \bar{Z} A_y$$

$$M_{m,st} = W_A \bar{Z} A_x + W_N \bar{X}_m A_z$$

$$M_{n,st} = -W_Y \bar{X}_m A_y - W_A \bar{Y} A_x$$

Differentiating the inertial force and moment equations with respect to the measured variables (A_x, A_y, and A_z) yields the following inertial force and moment uncertainty equations:

$$\Delta F_{N,st} = W_N \Delta A_z$$

$$\Delta F_{Y,st} = W_Y \Delta A_y$$

$$\Delta F_{A,st} = W_A \Delta A_x$$

$$\Delta M_{\ell,st} = [(W_N \bar{Y} \Delta A_z)^2 + (W_Y \bar{Z} \Delta A_y)^2]^{1/2}$$

$$\Delta M_{m,st} = [(W_A \bar{Z} \Delta A_x)^2 + (W_N \bar{X}_m \Delta A_z)^2]^{1/2}$$

$$\Delta M_{n,st} = [(W_Y \bar{X}_n \Delta A_y)^2 + (W_A \bar{Y} \Delta A_x)^2]^{1/2}$$

Since the aerodynamic loads are simply the difference between gross and inertial loads, the aerodynamic force and moment uncertainty equations are:

$$\Delta F_N = [(\Delta F_{N,g})^2 + (\Delta F_{N,st})^2]^{1/2}$$

$$\Delta F_Y = [(\Delta F_{Y,g})^2 + (\Delta F_{Y,st})^2]^{1/2}$$

$$\Delta F_A = [(\Delta F_{Y,g})^2 + (\Delta F_{Y,st})^2]^{1/2}$$

$$\Delta M_{\ell} = [(\Delta M_{\ell,g})^2 + (\Delta M_{\ell,st})^2]^{1/2}$$

$$\Delta M_{m} = [(\Delta M_{m,g})^2 + (\Delta M_{m,st})^2 + (X_{m_T}\ \Delta F_N)^2]^{1/2}$$

$$\Delta M_{n} = [(\Delta M_{n,g})^2 - (\Delta M_{n,st})^2 + (X_{n_T}\ \Delta F_Y)^2]^{1/2}$$

The equations for the aerodynamic coefficients are:

$$C_N = F_N/q_\infty S$$

$$C_Y = F_Y/q_\infty S$$

$$C_A = F_A/q_\infty S$$

$$C_{\ell} = M_{\ell}/q_\infty Sb$$

$$C_m = M_m/q_\infty Sb$$

$$C_n = M_n/q_\infty Sb$$

Differentiating the aerodynamic coefficient equations with respect to the measured variables (F_N, F_Y, F_A, M_{ℓ}, M_m, M_n, and q_∞) yields the following aerodynamic coefficient uncertainty equations:

$$\Delta C_N = \left[\left(\frac{\Delta F_N}{q_\infty S}\right)^2 + \left(C_N\ \frac{\Delta q_\infty}{q_\infty}\right)^2\right]^{1/2}$$

$$\Delta C_Y = \left[\left(\frac{\Delta F_Y}{q_\infty S}\right)^2 + \left(C_Y\ \frac{\Delta q_\infty}{q_\infty}\right)^2\right]^{1/2}$$

$$\Delta C_A = \left[\left(\frac{\Delta F_A}{q_\infty S}\right)^2 + \left(C_A\ \frac{\Delta q_\infty}{q_\infty}\right)^2\right]^{1/2}$$

$$\Delta C_{\ell} = \left[\left(\frac{\Delta M_{\ell}}{q_{\infty} S b} \right)^2 \left(C_{\ell} \frac{\Delta q_{\infty}}{q_{\infty}} \right)^2 \right]^{1/2}$$

$$\Delta C_{m} = \left[\left(\frac{\Delta M_{m}}{q_{\infty} S b} \right)^2 + \left(C_{m} \frac{\Delta q_{\infty}}{q_{\infty}} \right)^2 \right]^{1/2}$$

$$\Delta C_{n} = \left[\left(\frac{\Delta M_{n}}{q_{\infty} S b} \right)^2 + \left(C_{n} \frac{\Delta q_{\infty}}{q_{\infty}} \right)^2 \right]^{1/2}$$

VITA

Gary Richard Mattasits was born in South Bend, Indiana, on March 4, 1948. He entered the Indiana University, South Bend Extension, upon graduating from the Central High School in June, 1966. After completing three and one-half years of general science study at Indiana University, he transferred to the Purdue University to complete studies in Aeronautical Engineering and received a Bachelor of Science Degree in June, 1972.

On November 6, 1972, he was employed by ARO, Inc. at the Arnold Engineering Development Center, Arnold Air Force Station, Tennessee, as a Project Engineer in the Propulsion Wind Tunnel Facility. He worked on many aircraft external store programs in the four-foot transonic tunnel. The author has published fourteen works relating to external store aerodynamics.

The author is married to the former Phyllis Ann Simms of South Bend, Indiana, and is the father of three children: Marc Richard age five, Marcia Ann age three, and Keith Louis age eleven months.